NASA Technical Paper 2011

1982

Effects of Wing-Leading-Edge Modifications on a Full-Scale, Low-Wing General Aviation Airplane

Wind-Tunnel Investigation of High-Angle-of-Attack Aerodynamic Characteristics

William A. Newsom, Jr.,
Dale R. Satran, and
Joseph L. Johnson, Jr.
Langley Research Center
Hampton, Virginia

National Aeronautics and Space Administration

Scientific and Technical Information Branch

SUMMARY

A static-force-test investigation has been made on a full-scale, low-wing general aviation airplane in the Langley 30- by 60-Foot Tunnel to determine the effects of wing-leading-edge modifications on the high-angle-of-attack aerodynamic characteristics. The leading-edge modifications included leading-edge droop and slat configurations having full-span, partial-span, or segmented arrangements. Other devices included wing-chord extensions, fences, and leading-edge stall strips. Some tests were made to determine control effectiveness and the effects of power.

The investigation showed that good correlation exists between the results of wind-tunnel data and the results of flight tests, on the basis of autorotational stability criterion, for a wide range of wing-leading-edge modifications. It was found that the addition of a drooped leading edge on the outboard wing panel delayed tip stall to a very high angle of attack and resulted in a relatively small drag penalty in cruise. Segmented leading-edge droop or slats were found to be equally effective, but the drag penalties were much higher. Wing-chord extensions, fences, or leading-edge stall strips were generally ineffective. The outboard leading-edge-droop modification, which was most promising from the standpoint of stall departure and spin resistance, had little effect on static longitudinal stability, increased lateral stability, and generally provided an increase in lateral control at high angles of attack. Full-span leading-edge modifications tended to degrade airplane stall-departure and spin-resistance characteristics.

INTRODUCTION

The NASA Langley Research Center is currently conducting a broad research program to develop the technology required to provide improved stall departure and spin resistance of light general aviation airplanes. The program was initiated because stalling and spinning have been identified as major causes of fatal general aviation accidents (refs. 1 and 2). The research encompasses a wide variety of test techniques involving wind-tunnel tests, radio-controlled-model tests, and full-scale flight tests. Presented in references 3 to 10 are some results obtained in the research effort thus far. Included in this program are studies to define concepts which improve the stall characteristics and spin resistance of light general aviation aircraft as well as studies of the fully developed spin and recovery. Given in references 8 to 10 is a summary of the significant results obtained to date relative to the effects of wing-leading-edge modifications on the stall/spin behavior of a typical, light general aviation airplane.

The present research effort on wing modifications was inspired to a great extent by recent research conducted at the University of Michigan and at NASA Ames Research Center, in addition to earlier work conducted by the National Advisory Committee for Aeronautics (NACA) to investigate the effects of wing-leading-edge modifications on the lateral-directional characteristics of wings near stall (refs. 11 to 17). In the studies of references 16 and 17, the concept of a segmented wing leading edge was developed to control stall progression and to produce a "flat-top" wing lift curve to minimize or eliminate loss of damping in roll at the stall. In the tests summarized in references 8 to 10, an outboard wing-leading-edge modification was developed which significantly improved lateral-stability characteristics at the stall, spin-

resistance, and developed-spin characteristics as determined by a radio-controlled-model and by full-scale flight tests. Because of the need for full-scale-Reynolds-number aerodynamic data for analysis of airplane flight-test results, an investigation has been conducted in the Langley 30- by 60-Foot Tunnel using an airplane similar to the flight-test configuration. Some of the results of the wind-tunnel tests are summarized in reference 9. This paper includes that summary, augmented with data for additional configurations, pressure distributions, and associated analysis.

This investigation was directed at determining the effects of wing-leading-edge modifications on the high-angle-of-attack aerodynamic characteristics of the subject airplane configuration. Particular emphasis is placed on those configurations for which flight-test results were obtained. The leading-edge modifications included leading-edge-droop configurations and slat configurations having full-span, partial-span, or segmented arrangements. Other devices tested included wing-chord extensions, fences, and leading-edge stall strips. Most of the tests to investigate leading-edge devices were made for the configuration with the horizontal tail removed, but the effects of the most promising leading-edge device determined in the flight tests of references 9 and 10 were documented for the complete airplane. Tests of the complete airplane included rudder and elevator deflections and effects of power.

In addition to measurements of the forces and moments of the airplane made on the tunnel balance system, the forces and moments on the left outboard wing panel were recorded independently by a strain-gauge balance, and the right wing of the airplane was provided with several rows of pressure ports to provide pressure measurements for many of the tests. Flow surveys and flow-visualization studies utilizing a tuft grid, smoke, and "mini-tufts" were also employed during the investigation. The investigation was conducted at angles of attack ranging from -9° to 41° and at sideslip angles ranging from -15° to 15° for a Reynolds number of about 2.5×10^6, based on the mean aerodynamic chord.

SYMBOLS

All longitudinal forces and moments are referred to the wind-axis system and all lateral-directional forces and moments are referred to the body-axis system. Moment data are presented with respect to a center-of-gravity position of 25 percent of the wing mean aerodynamic chord at fuselage water line 34.87 (in.). Dimensional quantities are presented in U.S. Customary Units.

b wing span, ft

c local wing chord, ft

$\bar{c}$ mean aerodynamic chord, ft

c_n section normal-force coefficient, $\int_0^1 (c_{p,l} - c_{p,u})\, d\left(\frac{x}{c}\right)$

c_p section wing-pressure coefficient, $(p - p_\infty)/q_\infty$

C_D airplane drag coefficient, $\text{Drag}/q_\infty S$

$C_{D,wp}$ outboard-wing-panel drag coefficient, Drag(wing panel)/$q_\infty S_{wp}$

C_L airplane lift coefficient, Lift/$q_\infty S$

$C_{L,wp}$ outboard-wing-panel lift coefficient, Lift(wing panel)/$q_\infty S_{wp}$

C_l rolling-moment coefficient, positive right wing down, Rolling moment/$q_\infty Sb$

C_m pitching-moment coefficient, positive nose up, Pitching moment/$q_\infty Sc$

C_n yawing-moment coefficient, positive nose right, Yawing moment/$q_\infty Sb$

C_R resultant-force coefficient, $\sqrt{C_{L,wp}^2 + C_{D,wp}^2}$

C_T' effective propeller-thrust coefficient,

$$\frac{\text{Drag(prop off) - Drag(prop running)}}{q_\infty S}$$

C_Y side-force coefficient, Side force/$q_\infty S$

D propeller diameter, ft

n propeller speed, rps

p local static pressure, lb/ft^2

p_∞ free-stream static pressure, lb/ft^2

q_∞ free-stream dynamic pressure, lb/ft^2

S wing area, ft^2

S_{wp} outboard-wing-panel area, ft^2

V velocity, ft/sec

x chordwise distance from leading edge, ft

y spanwise distance from plane of symmetry, ft

α angle of attack, deg or rad

β angle of sideslip, deg

δ_e elevator deflection, positive trailing edge down, deg

δ_f flap deflection, positive trailing edge down, deg

δ_r rudder deflection, positive for left yaw, deg

ΔC_D incremental drag coefficient relative to basic airplane configuration

ΔC_l incremental rolling-moment coefficient

ΔC_n incremental yawing-moment coefficient

ΔC_Y incremental side-force coefficient

Stability derivatives:

$$C_{l_\beta} = \frac{\partial C_l}{\partial \beta} \qquad C_{n_\beta} = \frac{\partial C_n}{\partial \beta} \qquad C_{Y_\beta} = \frac{\partial C_Y}{\partial \beta}$$

Subscripts:

l lower

u upper

DESCRIPTION OF AIRPLANE

Basic Configuration

A three-view sketch of the low-wing general aviation airplane used in these tests is presented in figure 1, and a photograph of the airplane mounted in the Langley 30- by 60-Foot Tunnel is shown in figure 2. This configuration differed externally from the flight-test airplane of reference 8 only in that the flight-test airplane was fitted with a tail-mounted spin-recovery parachute, streamlined wheel fairings, and wing-tip-mounted α/β sensor booms. Presented in tables I and II(a) are the geometry characteristics of the airplane tested in the wind tunnel and the coordinates of the basic-wing airfoil section, respectively.

The location of the balance used to measure loads on the left outboard wing panel during the wind-tunnel tests is also shown in figure 1. For this installation, the wing panel was separated from the airplane along the line shown and reattached with all loads carried through an internal strain-gauge balance. The opening at the separation line was sealed with a thin rubber membrane. The right wing of the airplane was provided with static-pressure ports to provide pressure measurements for most of the tests. Figure 3 is a drawing of the right wing panel showing the spanwise locations of the 6 rows of pressure ports. Each row consisted of 15 chordwise ports on the upper surface and 8 on the lower surface. When the leading-edge-droop modifications were added, they were provided with ports in their upper and lower surfaces to replace the wing ports covered.

Wing-Leading-Edge Modifications

Leading-edge droop.- Most of the tests using a drooped leading edge were made with the leading-edge airfoil configuration developed in reference 8 as a device which would improve lateral stability at the stall. The modification to the basic wing consisted of a glove installed over the forward part of the airfoil which provided a 3-percent-chord extension and a droop which increased the leading-edge camber and radius as shown in figure 4. Coordinates of the new airfoil section created by this basic-droop piece are presented in table II(b). Several different configurations using various spanwise segments of the basic leading-edge droop were

tested in flight and in the wind tunnel as shown in figure 5. These modifications were created by changing the spanwise location of the abrupt discontinuity at the inboard end of the droop piece (figs. 5(a), (b), (d), and (e)), creating a gap in what would otherwise be a full-span droop (figs. 5(f) and (g)), or fairing the inboard edge of the discontinuity (fig. 5(c)).

An exaggerated leading-edge-droop configuration was created for the wind-tunnel tests by using the basic leading-edge droop as a starting point. Shown in figure 6 is the configuration resulting from mounting an additional drooped portion onto the outboard panels of the wing with the original drooped-leading-edge glove still in place. Coordinates of the airfoil section resulting from this leading-edge configuration are presented in table II(c).

A third leading-edge-droop configuration, shown in figure 7, was made by superimposing the leading edge of a NASA LS(1)-0417 airfoil section onto the leading edge of the basic wing. This airfoil section was selected primarily because of its large, rounded leading edge. The chord line of the LS(1)-0417 was tilted downward 1.5° to accomplish the upper-surface alignment. The resultant airfoil section was faired back into the lower surface of the basic wing starting about 0.10c behind the leading edge. Coordinates for the LS(1)-0417 drooped section are given in table II(d).

Upper-surface modification.- A modification to the upper surface of the basic wing was designed in reference 18 to improve maximum lift of the NACA 64-series airfoil used for the basic wing of the test airplane. This increase in thickness of the airfoil, as shown in figure 8, extended over the forward 42 percent of the wing chord. Coordinates of the new airfoil created by this modification are presented in table II(e).

Leading-edge slats.- Two leading-edge-slat configurations were used in the tests. Sketches of the slat arrangements are presented as figures 9 and 10, and it can be seen that the slats, which differed only in chord width, were tested in both partial- and full-span configurations.

Leading-edge stall strips.- Two sets of leading-edge stall strips were used in the tests. The stall strips were made to mount on the basic wing and on the original drooped leading edge at the same spanwise location as the gap of figure 5(g). As shown in the sketches of figure 11, the stall strips were triangular in cross section and were made in three chord widths.

Wing fences.- Sketches of wing-fence arrangements used in the tests are shown in figures 12(a) and (b). The fences were located at 57-percent semispan and were made in 2 chord lengths. The long fence was full chord and the short fence, which was tested only in skewed-in and skewed-out configurations, had a chord length of 23 percent of the wing chord.

Chord extension.- The leading-edge extension to the chord of the wing is shown in figure 12(c). A simple glove made to fit over the wing leading edge was used to increase the wing chord by 8 percent. The leading edge of the glove was made using the same coordinates as those of the basic wing.

Fillet droop.- In order to carry the lines of the basic leading-edge-droop airfoil into the side of the fuselage, a tapered fairing was made which mounted on the wing fillet. This fillet fairing is shown in the sketch of figure 12(d).

TESTS

The investigation was conducted in the Langley 30- by 60-Foot Tunnel. Except for the loads on the left outboard wing panel being measured by the internal balance mentioned previously, all forces and moments were measured on the tunnel scale system. The static pressures on the right wing were recorded by using a set of scanivalve units. Forces and moments presented are the average of 10 sets of data recorded at 1-sec intervals for each test condition.

During the tests of the complete airplane configurations, measurements were included with both ailerons deflected ±25° and the elevator deflected 12° to -23°.

Most of the tests were made with power off, but for some tests of the complete airplane, power was set to produce an advance ratio (V/nD) of 0.5 ($C_T' = 0.11$). Reynolds number for the tests was about 2.5×10^6 based on the mean aerodynamic chord ($\bar{c}$) for a free-stream dynamic pressure q_∞ of about 11 lb/ft^2. The test angle of attack, which was set using an accelerometer mounted in the model, ranged from -9° to 41° and the sideslip angle ranged from -15° to 15°.

In addition to the measurement of forces and moments on the airplane during the investigation, flow surveys and flow-visualization studies were made. These studies included the use of a tuft grid, smoke, and "mini-tufts" which were illuminated by ultraviolet light.

The longitudinal data from the tests have been corrected for blockage, airstream misalignment, buoyancy effects, mounting strut tares (including propeller slipstream effects), and wind-tunnel jet-boundary effects on the wing and the tail. Effects of the propeller slipstream at the tail are also accounted for in the tail-on jet-boundary corrections. Lift and drag corrections have been made for the integrated average airstream misalignment, and lateral-directional data are referenced to sideslip angles which include a correction for the integrated average lateral-airstream angle. An indication of the correction involved and a plot of the actual flow distribution in the tunnel is presented in appendix A of reference 19.

PREVIOUS FLIGHT RESULTS

In order to provide the reader with additional background information to aid in the interpretation of this paper, a brief discussion of the flight tests (refs. 8 and 10) conducted with several of the wing-leading-edge modifications is presented. Shown in figure 13 are sketches of the eight principal wing configurations previously studied in flight. Shown under each configuration are summary comments describing the spin results obtained in flight tests.

The airplane with the basic wing had two spin modes: one moderately flat and the other flat. The moderately flat spin mode was characterized by an angle of attack of about 50°, and recovery from this mode occurred 1 1/2 turns after applying normal recovery controls. The flat spin mode was characterized by an angle of attack of about 70°. Airplane controls were found to be ineffective for recovery, and the use of a spin-recovery parachute was required. During the flight program, the airplane exhibited a strong tendency to enter the moderately flat spin mode, but it was reluctant to enter the flat spin mode with normal prospin controls.

The full-span-droop configuration (modification A) was found to readily enter a flat spin, regardless of the prospin controls employed. The flat spin mode was

characterized by an angle of attack of 60° to 70°, which was comparable with the flat spin mode of the basic configuration. The airplane controls were ineffective for providing acceptable spin recovery, and the spin-recovery parachute was required.

The airplane with the outboard wing-leading-edge droop (modification B) exhibited a steep, slow spiral-type motion following prospin control inputs. Immediate recovery was achieved (1/8 turn) by simply relaxing either prospin rudder or elevator.

Addition of the fairing to the outboard leading-edge droop (modification C) caused the spin characteristics to be severely degraded. The spin entry appeared identical to that for the basic, outboard leading-edge-droop configuration, but after 1 1/2 turns the rotation rate increased rapidly, the angle of attack increased, and the airplane entered a flat spin mode. The spin mode was characterized by an angle of attack of about 74°. Recovery controls were ineffective and the spin-recovery parachute was deployed for recovery.

Spin characteristics relative to those obtained for the basic airplane were degraded by shortening the outboard leading-edge droop to modification D. This configuration also entered the flat spin easily. When the outboard leading-edge droop was lengthened to modification E, no change was noted from results obtained with modification B (that is, the very steep, easily recoverable spin was obtained).

Finally, it was found that both of the segmented leading-edge-droop modifications (F and G) resulted in flat spins.

The foregoing flight-test results indicate extremely large effects of wing-leading-edge modifications on spinning, and these results imply large variations of aerodynamic autorotational tendencies for the various wing configurations. These trends were quite evident in examination of the wind-tunnel data, as will be discussed. Also, the detailed flow phenomena and pressures responsible for the trends were identified.

WIND-TUNNEL RESULTS

The results of this wind-tunnel investigation are presented in the figures listed in table III.

Lift Characteristics

Basic wing.- Presented in figure 14 is the variation of lift coefficient with angle of attack measured on the outboard wing panel during one test run of the airplane with the tail removed. The data show a normal trend and repeatability at the lower angles of attack. Above an angle of attack of about 12°, however, the data show a scatter band of lift values corresponding to random fluctuations in the wing-balance readings. The lift fluctuations were periodic and did not appear to be related to hysteresis effects; but rather, they appeared to be caused by random flow separation and flow reattachment on the outboard wing panel.

The results of tuft studies for the basic configuration (presented in fig. 15) illustrate the random-flow-separation problem on the outboard wing panel and provide basic flow information for correlation with the lift data of figure 14. Two photographs of the flow patterns are presented for different time intervals corresponding

to the high- and low-lift readings at $\alpha = 20°$. The flow pattern for the high-lift condition shows separated flow inboard on the wing but attached flow on the outboard wing panel. For the low-lift condition, the flow on the outboard wing panel is shown to be separated. The results of oil-flow studies (fig. 16) obtained on a 1/3-scale model in the University of Maryland's Glenn L. Martin Wind Tunnel illustrate even more clearly the fluctuations in surface flow conditions for the basic configuration near the stall angle of attack. It is interesting to note the similarity in flow patterns for the model and the aircraft. The two photographs of the model at $\alpha = 14°$ are presented to illustrate the random flow changes in flow patterns which occurred at different time intervals - a result similar to that for the full-scale aircraft at $\alpha = 20°$. In one photograph, the oil-flow studies show attached flow on the outboard panel of the right wing and stalled flow on the left wing panel; whereas, the other photograph, taken at a different time interval, shows the opposite trends with flow attachment on the left outboard wing panel and separated flow on the right wing panel. For angles of attack greater than about 25°, the flow-visualization tests indicated that the entire wing of the basic configuration was stalled. In view of the conditions described, it is necessary that some of the data herein be used with caution.

Modified wing.- As mentioned previously, photographs were made of the flow across the wing surface for each configuration tested. An example of the results obtained is presented in figure 17. Shown are the stall patterns at $\alpha = 30°$ and 35° for the wing with the addition of a drooped leading edge on the outboard portion of the wing (modification B). It can be seen that this leading-edge-droop configuration tended to have attached wing-tip flow to very high angles of attack. Closer examination of the flow associated with the outboard-droop configuration, using a tuft grid and a smoke generator, indicated that the effectiveness of this configuration in maintaining attached flow at the wing tips was the result of a vortex flow generated at the inboard edge of the droop. The vortex flow apparently acted as an aerodynamic fence to stop the spanwise progression of the separated flow region toward the wing tips such that the tips continued to generate lift to high angles of attack. The outboard wing panel then appeared to have aerodynamic characteristics generally similar to those of a low-aspect-ratio wing.

Comparison of Wing Modifications

Basic leading-edge droop.- The significance of maintaining attached flow on the wing tips to high angles of attack is illustrated in figure 18 by plots of the lift and drag coefficients measured on the wind-tunnel scale system and plots of the resultant-force coefficient measured on the wing-tip balance. The wing-tip-balance data are included because the wing-tip aerodynamics on unswept wings are believed to be closely related to the damping or autorotational tendencies exhibited by the wing. As pointed out in reference 8, previous research has indicated that autorotation is encountered when the variation of the resultant-force coefficient of the wing angle of attack becomes negative; that is, when $\partial C_R/\partial\alpha < 0$. For the subject configurations, the variation in the slope of the resultant-force coefficient of the wing tip with α is expected to provide information for a good prediction of autorotational tendencies. The data of figure 18 show that the tip of the basic wing stalled abruptly at an angle of attack of 20° and the lift decreased rapidly at higher angles of attack. The addition of an outboard leading-edge droop (modification B) is shown to eliminate the abrupt stall of the wing tip and to maintain or increase lift up to $\alpha = 40°$. The change in slope of the resultant-force-coefficient curve from negative to positive values at the higher angles of attack is believed to be important in indicating the elimination of autorotation and the improvement of spin

resistance. It is interesting to note that the addition of a fairing on the inboard end of the outboard droop (modification C) to eliminate leading-edge discontinuity, or the addition of a full-span leading-edge droop (modification A), reintroduced abrupt tip stall and caused the slope of the resultant-force-coefficient versus α curve to become very negative at high angles of attack. This is probably the result of eliminating the vortex formerly generated by the discontinuity. In flight tests reported in reference 8, modification B was very spin resistant; whereas, the basic-wing configuration showed a flat spin mode. Modifications C and A also exhibited a flat spin mode in the airplane flight tests. Correlation of the values of $\partial C_R/\partial\alpha$ for the four configurations of figure 18 with the airplane flight-test results from reference 8 can be made on the basis of figure 19. The values of $\partial C_R/\partial\alpha$ plotted against angle of attack in figure 19 predict autorotation for all configurations except B. It is interesting to note that all leading-edge modifications extended the angle of attack at which $\partial C_R/\partial\alpha$ became zero, but apparently the elevator power was great enough to drive the airplane to angles of attack where only modification B could provide attached flow on the wing tips.

Static aerodynamic data for correlation with flight-test data on the effect of spanwise variation of the length of the leading-edge droop are shown in figure 20. The test configurations included full-span droop (modification A) and partial-span droop with inboard discontinuity at semispan stations of 72 percent (modification D), 57 percent (modification B), and 38 percent (modification E). The data of figure 20 show trends similar to those previously discussed in figure 18, but bring out two additional points. First, shortening the outboard-droop length by moving the inboard end of the droop from 57 to 72 percent of the semispan eliminates almost all the effectiveness of the outboard-droop arrangement for providing stall departure and spin resistance. In fact, the data show droop-modification D to have aerodynamic characteristics very similar to those of the basic wing. The second significant point regarding figure 20 is that droop-modification E provided aerodynamic data generally similar to modification A, except modification E tended to delay to a higher angle of attack the rapid destabilizing change in C_R near $\alpha = 30°$ which was noted for the full-span droop.

A summary of the data of figure 20 is presented in figure 21 in terms of $\partial C_R/\partial\alpha$ plotted against wing lateral stations in percent of wing semispan. Presented in figure 21 are the values of $\partial C_R/\partial\alpha$ for angles of attack from 20° to 40° along with results of flight tests (ref. 10) which define boundaries of inboard discontinuity of leading-edge droop which effectively prevent entry of the airplane into the flat spin mode. The data of figure 21 indicate fairly good qualitative agreement between the flight data and wind-tunnel static data, based on the criterion that autorotation is encountered when $\partial C_R/\partial\alpha < 0$. Modification B is seen to provide stabilizing tendencies over the angle-of-attack range, but shortening the length of the droop is seen to produce negative values of $\partial C_R/\partial\alpha$ at semispan stations corresponding very closely to that identified in flight tests (67 percent of $b/2$) for loss of effectiveness of the drooped leading edge. In the flight tests (ref. 10), an inboard wing station was identified for loss of effectiveness of the leading-edge droop in providing resistance to the flat spin mode (35 percent of $b/2$). The wind-tunnel data show that large negative values of $\partial C_R/\partial\alpha$ can be encountered at that point for angles of attack above 30°. Apparently, angles of attack of 30° or above can be induced at the wing tips by rotation under spin conditions.

Wing-fillet droop.- With regard to modifications A, E, and B, an interesting point brought out in the tests was that adding a leading-edge-droop modification to the wing/fuselage fillet (see fig. 12(d)) altered the aerodynamic characteristics of these configurations considerably. The data for the fillet droop modification on

modification A is shown in figure 22(a). It can be seen that the addition of the droop to the fillet eliminated the initial break in the total wing-lift curve. Without the wing-fillet droop, the initial lift-curve break in modification A data occurred near $\alpha = 10°$ and a stall break occurred near $\alpha = 25°$. Values of C_R in figure 22(a) indicate that the addition of droop to the fillet decreased the angle of attack at which $\partial C_R/\partial\alpha$ for the wing tip changed from positive to negative values, which suggests that the fillet droop would introduce autorotative tendencies at lower angles of attack than the basic full-span-droop configuration.

The effect of adding the wing/fuselage-fillet droop to modification E or to modification E with a spanwise, inboard droop extension with length equal to 0.095b/2 is shown in figure 22(b). The total lift data for all configurations show an initial break near $\alpha = 10°$ with a stall break near $\alpha = 30°$. Values of C_R in figure 22(b) show that addition of the drooped fillet to modification E provided a slight increase in angle of attack at which $\partial C_R/\partial\alpha$ changed from positive to negative values, indicating a stabilizing effect on autorotation tendencies. However, modification E with the inboard droop extension and the fillet droop appeared to be less stable on the basis of the variation of C_R with α.

The addition of the fillet droop to the modification-B wing arrangement (fig. 22(c)) was also found to increase the autorotational tendencies of the airplane on the basis of the variation of C_R with α.

Segmented leading-edge droop.- Presented in figure 23 is a comparison of data measured on the airplane with two configurations of segmented leading-edge droop. The segmented configurations (figs. 5(f) and (g)) are geometrically similar to those tested in reference 8. The lift data of figure 23 show trends similar to those reported in reference 8 in that initial stall occurs around $\alpha = 10°$ and a secondary stall occurs at a higher angle of attack, resulting in a double-peak lift curve. Values of C_R show that the wing-tip stall is delayed by the segmented leading edge from $\alpha = 20°$ to $\alpha = 30°$. Values of $\partial C_R/\partial\alpha$ for the segmented configurations are compared with those of the basic wing and of modification B in figure 24. The segmented leading edges were not as effective as modification B in providing positive values of $\partial C_R/\partial\alpha$ to high angles of attack. The segmented leading edge with the larger cutout (modification G) shows only small negative values of $\partial C_R/\partial\alpha$ at $\alpha = 40°$; whereas, the smaller segmented cutout (modification F) produced large unstable values at $\alpha = 40°$.

LS(1)-0417 leading-edge droop.- As described previously, a modified leading-edge droop was created on the wing by superimposing the lines of an LS(1)-0417 airfoil. Tests of this configuration (see fig. 7) provided the results shown plotted and compared with the basic wing in figure 25. The figure shows an initial break near $\alpha = 10°$ for all configurations. The outboard LS(1)-0417 droop provided some protection in preventing autorotational tendencies by delaying the angle of attack at which stall occurred from $\alpha = 20°$ to $\alpha = 30°$. The full-span LS(1)-0417 droop provided some increase in maximum lift coefficient after the initial stall break. The initial stall break apparently was associated with wing-root flow-separation problems, and the use of a droop on the fillet in combination with the full-span LS(1)-0417 droop probably would have provided an increase in maximum lift coefficient at the initial stall break. The resultant-force coefficient, however, indicates that the full-span LS(1)-0417 droop provided no improvement in tip stall characteristics compared with those of the basic wing.

Exaggerated leading-edge droop.- To determine the aerodynamic effectiveness of increasing the radius of the leading-edge droop, tests were conducted using modifica-

tions A and B with an extra droop section mounted outboard, as shown in figure 6. The results presented in figure 26 show generally similar trends of lift, drag, and wing-tip resultant force as those shown for the basic droop configurations (fig. 18), which indicates that increasing the leading-edge radius provided little or no benefit on the stall departure and spin resistance relative to those of the basic droop configurations. Detailed studies of the penalties introduced on performance characteristics of the airplane by modifying the leading-edge radius will be discussed in a subsequent section.

Leading-edge slats.- The results of the tests of various slat configurations are compared in figure 27. As shown by the data in figure 27(a), outboard-slat arrangements provided trends in lift and drag generally similar to those of modification B (basic leading-edge droop), but the outboard slat provided more lift on the outboard wing panel. The full-span slats gave large increases in maximum lift coefficient and delayed tip stall to very high angles of attack as seen in the data of figure 27(b). The outboard-wing-panel data of figure 27 are summarized in figure 28 in terms of $\partial C_R/\partial\alpha$ plotted against α. Figure 28 is a very clear illustration of the similarity in autorotational stability of the outboard-droop and outboard-slat configurations. The full-span slat arrangements are shown to provide autorotational stability except near an angle of attack of 35° for the small-chord slat.

Chord extension.- The aerodynamic data obtained in tests of the extended-chord configuration are shown in figure 29 compared with the basic wing data. It can be seen that the extended chord on the outboard wing section had little effect on the aerodynamic characteristics of the airplane. The results of figure 29 suggests that the effectiveness of the outboard-leading-edge-droop configuration is apparently associated to a great extent with the droop shape as well as with the abrupt discontinuity of the inboard end of the drooped section.

Wing fences.- Figure 30 is a summary of the results of tests made with the various fence arrangements on the wing. The figure shows that the long-chord fence provided some delay in the angle of attack at which the lift-curve slope changes from positive to negative values; but, based on values of C_R for the wing tip, the fences were not very effective in improving the stall characteristics or the autorotational tendencies.

Leading-edge stall strips.- Presented in figure 31 are the data from the tests of the stall strips on the leading edge of the basic wing and on modification A of the basic leading-edge-droop arrangement. Results for only the smallest chord stall strips are shown, but the results were the same for the other stall-strip chord widths. In general, the stall strips provided little if any aerodynamic benefits in terms of improved stall characteristics or improved autorotational tendencies.

Wing upper-surface modification.- Data for the tests involving the configuration having a modified upper wing surface show in figure 32 that there was some improvement in maximum lift coefficient at the stall break for the full-span arrangement, but very little improvement in extending the angle of attack at which autorotational tendencies begin.

Chordwise Pressure Coefficients

Presented in figures 33 to 36 are representative plots of the chordwise pressure coefficients obtained in the test. Data are included for: the basic wing (fig. 33); modification B (fig. 34), which showed improved aerodynamic characteristics; modifi-

cation C (fig. 35), wherein the improved aerodynamic characteristics of modification B were lost; and modification A (fig. 36), which had increased lift but poor autorotational characteristics.

Basic wing.- The data of figure 33(a) show that the basic wing had peak negative pressures near the wing leading edge and relatively high loading along the inboard and forward portion of the wing. Increasing the angle of attack to 21.6° (fig. 33(b)) reduced the loading inboard because of stalling and increased the peak leading-edge loading near the wing tip. At angles of attack of 31.9° and 41.5°, the chordwise stations show mostly zero pressure gradients along the wing chord with values of c_p about 0.6, indicating flow separation over the entire wing.

Modification B.- The pressure data for the best outboard-droop configuration near $\alpha = 11°$ (fig. 34(a)) show chordwise variations very similar to those of the basic wing (fig. 33(a)). However, at $\alpha = 21.6°$ (fig. 34(b)) the outboard-droop configuration shows decreased values of wing-leading-edge peak pressures at the spanwise stations along the droop portion of the wing (stations 0.63b/2 to 0.92b/2). As shown in figures 34(c) and (d), the peak pressures along the drooped leading edge maintained relatively high values even to an angle of attack of 41.5°.

Modification C.- Comparison of the chordwise pressure data for modification C (fig. 35) with the data for modification B (fig. 34), with its abrupt discontinuity at the inboard edge, shows that similar chordwise pressure variations and peak values of pressure coefficients were obtained for both configurations except near $\alpha = 40°$. Comparison of the data of figures 34(d) and 35(d) indicates that the creation of modification C by adding the inboard fairing to modification B reduced the peak values of the leading-edge pressure coefficients along the drooped portion of the leading edge and resulted in separated flow behind the wing leading edge as indicated by the low, constant values of pressure coefficient ($c_p = 0.60$) aft of the wing leading edge.

Modification A.- Comparison of the pressure data for the full-span-droop configuration (fig. 36) with those for modification B (fig. 34) shows, as expected, increased loading inboard along the wing for the full-span-droop configuration. Outboard, the pressure data are very similar for the two configurations except for angles of attack near 40°. The pressure data for modification A near $\alpha = 40°$ show reduced values of peak pressure coefficients near the leading edge and separated flow behind the leading edge. These data very closely resemble the data for modification C.

Spanwise Load Distribution

Values of section normal-force coefficient obtained from figures 33 to 36 were integrated and plotted as a function of semispan location in figure 37. In addition, similar plots are included for the segmented leading-edge-droop configurations investigated (fig. 38) and for the slat configurations in figures 39 and 40.

The data of figure 37 show generally similar span-load distributions for all the configurations at an angle of attack of 11.2°. Modification A, as expected, showed much higher inboard loading than the other configurations. Increasing the angle of attack to 21.6° resulted in modification A having the highest loading, and all configurations show a general trend of increased loading at the outboard stations. At $\alpha = 31.7°$, modifications B and C continued to show heavy loading near the wing tips;

whereas, modification A showed reductions in loading near the tips. At $\alpha = 41.5°$, the data show trends in span loading that are generally in good agreement with the static-force-test results of figure 18 in that modification B provided high loading at the tips, whereas the other configurations show reduced loading over the wing span, especially at the wing tips.

Span-load distribution data for the segmented leading-edge droop (modifications F and G), presented in figure 38, show changes in span loading with increases in angle of attack that are generally similar to those noted in figure 37 for the outboard droop arrangements. The segmented leading edge with the largest cutout (G) provided higher wing-tip loading than the configuration with the smaller cutout (F). These results are generally as expected, based on the static-force-test data of figure 23.

Span-load data for the small-chord slat (fig. 39) and for the large-chord slat (fig. 40) are in good agreement with the static-force-test data of figure 27. The data of figures 39 and 40 show that the slats increased the span loading outboard on the wing as the angle of attack was increased and maintained the high outboard loading up to the highest test angle of attack.

Drag Characteristics

In order to provide drag coefficient data for use in determining the performance penalties of the leading-edge devices under investigation, the drag coefficient data presented earlier were replotted to an expanded scale and incremental drag values were determined for the configurations which appeared most promising for improved stall departure and spin resistance. The curves of figure 41 show incremental drag values plotted against C_L for various configurations. Incremental drag values in the cruise range ($C_L = 0.4$) of 0.002 are shown for modification B, whereas modification C has $\Delta C_D = 0.0054$ and modification A has $\Delta C_D = 0.007$. Calculated performance figures indicate that ΔC_D of 0.002 would reduce the airplane cruise speed about 2 mph and ΔC_D of 0.007 would penalize the airplane cruise speed about 6 mph. The data of figure 41 show that the addition of the droop on the fillet would reduce the drag penalty of modification A in cruise to a value of $\Delta C_D = 0.004$. Modification B is shown to produce no penalty on the climb performance of the airplane ($C_L = 0.75$).

Incremental-drag-coefficient data for the segmented leading-edge-droop configurations are presented in figure 42. They show that the segmented leading edge with the smaller cutout had the lower drag penalty but that both segmented configurations generally produced a higher drag penalty than modification B.

The incremental-drag-coefficient data for the slat configurations are presented in figure 43. The data show, as expected, that all slat arrangements produced very large drag penalties on the airplane. The large-chord full-span-slat configuration showed values of ΔC_D at $C_L = 0.4$ that almost doubled the drag of the basic airplane in cruise.

Complete Airplane

The aerodynamic characteristics of the complete airplane are presented in figures 44 to 56.

Longitudinal characteristics.- The effects of power and flap deflection on the longitudinal characteristics are shown in figure 44. Power had about the same incremental effect on maximum lift as deflecting the flaps 30°, but neither power nor flap deflection had any significant effect on the pitching moment. The effects of elevator deflection with power off and on are shown in figure 45. The elevator was effective for producing incremental pitching moment over the whole angle-of-attack range and elevator deflection range, and as would be expected, the presence of increased slipstream velocity with power on gave increased elevator effectiveness. In the data of figure 46 which show the effect of the horizontal tail on the longitudinal characteristics, it can be seen that the airplane has good static longitudinal stability with the tail on and is unstable with the tail off.

Presented in figures 47 to 49 are the longitudinal aerodynamic characteristics of the complete airplane with wing-leading-edge droop pieces in place. The leading-edge modifications had little effect on static longitudinal stability of the airplane, indicating that the downwash characteristics in the vicinity of the horizontal tail were unaffected by the wing-leading-edge modifications.

Lateral characteristics.- Wide variations in effective dihedral and directional stability occurred starting at about $\alpha = 15°$. These variations are apparently associated with random asymmetric wing stall. The effect of this asymmetric stall, which was first mentioned in the discussion of figure 14, on the measured rolling moment is illustrated in figure 50. The data plotted in this report are averages of 10 measurements made at each test condition. In addition, data are presented, between $\alpha = 12°$ and $\alpha = 36°$, for the maximum and minimum values of rolling moment measured on the tunnel scale system to emphasize the unusually large variations of the readings in that angle-of-attack range. These variations in rolling moment and yawing moment could adversely affect the accuracy of C_{l_β} and C_{n_β} between $\alpha = 15°$ and $\alpha = 30°$ because these derivatives were calculated using the average of the tunnel scale readings. Therefore, the values of lift, rolling moment, and yawing moment at any given time during a test could, as shown in figures 14 and 50, be varying drastically as flow is detached and reattached on the wing panels.

The static lateral-stability characteristics of the complete basic airplane are shown in figure 51. With the vertical tail on, the airplane was directionally stable with power on up to about $\alpha = 25°$. The level of directional stability was higher with power on than with power off. It is interesting to note, however, that in the range of angles of attack between 0° and about 12° the airplane had more positive effective dihedral ($-C_{l_\beta}$) with the vertical tail off than with the tail on. Above 15° angle of attack, effective dihedral and directional stability were subject to wide variations.

The static lateral-directional characteristics of the complete airplane with wing-leading-edge droop pieces in place are presented in figures 52 to 54. A comparison of the basic configuration and modification B (figs. 51 and 52) shows that the addition of the outboard leading-edge droop reduced the directional stability and provided a large increase in the effective dihedral at angles of attack greater than 15°. The increase in dihedral effect was, as expected, based on longitudinal data which showed that the outboard droop modification provided attached flow on the wing outboard span up to angles of attack near 40°. Between $\alpha = 0°$ and $\alpha = 20°$, lateral-directional stability data for modification A presented in figure 53 show a slight increase in directional stability and an increase in effective dihedral rela-

tive to the basic configuration. When the fillet droop was added to modification A, the data (fig. 54) show that, compared to the data of figure 53, the directional stability was reduced over the whole high-angle-of-attack range, but there was an increase in $-C_{l_\beta}$ at angles of attack between 15° and 40°. Comparison of the data of figures 52 and 54, however, show that the increase in $-C_{l_\beta}$ provided by modification A with drooped fillet was not as large as that provided by modification B in the high-angle-of-attack range.

Rudder effectiveness of the airplane is shown in figure 55 and the aileron effectiveness is shown in figure 56. In general, the rudder provided substantial increments of yawing moment and the aileron provided substantial increments of rolling moment over most of the angle-of-attack range. Presented in figure 56 are values of ΔC_Y, ΔC_n, and ΔC_l provided by maximum deflection of the ailerons for right roll. The data show that modification B provided relatively small increases in aileron effectiveness even though attached flow was maintained to angles of attack near 40°.

Results of the pressure surveys indicated that most of the benefits of the outboard droop in delaying flow separation of the wing tips were near the wing leading edge. The ailerons were apparently exposed to regions of separated flow despite the benefits of the leading-edge droop in maintaining attached flow forward of the ailerons. The data of figure 56 do show, however, that modification A apparently provided improved flow conditions over the ailerons between $\alpha = 10°$ and $\alpha = 30°$ as indicated by the increased aileron effectiveness in that region. At angles of attack above 30°, modification-A data indicated a sharp decrease in aileron effectiveness, apparently because of flow separation on the outboard wing panel.

SUMMARY OF RESULTS

The results of an investigation to determine the effects of wing-leading-edge modifications on the aerodynamic characteristics of a full-scale low-wing general aviation airplane may be summarized as follows:

1. Good correlation was obtained between the results of wind-tunnel static data and the results of airplane flight tests, on the basis of the autorotational stability criterion, for a wide range of wing-leading-edge modifications.

2. The addition of a drooped leading edge on the outboard wing panel delayed tip stall to a very high angle of attack and resulted in a relatively small drag penalty in cruise.

3. The effectiveness of the outboard-droop arrangement in delaying tip stall is attributed to a vortex flow field at its inboard discontinuity which prevented separated flow from progressing outboard on the wing. The outboard wing panel, with the addition of the drooped leading edge, appeared to have aerodynamic characteristics generally similar to those of a low-aspect-ratio wing with significant delay in wing-tip stall.

4. The use of segmented leading-edge droop, slats, or exaggerated leading-edge droop on the outboard wing panel was effective for delaying tip stall, but was accompanied by increased drag penalties.

5. Leading-edge droop on the wing/fuselage fillet minimized flow separation problems at the wing/fuselage juncture. The fillet droop eliminated the initial lift-curve break and reduced drag for most of the full-span leading-edge modifications.

6. The outboard leading-edge-droop modification, which was most promising from the standpoint of stall departure and spin resistance, had little effect on static longitudinal stability, increased lateral stability, and generally provided some increase in lateral control at high angles of attack.

7. Full-span leading-edge droop, wing/fillet droop, full-span slats, and segmented leading-edge droop (with small gap) degraded airplane stall-departure and spin-resistance characteristics based on the autorotational stability criterion.

8. The wing upper-surface modification, leading-edge stall strips, wing-chord extension, wing fences, and LS(1)-0417 leading-edge droop provided little or no improvement in airplane autorotational characteristics.

Langley Research Center
National Aeronautics and Space Administration
Hampton, VA 23665
May 11, 1982

REFERENCES

1. Silver, Brent W.: Statistical Analysis of General Aviation Stall Spin Accidents. [Preprint] 760480, Soc. Automot. Eng., Apr. 1976.

2. Ellis, David R.: A Study of Lightplane Stall Avoidance and Suppression. FAA-RD-77-25, Feb. 1977.

3. Bowman, James S., Jr.; Stough, Harry P.; Burk, Sanger M., Jr.; Patton, and James M., Jr.: Correlation of Model and Airplane Spin Characteristics for a Low-Wing General Aviation Research Airplane. AIAA Paper 78-1477, Aug. 1978.

4. Burk, Sanger M., Jr.; Bowman, James S., Jr.; and White, William L.: Spin-Tunnel Investigation of the Spinning Characteristics of Typical Single-Engine General Aviation Airplane Designs. I - Low-Wing Model A: Effects of Tail Configurations. NASA TP-1009, 1977.

5. Burk, Sanger M., Jr.; Bowman, James S., Jr.; and White, William L.: Spin-Tunnel Investigation of the Spinning Characteristics of Typical Single-Engine General Aviation Airplane Designs. II - Low-Wing Model A: Tail Parachute Diameter and Canopy Distance for Emergency Spin Recovery. NASA TP-1076, 1977.

6. Bihrle, William, Jr.; Barnhart, Billy; and Pantason, Paul: Static Aerodynamic Characteristics of a Typical Single-Engine Low-Wing General Aviation Design for an Angle-of-Attack Range of -8° to 90°. NASA CR-2971, 1978.

7. Bihrle, William, Jr.; Hultberg, Randy S.; and Mulcay, William: Rotary Balance Data for a Typical Single-Engine Low-Wing General Aviation Design for an Angle-of-Attack Range of 30° to 90°. NASA CR-2972, 1978.

8. Staff of Langley Research Center: Exploratory Study of the Effects of Wing-Leading-Edge Modifications on the Stall/Spin Behavior of a Light General Aviation Airplane. NASA TP-1589, 1979.

9. Johnson, Joseph L., Jr.; Newsom, William A., Jr.; and Satran, Dale R.: Full-Scale Wind-Tunnel Investigation of the Effects of Wing Leading-Edge Modifications on the High Angle-of-Attack Aerodynamic Characteristics of a Low-Wing General Aviation Airplane. AIAA-80-1844, Aug. 1980.

10. DiCarlo, Daniel J.; Stough, Harry P., III; and Patton, James M., Jr.: Effects of Discontinuous Drooped Wing Leading-Edge Modification on the Spinning Characteristics of a Low-Wing General Aviation Airplane. AIAA-80-1843, Aug. 1980.

11. Weick, Fred E.; and Wenzinger, Carl J.: Effect of Length of Handley Page Tip Slots on the Lateral-Stability Factor, Damping in Roll. NACA TN No. 423, 1932.

12. Weick, Fred E.; and Wenzinger, Carl J.: Wind-Tunnel Research Comparing Lateral Control Devices, Particularly at High Angles of Attack. VII - Handley Page Tip and Full-Span Slots With Ailerons and Spoilers. NACA TN No. 443, 1933.

13. Weick, Fred E.; and Wenzinger, Carl J.: Wind-Tunnel Research Comparing Lateral Control Devices, Particularly at High Angles of Attack. I - Ordinary Ailerons on Rectangular Wings. NACA Rep. No. 419, 1932.

14. Weick, Fred Ernest; Sevelson, Maurice S.; McClure, James G.; and Flanagan, Marion D.: Investigation of Lateral Control Near the Stall. Flight Investigation With a Light High-Wing Monoplane Tested With Various Amounts of Washout and Various Lengths of Leading-Edge Slot. NACA TN 2948, 1953.

15. Weick, Fred E.; and Abramson, H. Norman: Investigation of Lateral Control Near the Stall. Flight Tests With High-Wing and Low-Wing Monoplanes of Various Configurations. NACA TN 3676, 1956.

16. Kroeger, R. A.; and Feistel, T. W.: Reduction of Stall-Spin Entry Tendencies Through Wing Aerodynamic Design. [Paper] 760481, Soc. Automot. Eng., Apr. 1976.

17. Feistel, T. W.; Anderson, S. B.; and Kroeger, R. A.: A Method for Localizing Wing Flow Separation at Stall To Alleviate Spin Entry Tendencies. AIAA Paper 78-1476, Aug. 1978.

18. Szelazek, C. A.; and Hicks, Raymond M.: Upper-Surface Modifications for $c_{\ell_{max}}$ Improvement of Selected NACA 6-Series Airfoils. NASA TM-78603, 1979.

19. Hassell, James L., Jr.; Newsom, William A., Jr.; and Yip, Long P.: Full-Scale Wind-Tunnel Investigation of the Advanced Technology Light Twin-Engine Airplane (ATLIT). NASA TP-1591, 1980.

TABLE I.- GEOMETRIC CHARACTERISTICS OF TEST AIRPLANE

Wing (basic):	
Span, ft	24.46
Area, ft^2	98.11
Design wing loading, lbf/ft^2	15.89
Root chord, ft	4.00
Tip chord, ft	4.00
Mean aerodynamic chord $\bar{c}$, ft	4.00
Aspect ratio	6.10
Dihedral, deg	5.0
Incidence:	
At root, deg	3.5
At tip, deg	3.5
Airfoil section	Modified NACA 64_2-415
Aileron (each):	
Area, ft^2	2.60
Span, ft	3.82
Chord, ft	0.68
Flap (each):	
Area, ft^2	2.72
Span, ft	3.76
Chord, ft	0.68
Horizontal tail:	
Span, ft	7.69
Incidence, deg	-3.0
Root chord, ft	3.60
Tip chord, ft	1.67
Mean aerodynamic chord, ft	2.75
Airfoil section	NACA 65_1-012
Tail length (distance 0.25$\bar{c}$ to 0.25 mean aerodynamic chord of tail), ft	11.62
Elevator:	
Area (total), ft^2	7.22
Root chord, ft	1.13
Tip chord, ft	0.70
Span, ft	7.69
Area (forward of hinge line at tip), ft^2	0.92
Vertical tail:	
Span, ft	4.09
Root chord, ft	3.60
Tip chord, ft	1.67
Airfoil section	NACA 65_1-012
Rudder:	
Area (total), ft^2	3.61
Root chord, ft	1.13
Tip chord, ft	0.70
Span, ft	4.09
Area (forward of hinge line at tip), ft^2	0.46
Propeller diameter, ft	5.92
Propeller pitch, in.	46

TABLE II.- COORDINATES OF AIRFOIL SECTIONS USED IN TESTS

[Stations and ordinates given in percent of airfoil chord]

(a) Coordinates of modified NACA 64_2-415 airfoil (basic wing)

Upper surface		Lower surface	
Station	Ordinates	Station	Ordinates
0	0	0	0
.299	1.291	.701	-1.091
.526	1.579	.974	-1.299
.996	2.038	1.504	-1.610
2.207	2.883	2.793	-2.139
4.673	4.121	5.327	-2.857
7.162	5.075	7.838	-3.379
9.662	5.864	10.338	-3.796
14.681	7.122	15.319	-4.430
19.714	8.066	20.286	-4.882
24.756	8.771	25.224	-5.191
29.803	9.260	30.197	-5.372
34.853	9.541	35.147	-5.421
39.904	9.614	40.096	-5.330
44.954	9.414	45.046	-5.034
50.000	9.016	50.000	-4.604
55.040	8.456	54.960	-4.076
60.072	7.762	60.000	-3.698
65.096	6.954	65.000	-3.281
70.111	6.055	70.000	-2.865
75.115	5.084	75.000	-2.343
80.109	4.062	80.000	-1.875
85.092	3.020	85.000	-1.458
90.066	1.982	90.000	-.990
95.032	.976	95.000	-.573
100.000	0	100.000	0

TABLE II.- Continued

(b) Coordinates of leading-edge-droop airfoil

Upper surface		Lower surface	
Station	Ordinates	Station	Ordinates
-2.769	-3.833	-2.769	-3.833
-2.658	-2.885	-2.658	-4.631
-2.217	-1.633	-2.217	-5.540
-1.773	-.817	-1.773	-5.983
-1.329	-.190	-1.329	-6.160
-.885	.350	-.885	-6.210
-.444	.875	-.700	6.225
.000	1.254	.000	-6.210
.444	1.604	.444	-6.201
.885	1.983	.885	-6.191
1.329	2.319	1.329	-6.182
2.206	2.883	2.206	-6.164
4.673	4.121	4.673	-6.111
7.163	5.075	7.163	-6.059
9.662	5.865	9.662	-6.006
14.681	7.123	14.681	-5.900
19.715	8.065	19.715	-5.793
24.756	8.771	24.756	-5.687
29.802	9.258	29.802	-5.580
34.852	9.542	38.585	-5.394
39.904	9.615	40.096	-5.330
44.952	9.415	45.046	-5.034
50.000	9.017	50.000	-4.604
55.040	8.456	54.960	-4.076
60.071	7.763	60.000	-3.698
65.096	6.954	65.000	-3.281
70.110	6.056	70.000	-2.865
75.115	5.085	75.000	-2.343
80.108	4.063	80.000	-1.875
85.092	3.021	85.000	-1.458
90.065	1.983	90.000	-.990
95.031	.977	95.000	-.573
100.000	.000	100.000	.000

TABLE II.- Continued

(c) Coordinates of exaggerated leading-edge-droop airfoil

Upper surface		Lower surface	
Station	Ordinates	Station	Ordinates
-5.500	-9.271	-5.500	-9.271
-5.250	-7.896	-5.250	-10.625
-5.000	-6.667	-5.000	-10.979
-4.167	-4.521	-4.167	-11.688
-3.333	-2.938	-3.333	-11.833
-2.500	-1.667	-2.500	-11.667
-1.667	-.625	-1.667	-11.537
-.833	.313	-.833	-11.406
.000	1.042	.000	-11.276
.417	1.417	.417	-11.210
1.042	1.896	1.042	-11.113
2.207	2.883	2.207	-10.930
4.673	4.121	4.673	-10.544
7.162	5.075	7.162	-10.155
9.662	5.864	9.662	-9.764
14.681	7.122	14.681	-8.678
19.714	8.066	19.714	-8.191
24.756	8.771	24.756	-7.401
29.803	9.260	29.803	-6.612
34.853	9.541	34.853	-5.811
39.904	9.614		
44.954	9.414	40.096	-5.330
50.000	9.016	45.046	-5.034
55.040	8.456	50.000	-4.604
60.072	7.762	54.960	-4.076
65.096	6.954	60.000	-3.698
70.111	6.055	65.000	-3.281
75.115	5.084	70.000	-2.865
80.109	4.062	75.000	-2.343
85.092	3.020	80.000	-1.875
90.066	1.982	85.000	-1.458
95.032	.976	90.000	-.990
100.000	0	95.000	-.573
		100.000	0

TABLE II.- Continued

(d) Coordinates of LS(1)-0417 leading-edge-droop airfoil

Upper surface		Lower surface	
Station	Ordinates	Station	Ordinates
-1.375	-2.000	-1.375	-2.000
-.833	0	-.833	-3.188
-.417	.604	-.417	-3.750
0	1.145	0	-4.063
.625	1.688	.625	-4.396
1.250	2.188	1.250	-4.646
2.207	2.883	1.875	-4.833
4.673	4.125	2.500	-5.042
7.162	5.075	3.750	-5.438
9.662	5.864	4.375	-5.604
14.681	7.122	6.250	-6.021
19.714	8.066	9.229	-6.417
24.756	8.771	12.333	-6.063
29.803	9.260	30.530	-5.417
34.853	9.541	35.147	-5.375
39.904	9.614	40.096	-5.330
44.954	9.414	45.046	-5.034
50.000	9.016	50.000	-4.604
55.040	8.456	54.960	-4.076
60.072	7.762	60.000	-3.698
65.096	6.954	65.000	-3.281
70.111	6.055	70.000	-2.865
75.115	5.084	75.000	-2.343
80.109	4.062	80.000	-1.875
85.092	3.020	85.000	-1.458
90.006	1.982	90.000	-.990
95.032	.976	95.000	-.573
100.000	0	100.000	0

TABLE II.- Concluded

(e) Coordinates of upper-surface-modification airfoil

Upper surface		Lower surface	
Station	Ordinates	Station	Ordinates
0	0	0	0
.104	1.250	.701	-1.091
.500	2.270	.974	-1.299
1.000	3.150	1.504	-1.610
2.000	4.290	2.793	-2.139
3.000	5.130	5.327	-2.857
5.000	6.310	7.838	-3.379
7.000	7.150	10.338	-3.796
10.000	8.020	15.319	-4.430
15.000	8.900	20.286	-4.882
20.000	9.333	25.244	-5.191
25.000	9.520	30.197	-5.372
30.000	9.600	35.147	-5.421
35.000	9.600	40.096	-5.330
40.000	9.600	45.046	-5.034
45.000	9.420	50.000	-4.604
50.000	9.016	54.960	-4.076
55.040	8.456	60.000	-3.698
60.072	7.762	65.000	-3.281
65.096	6.954	70.000	-2.865
70.111	6.055	75.000	-2.343
75.115	5.084	80.000	-1.875
80.109	4.062	85.000	-1.458
85.092	3.020	90.000	-.990
90.066	1.982	95.000	-.573
95.032	.976	100.000	0
100.000	0		

TABLE III.- PRESENTATION OF WIND-TUNNEL DATA

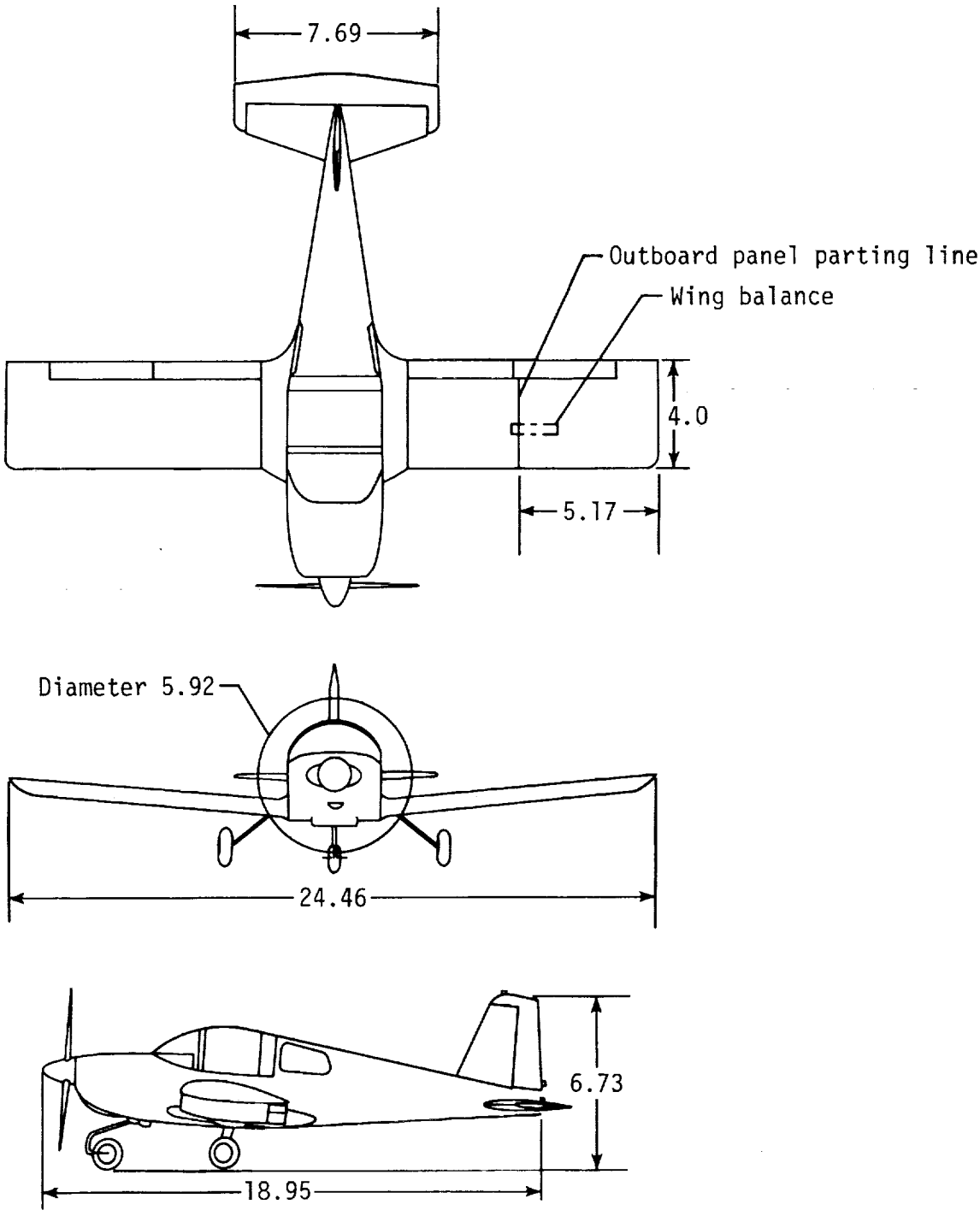

Figure 1.- Three views of test airplane. Dimensions are in feet.

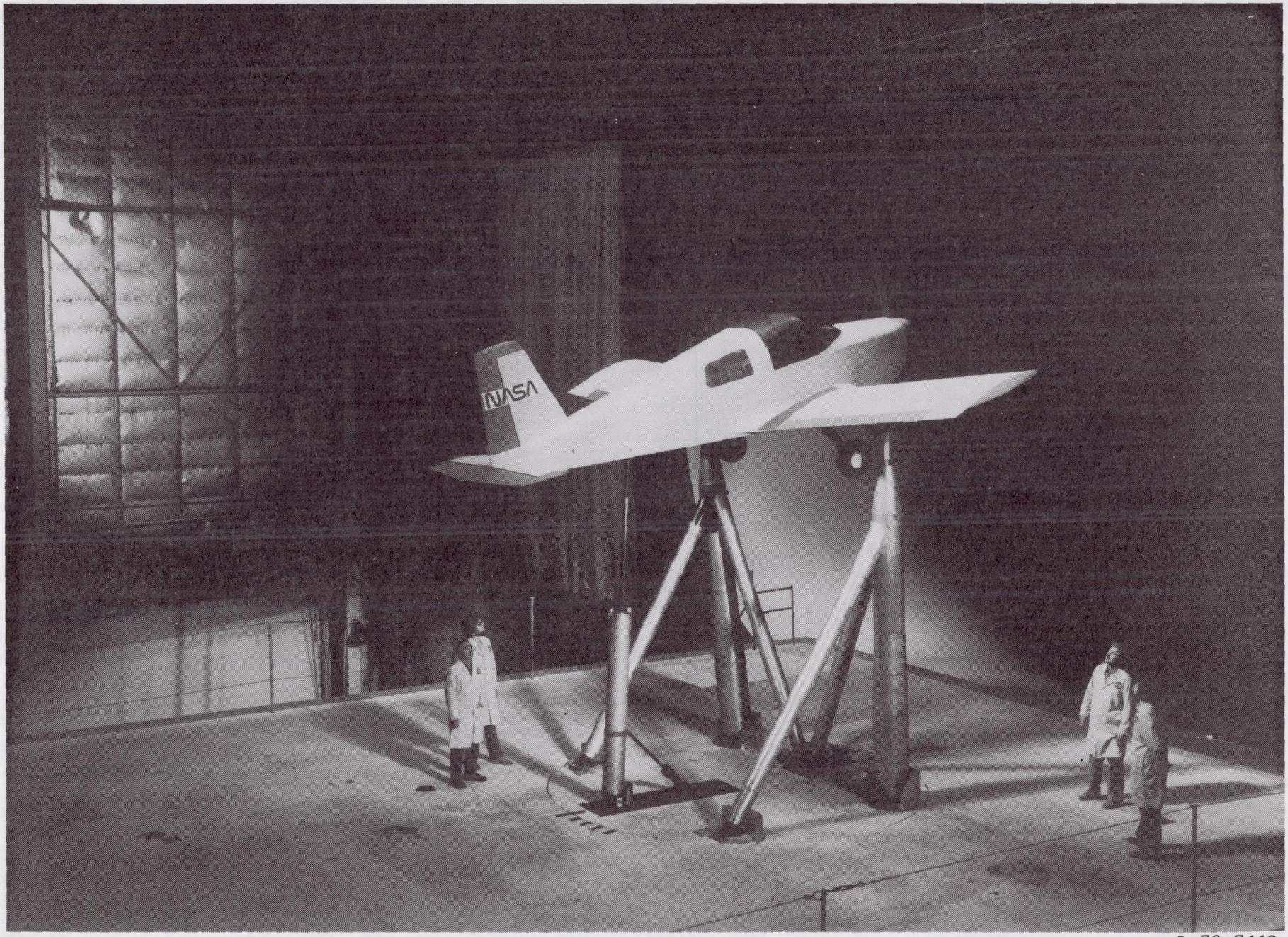

L-79-7119

Figure 2.- Test airplane in Langley 30- by 60-Foot Tunnel.

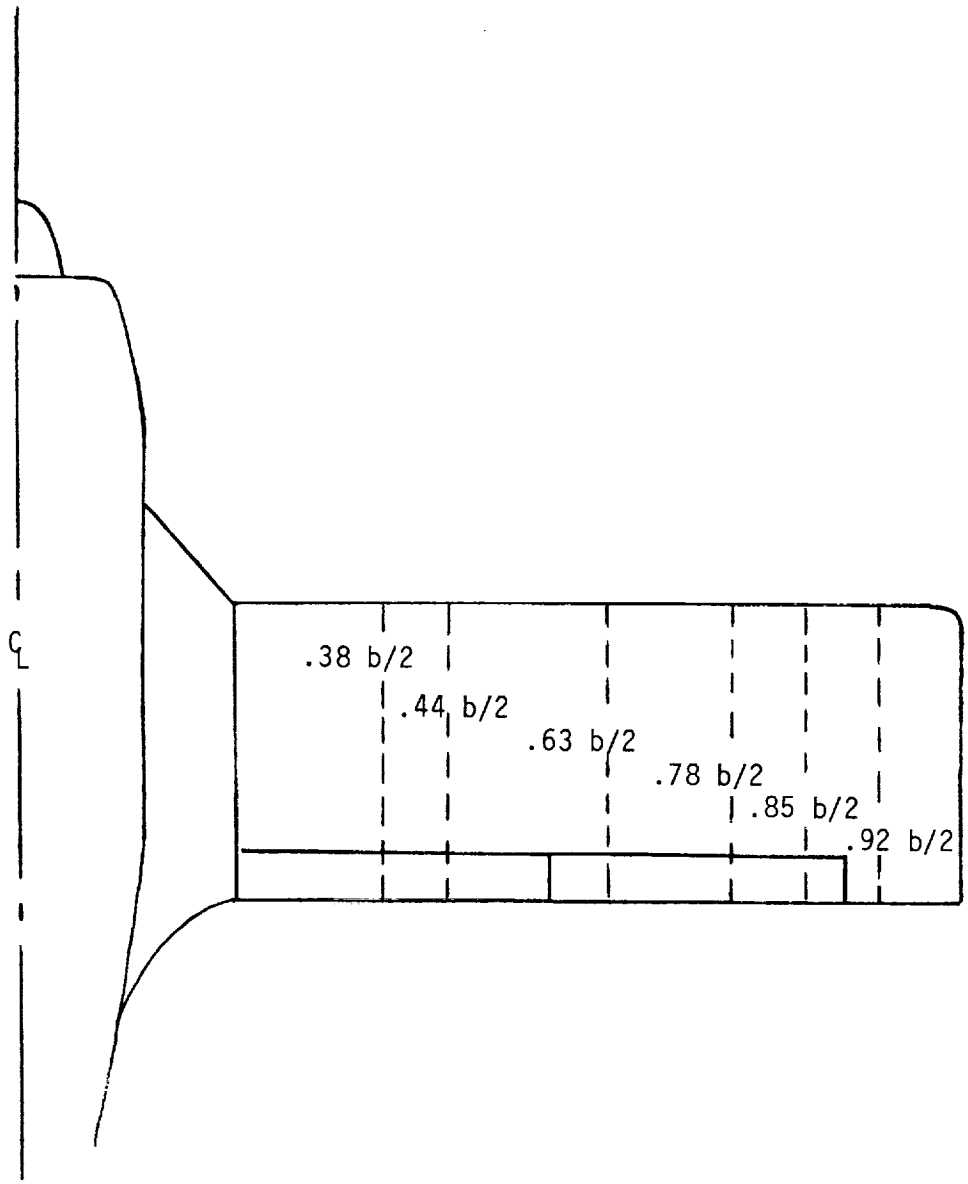

Figure 3.- Spanwise locations of rows of static-pressure ports on right wing of airplane.

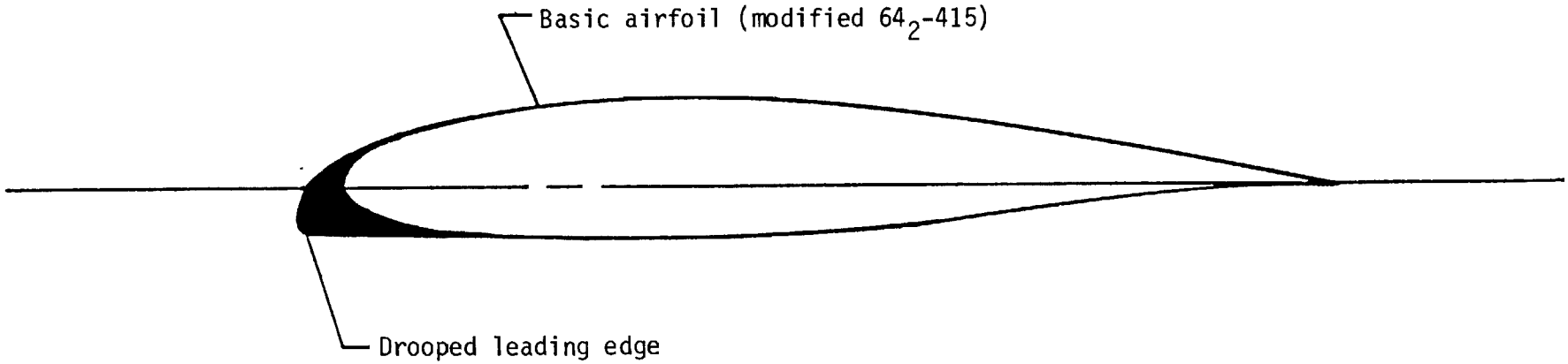

Figure 4.- Leading-edge-droop wing modification.

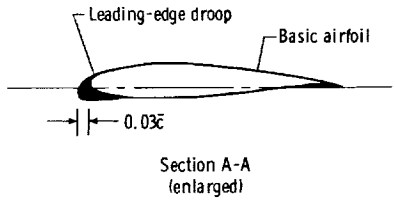

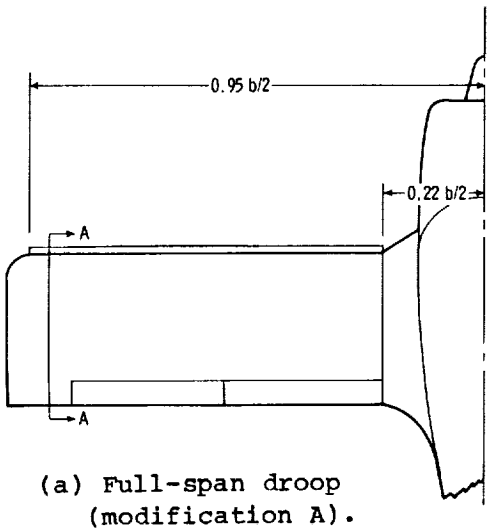

(a) Full-span droop (modification A).

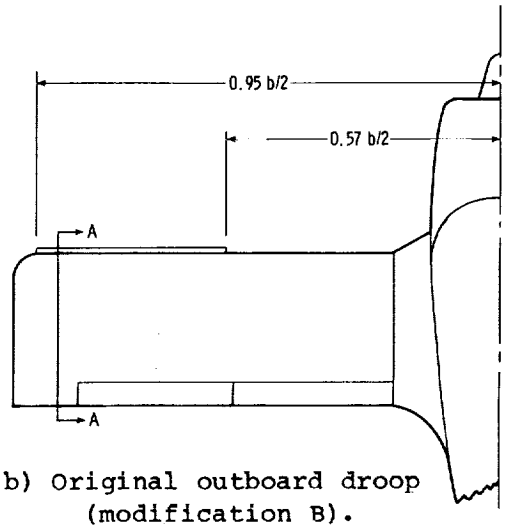

(b) Original outboard droop (modification B).

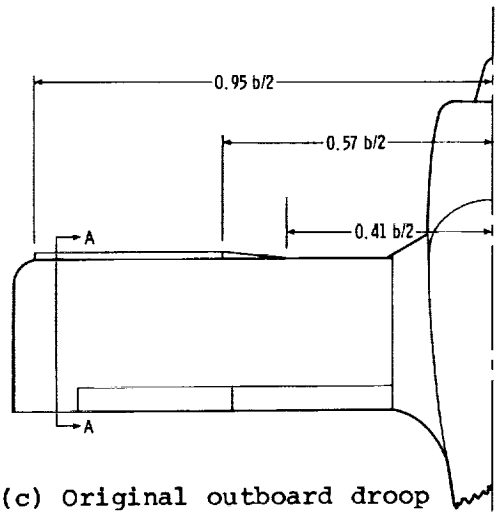

(c) Original outboard droop plus inboard fairing (modification C).

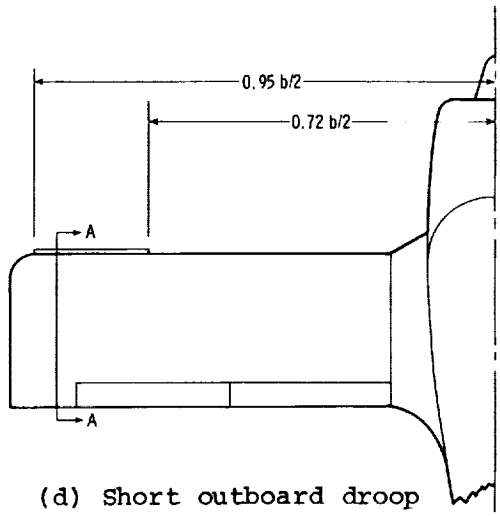

(d) Short outboard droop (modification D).

Figure 5.- Leading-edge-droop modifications studied in flight and wind-tunnel tests.

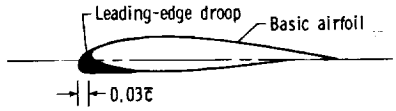

Section A-A
(enlarged)

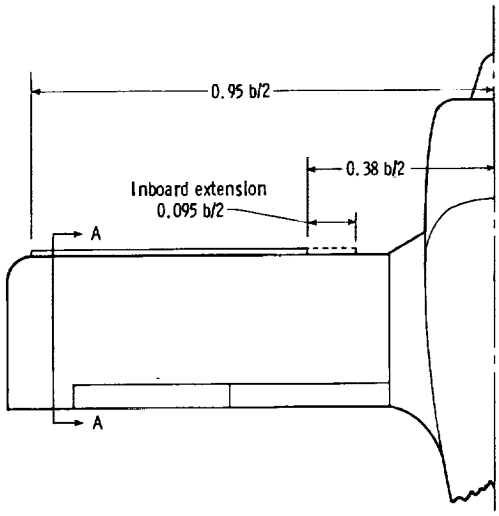

(e) Long outboard droop (modification E).

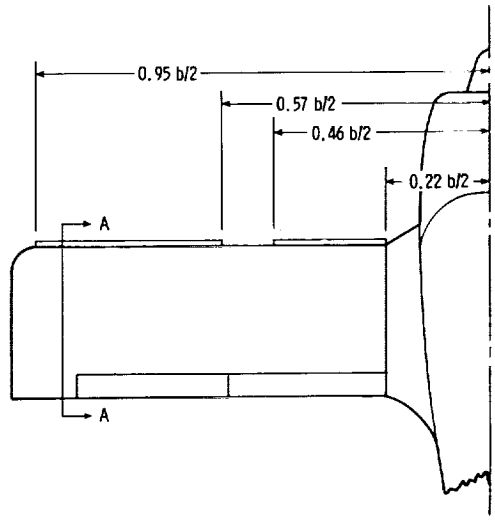

(f) Narrow-gap segmented droop (modification F).

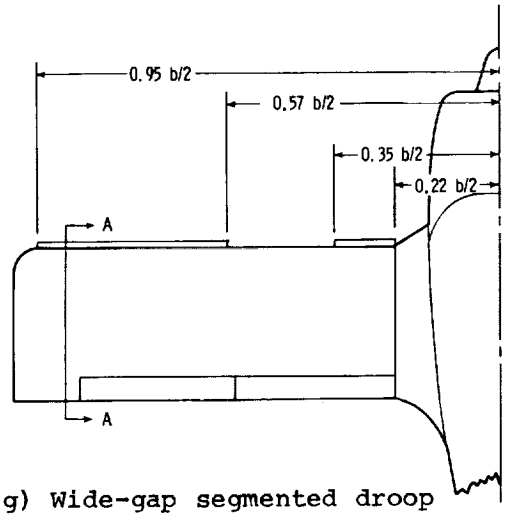

(g) Wide-gap segmented droop (modification G).

Figure 5.- Concluded.

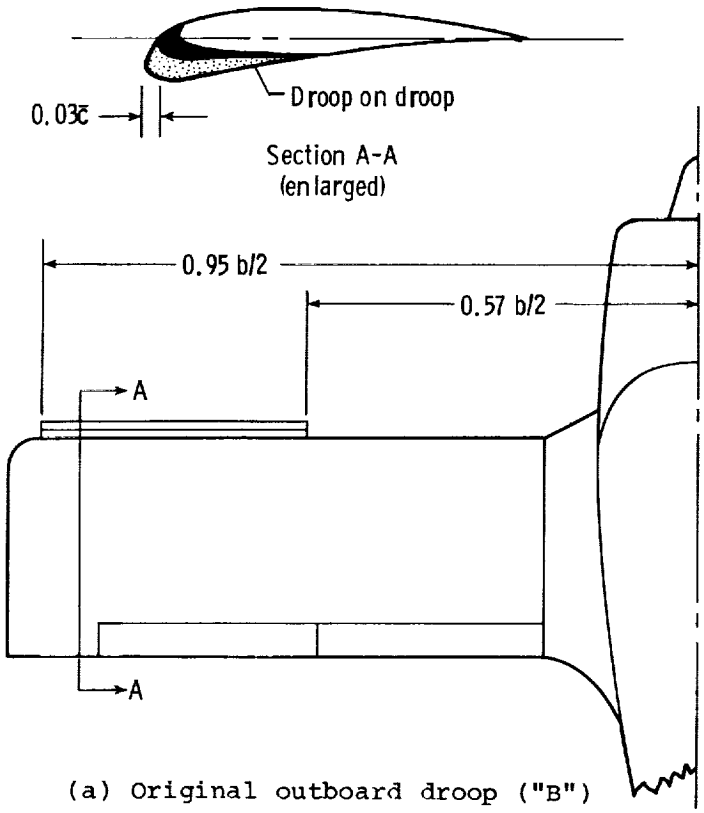

(a) Original outboard droop ("B") + Exaggerated droop.

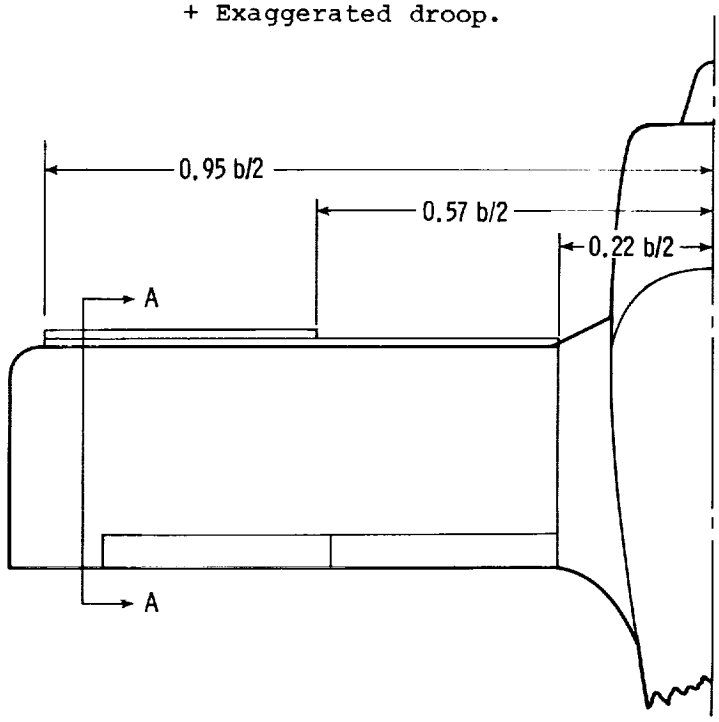

(b) Full-span droop ("A") + Exaggerated droop.

Figure 6.- Geometry of exaggerated leading-edge droop.

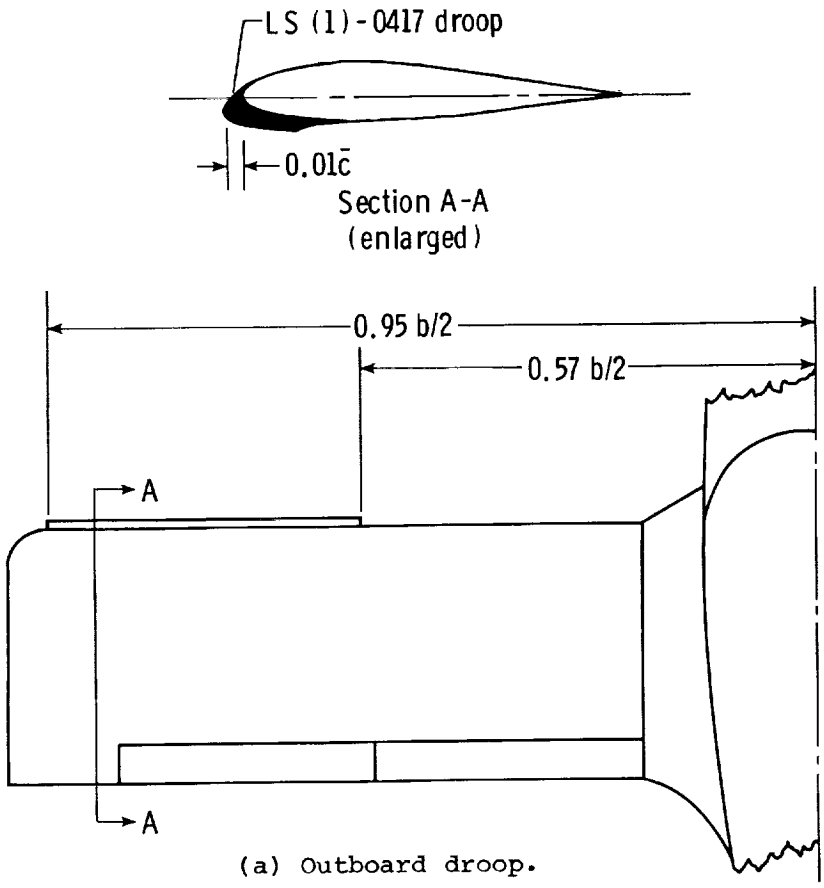

(a) Outboard droop.

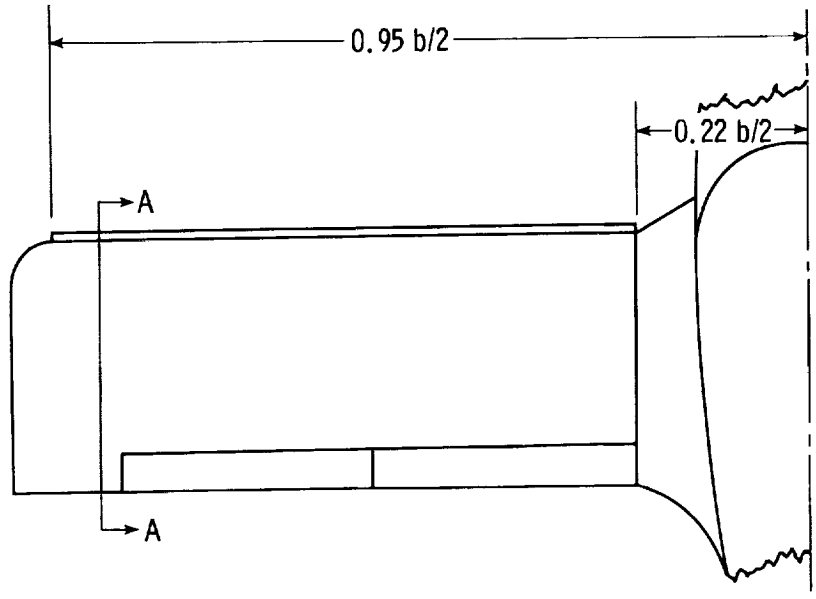

(b) Full-span droop.

Figure 7.- Geometry of LS(1)-0417 droop configuration used in tests.

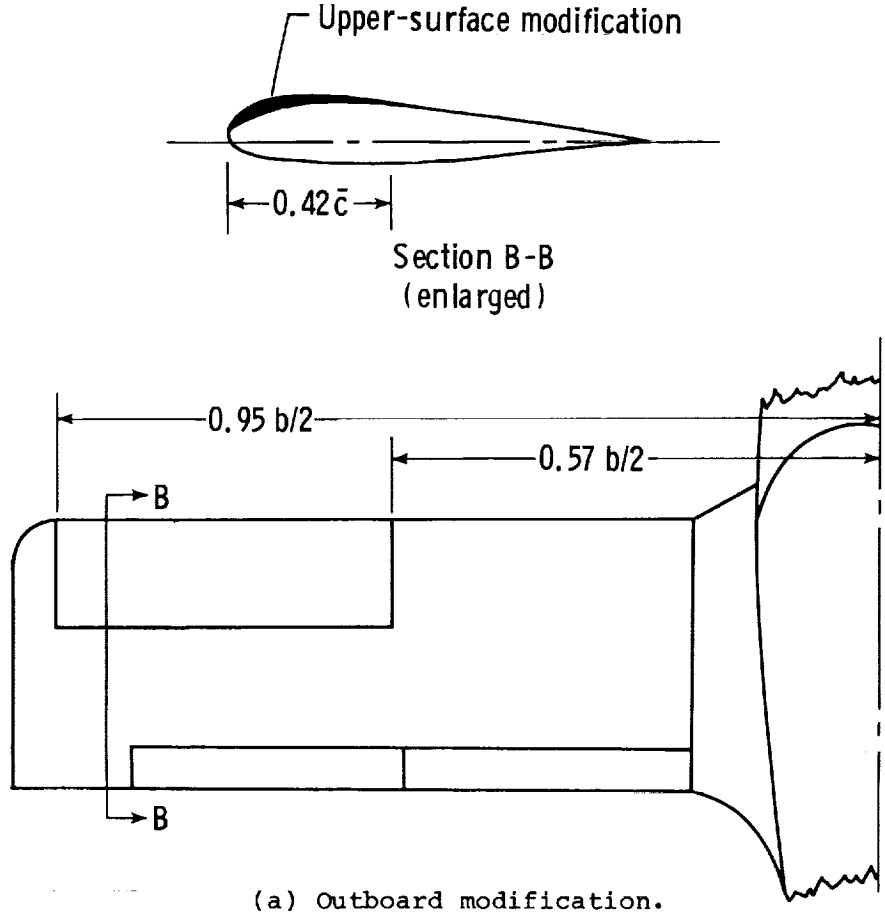

(a) Outboard modification.

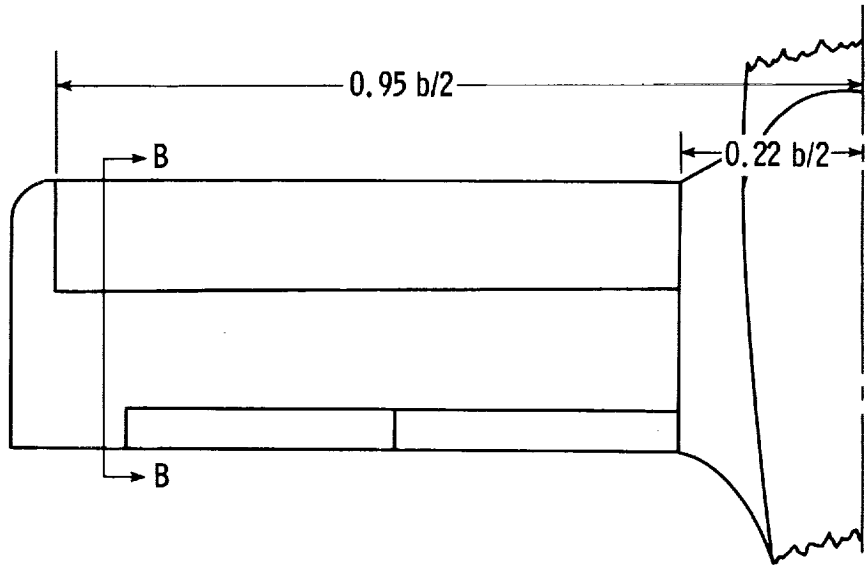

(b) Full-span modification.

Figure 8.- Geometry of upper-wing-surface modifications used in tests.

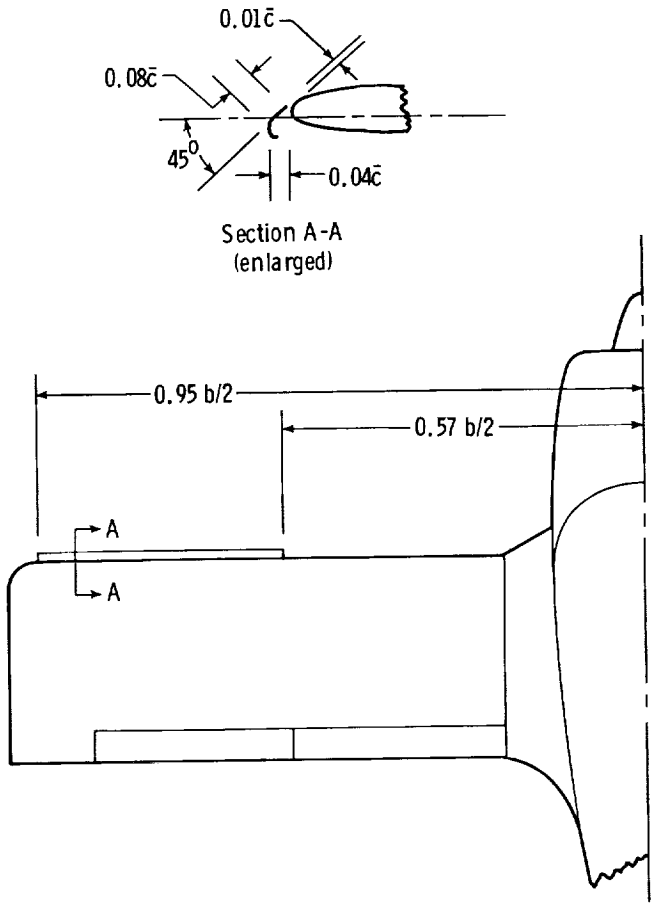

(a) Outboard slat.

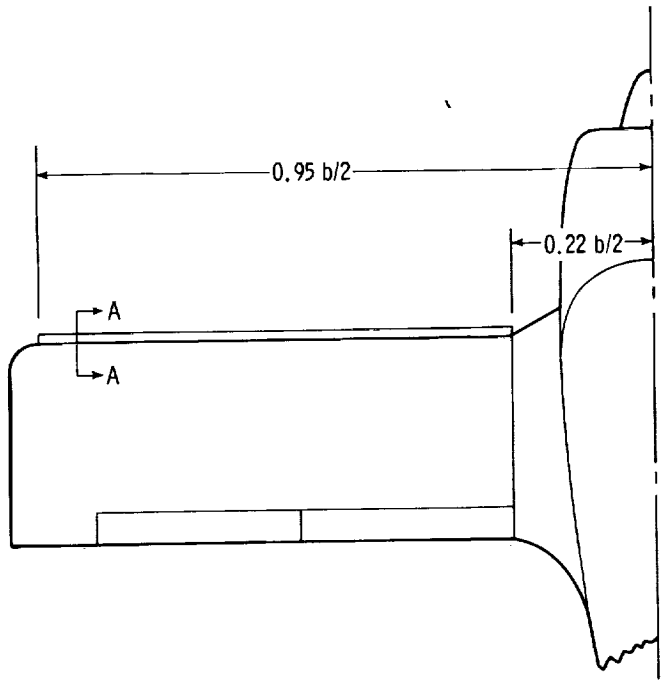

(b) Full-span slat.

Figure 9.- Geometry of $0.08\bar{c}$ slat used in tests.

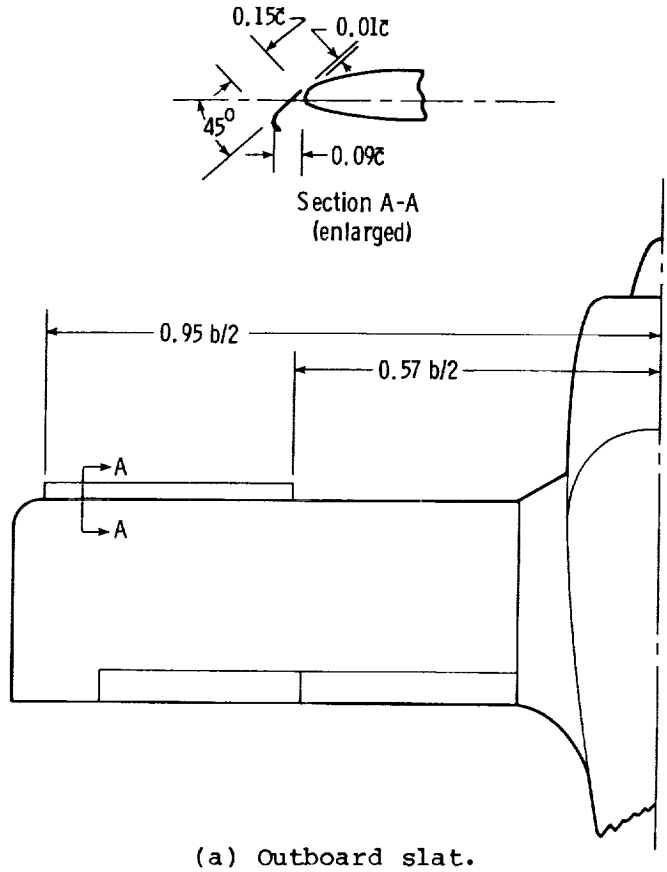

(a) Outboard slat.

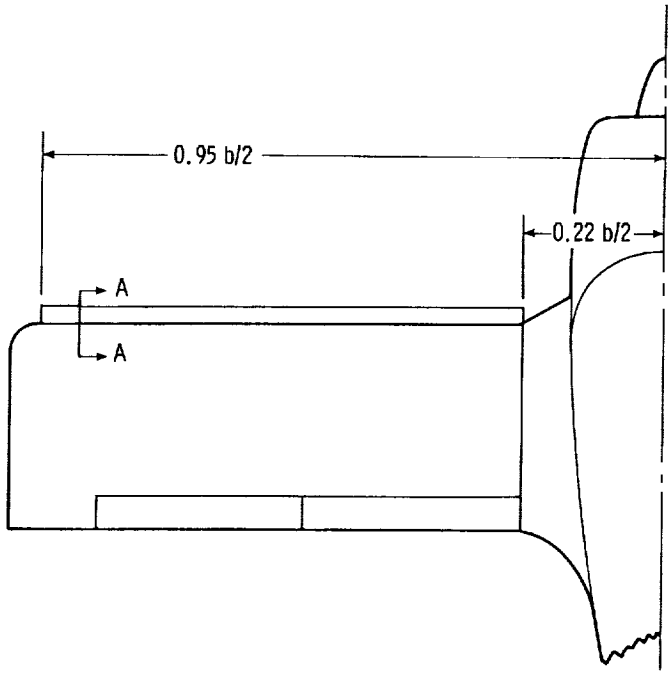

(b) Full-span slat.

Figure 10.- Geometry of 0.15$\bar{c}$ slat used in tests.

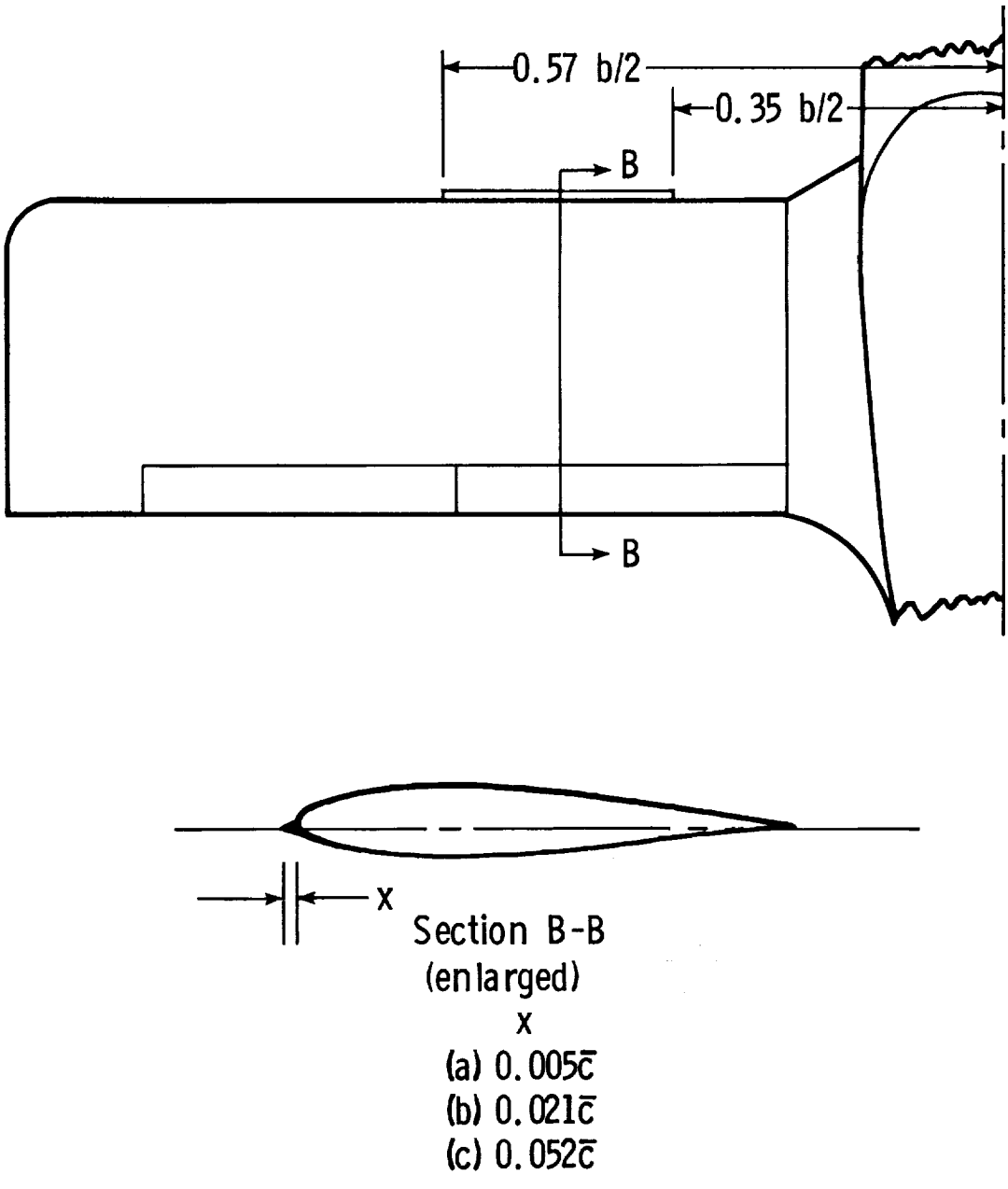

(a) Basic wing.

Figure 11.- Geometry of leading-edge stall strips used in tests.

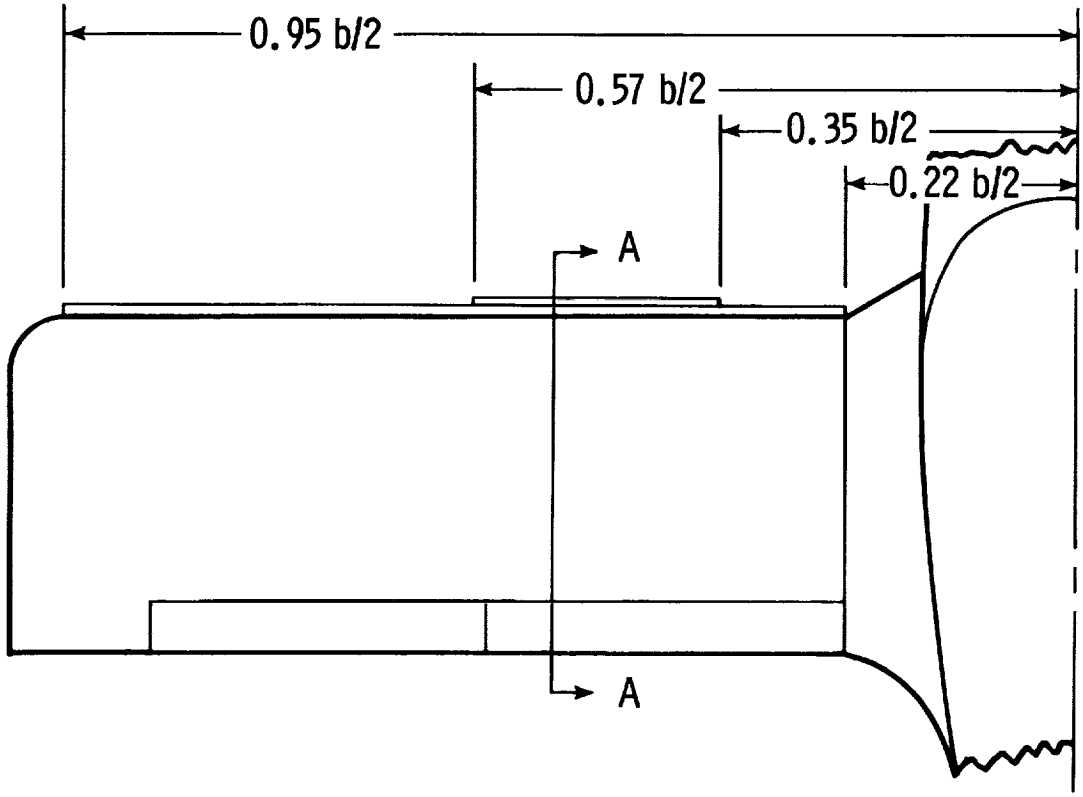

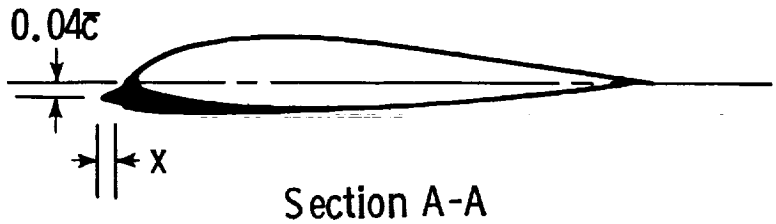

Section A-A
(enlarged)

x
(a) 0.005c̄
(b) 0.021c̄
(c) 0.052c̄

(b) Drooped leading edge.

Figure 11.- Concluded.

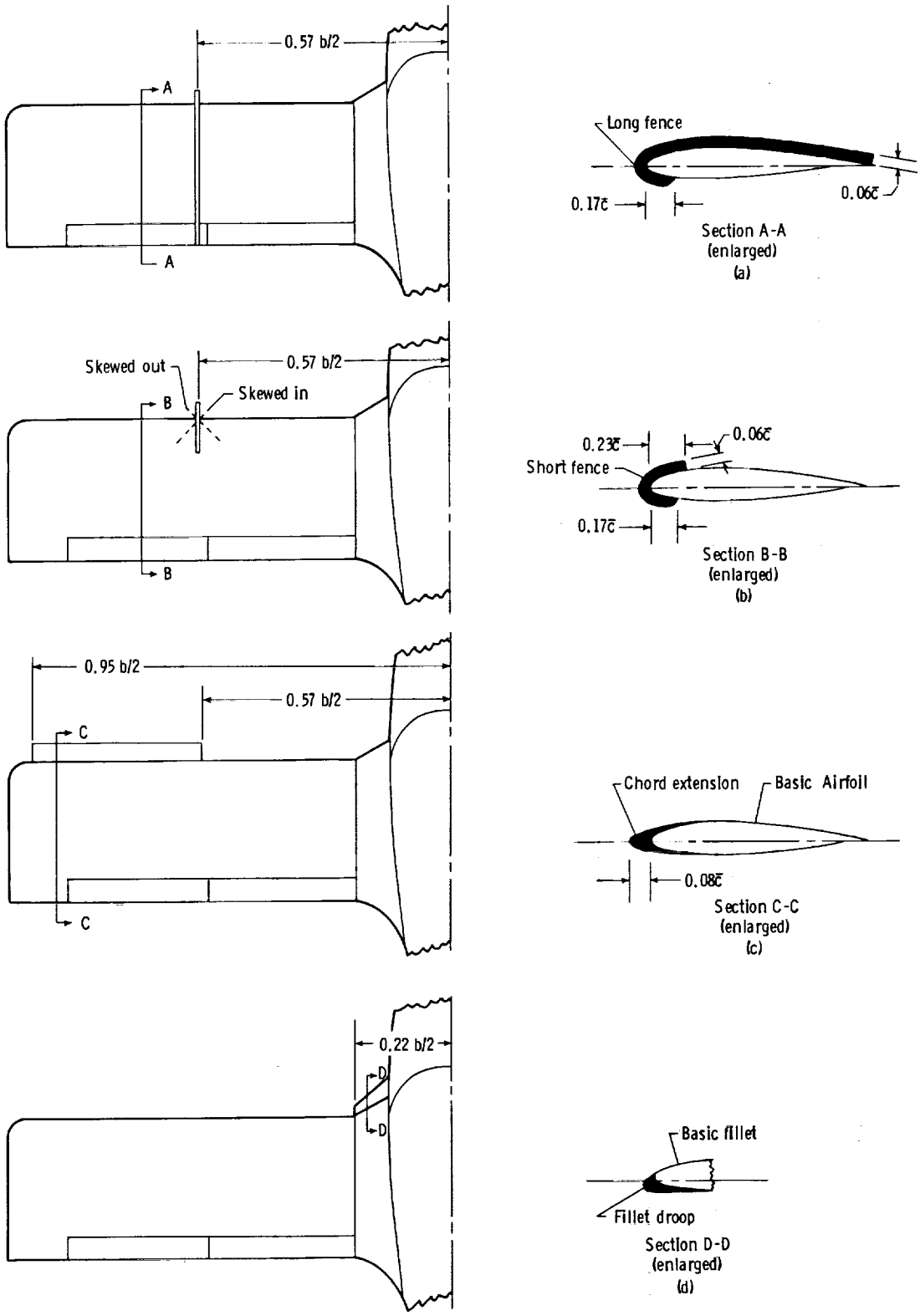

Figure 12.- Geometry of wing fences, chord extension, and fillet droop used in tests.

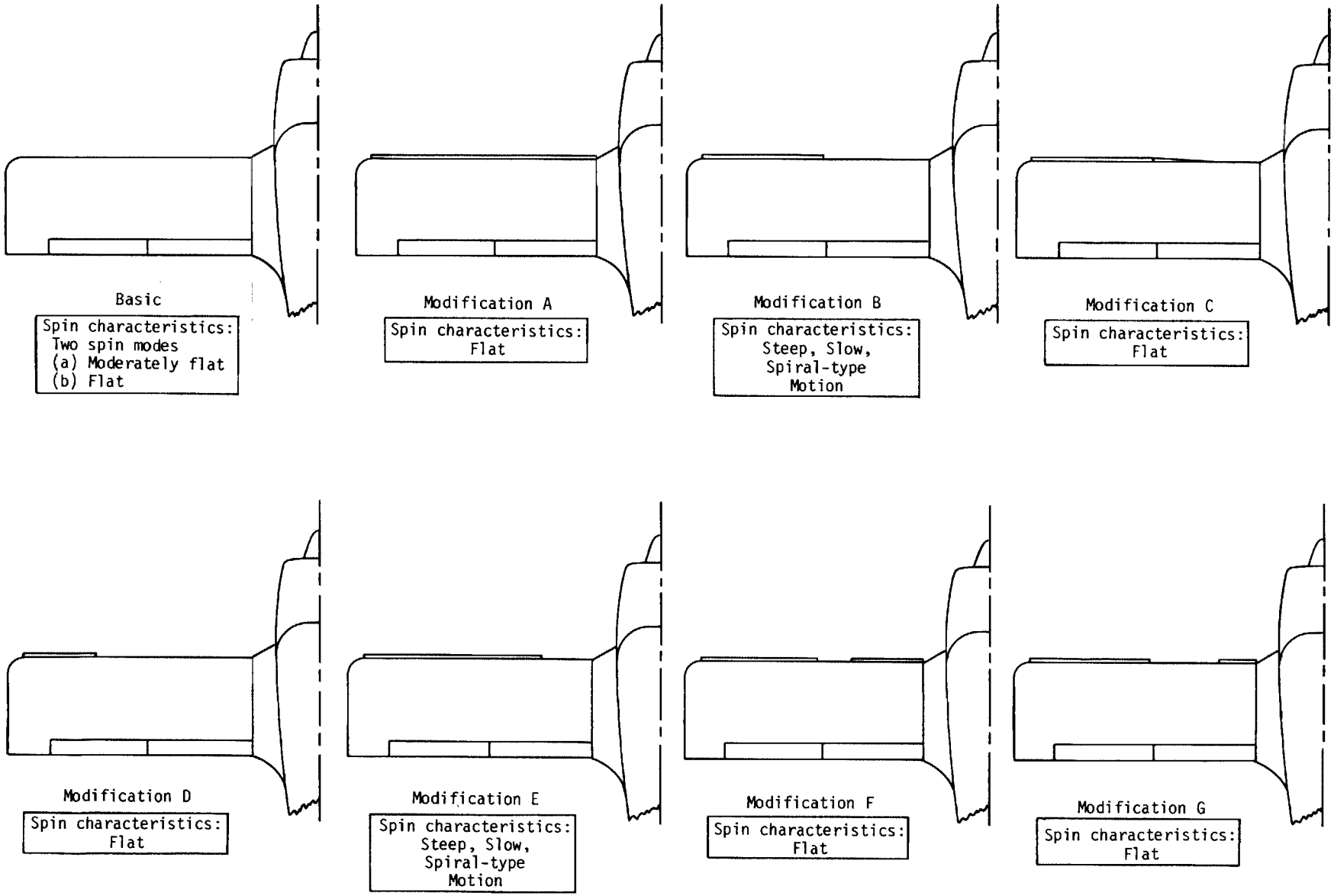

Figure 13.- Spin characteristics of wing configurations investigated in flight and force-test studies.

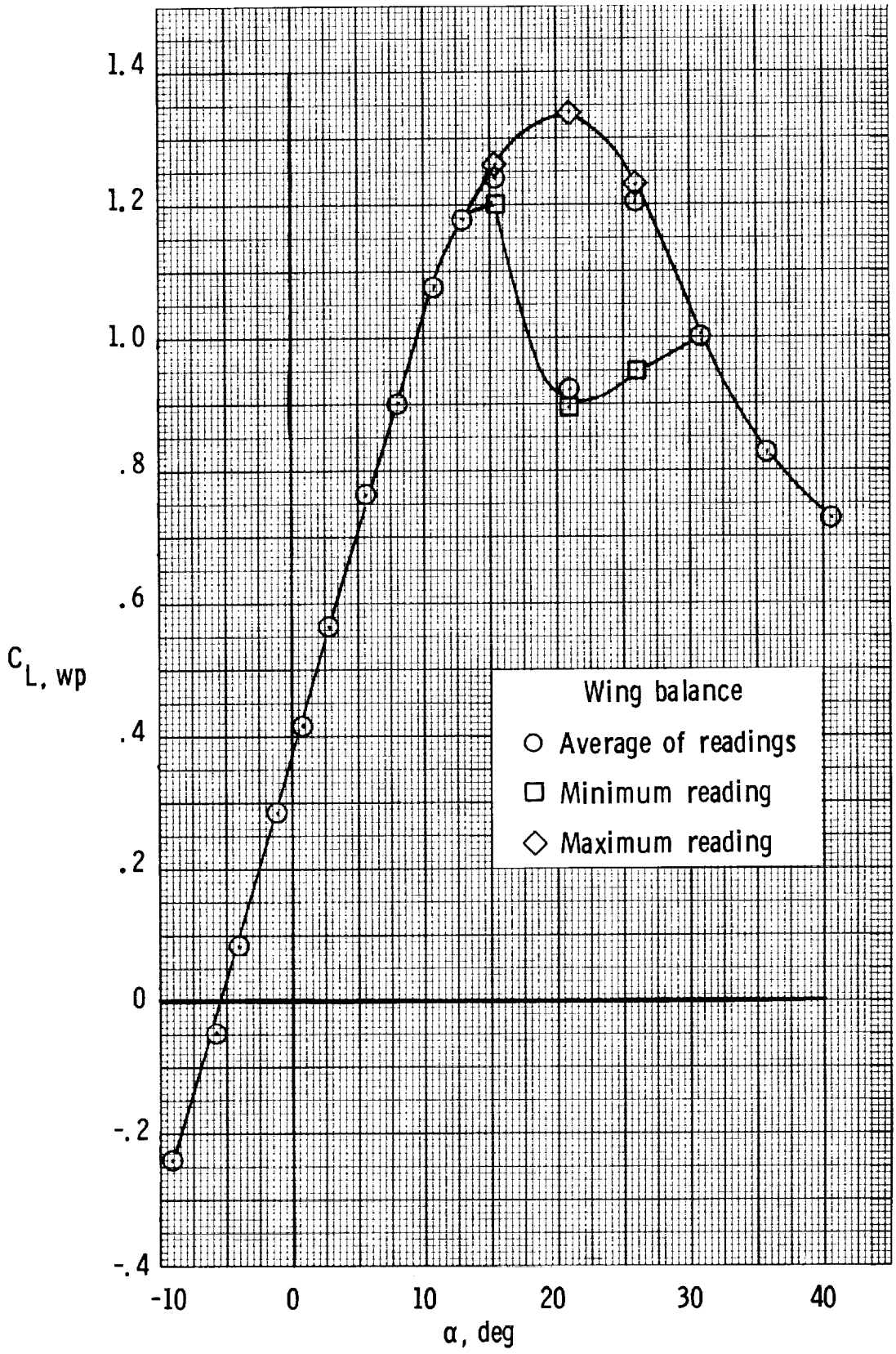

Figure 14.- Lift coefficient on outboard wing panel showing fluctuations in data at high angles of attack.

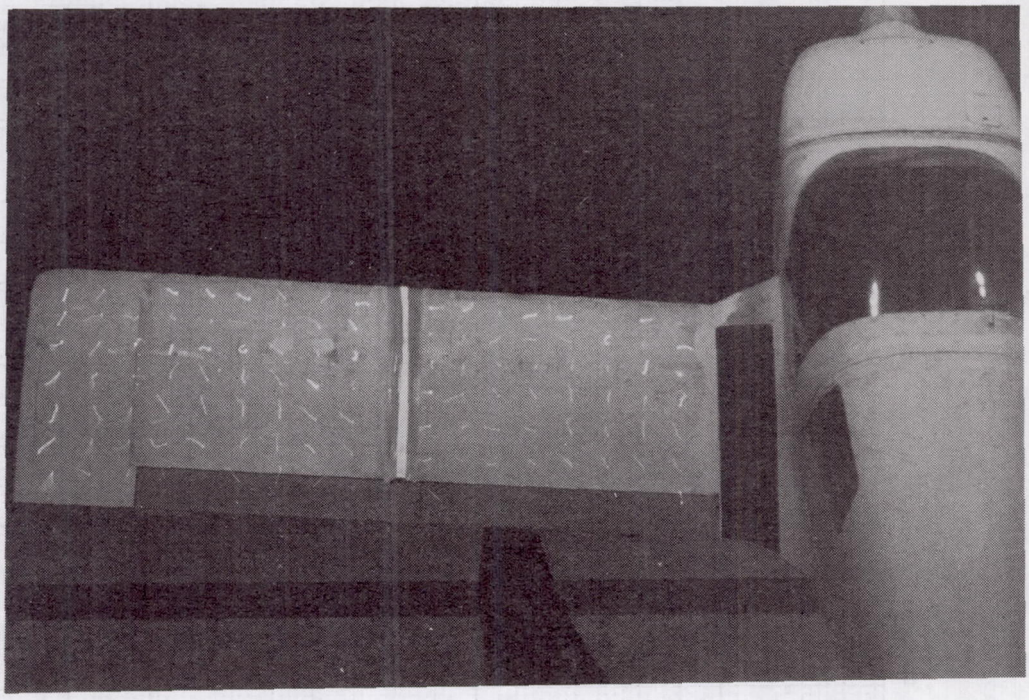

α = 20°, low lift

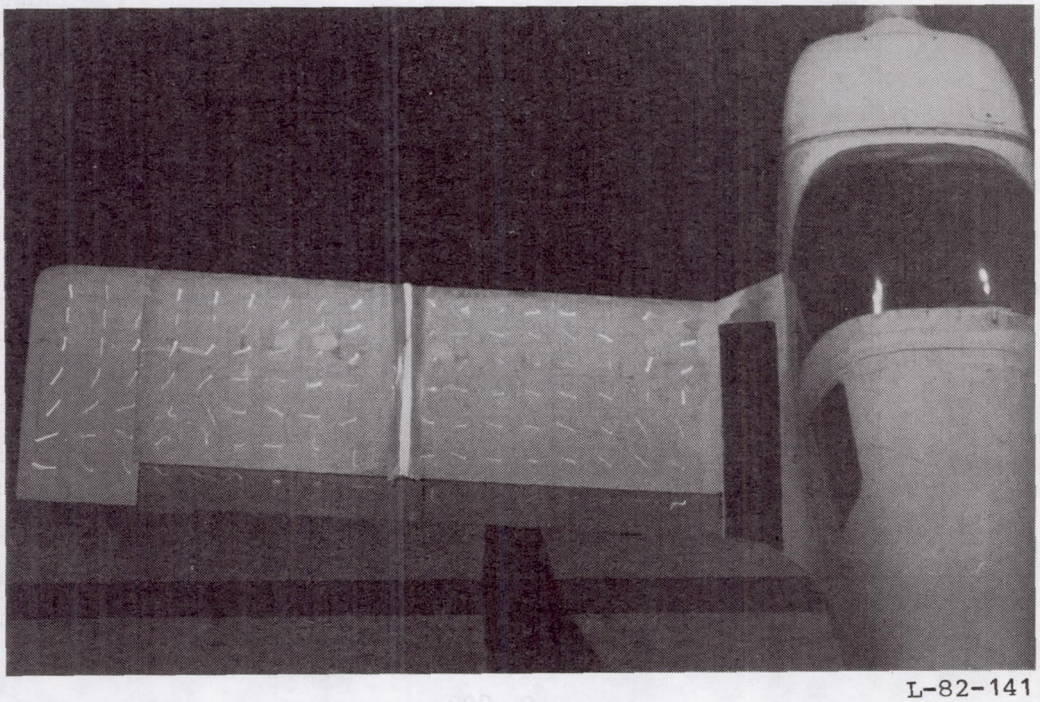

L-82-141

α = 20°, high lift

Figure 15.- Tuft surveys showing fluctuations in stall pattern on full-scale model with basic wing.

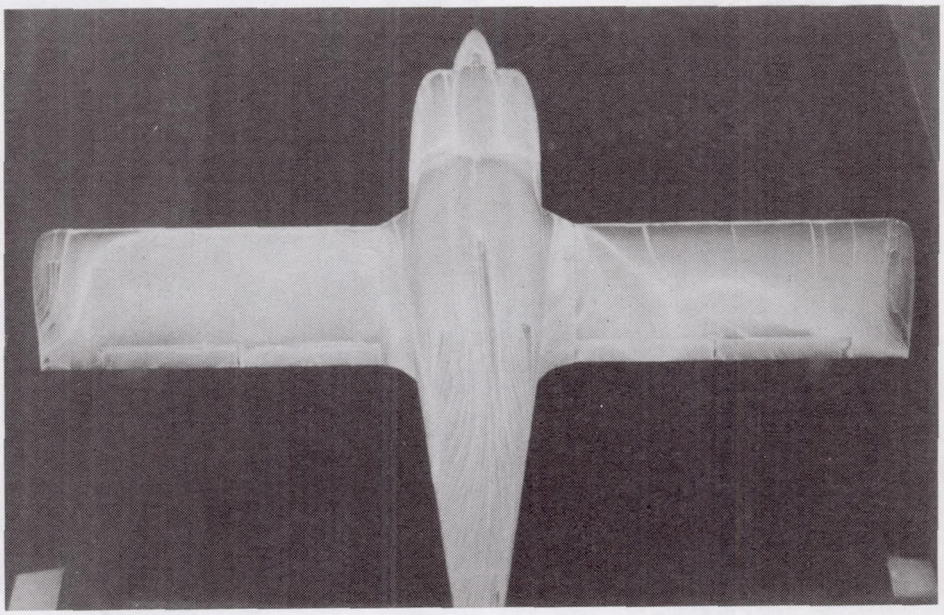

α = 14°

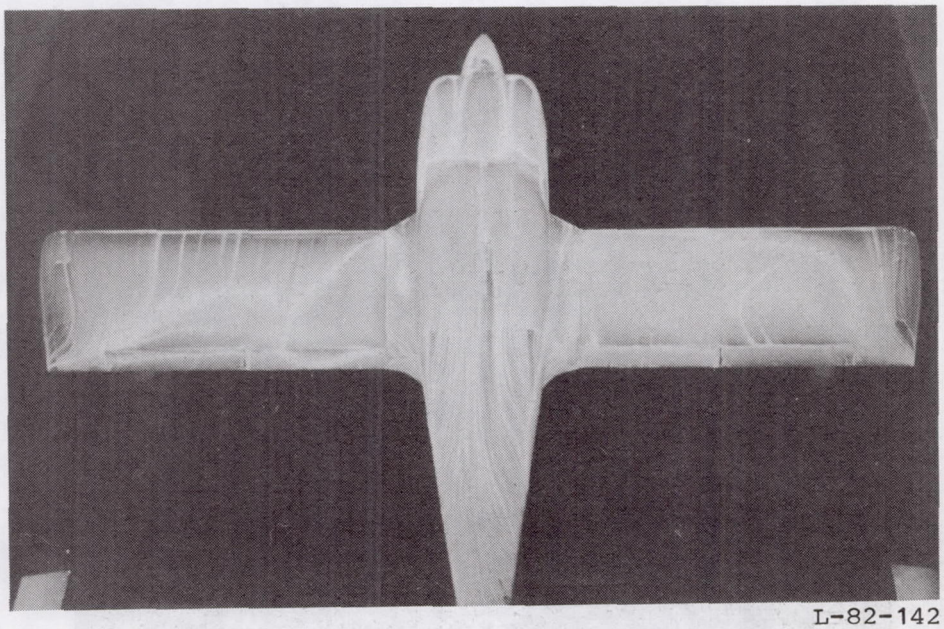

L-82-142

α = 14°

Figure 16.- Oil-flow surveys of 1/3-scale model with basic wing showing fluctuations in wing stall pattern.

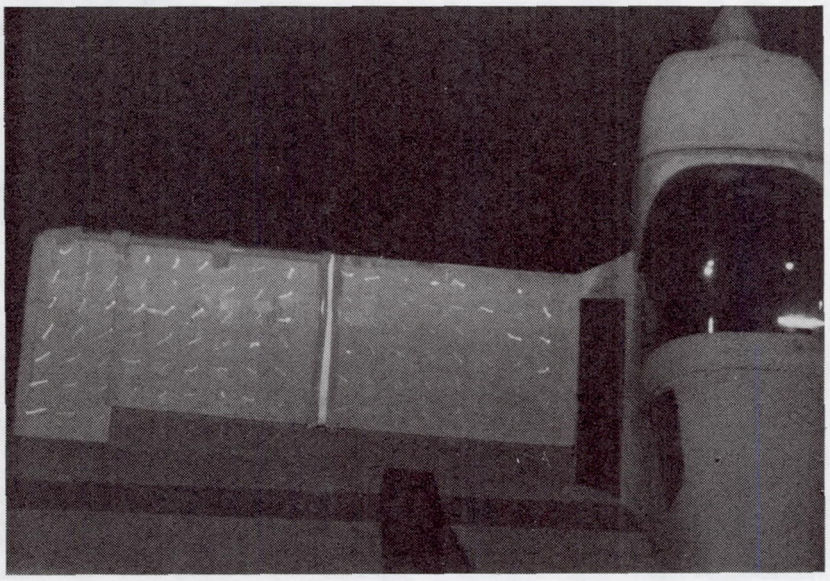

α = 30°

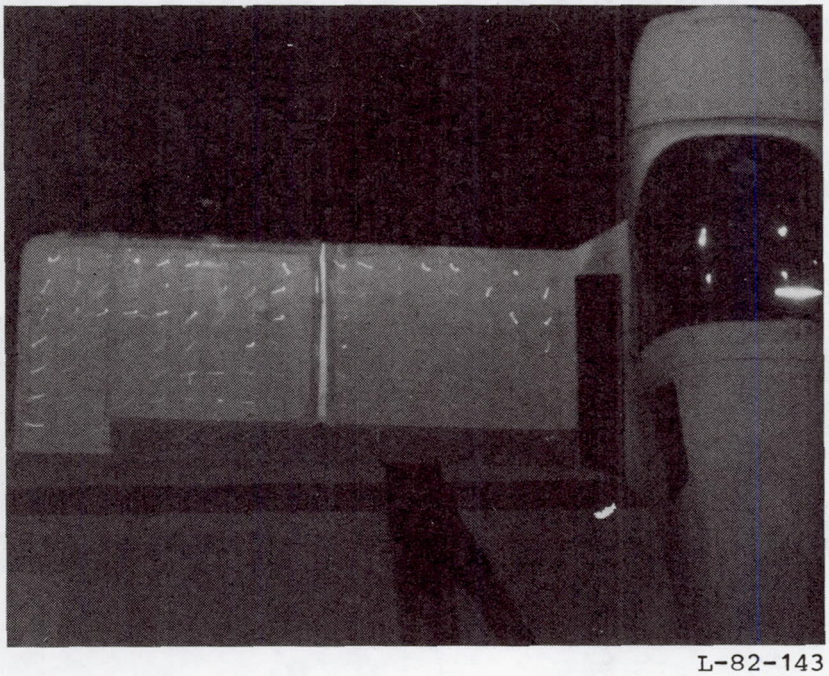

L-82-143

α = 35°

Figure 17.- Tuft surveys made on full-scale model with wing modification B.

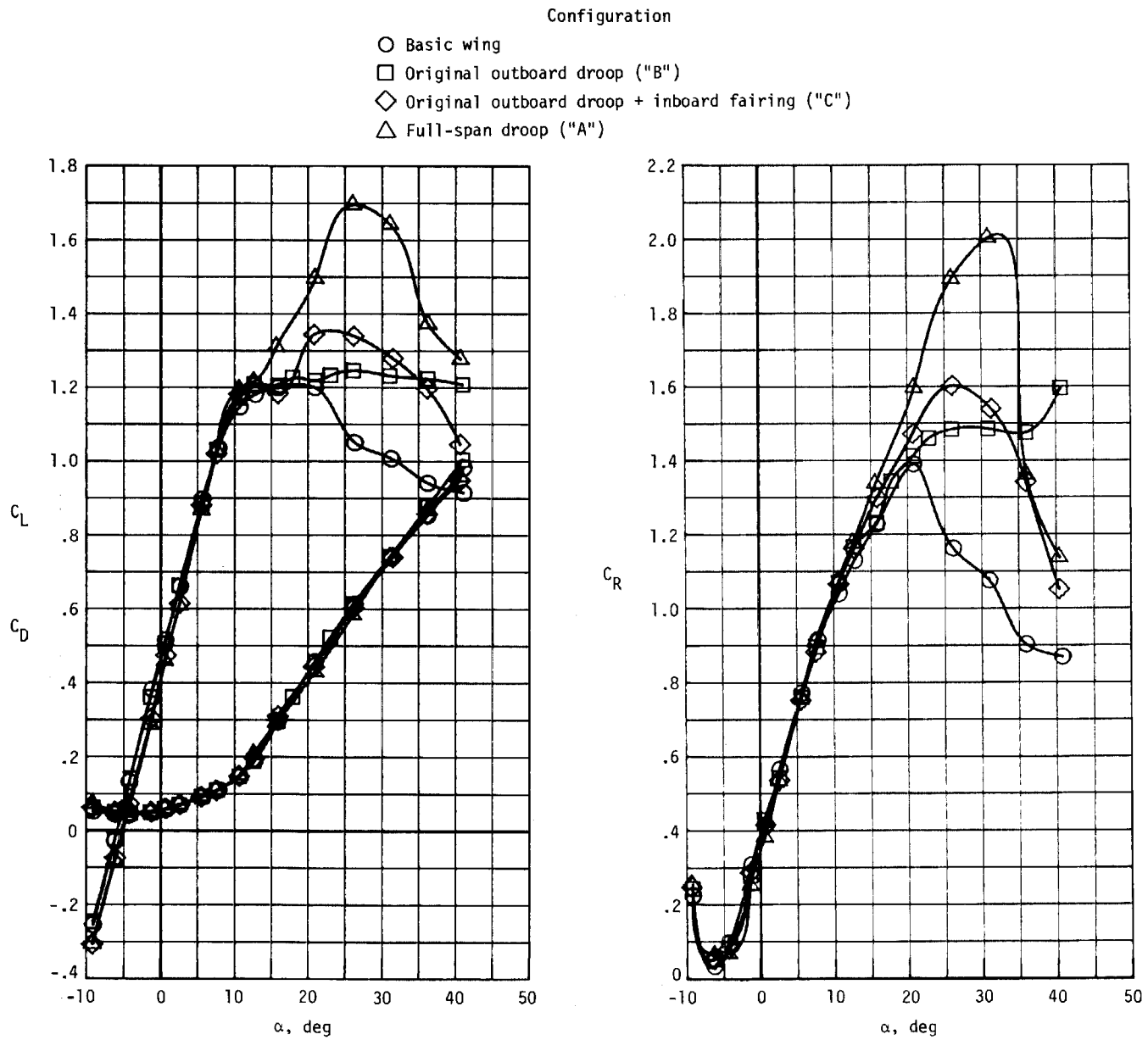

Figure 18.- Longitudinal aerodynamic characteristics of airplane with several wing leading-edge-droop modifications. Tails off.

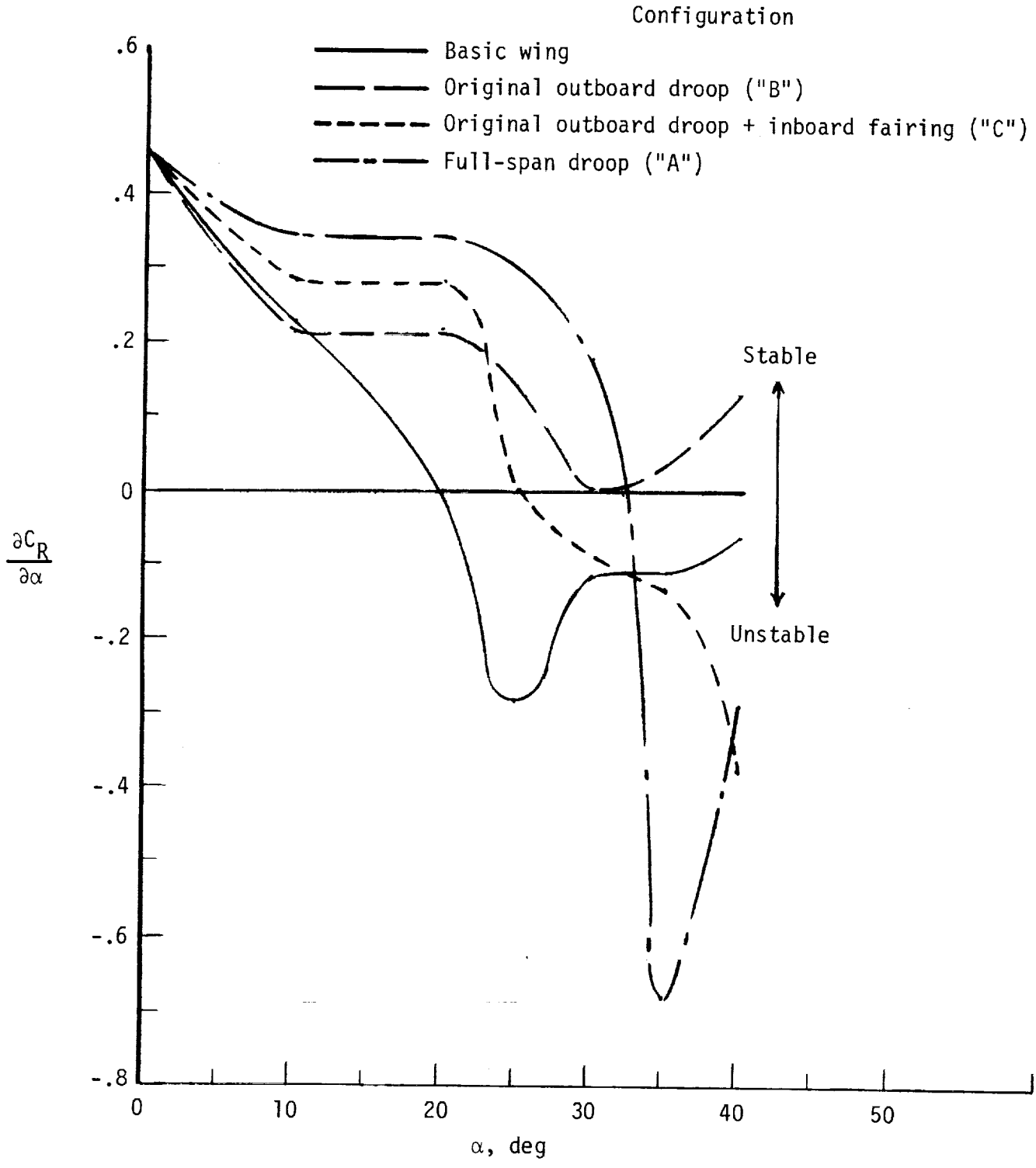

Figure 19.- Effect of leading-edge-droop modifications on autorotational characteristics of airplane.

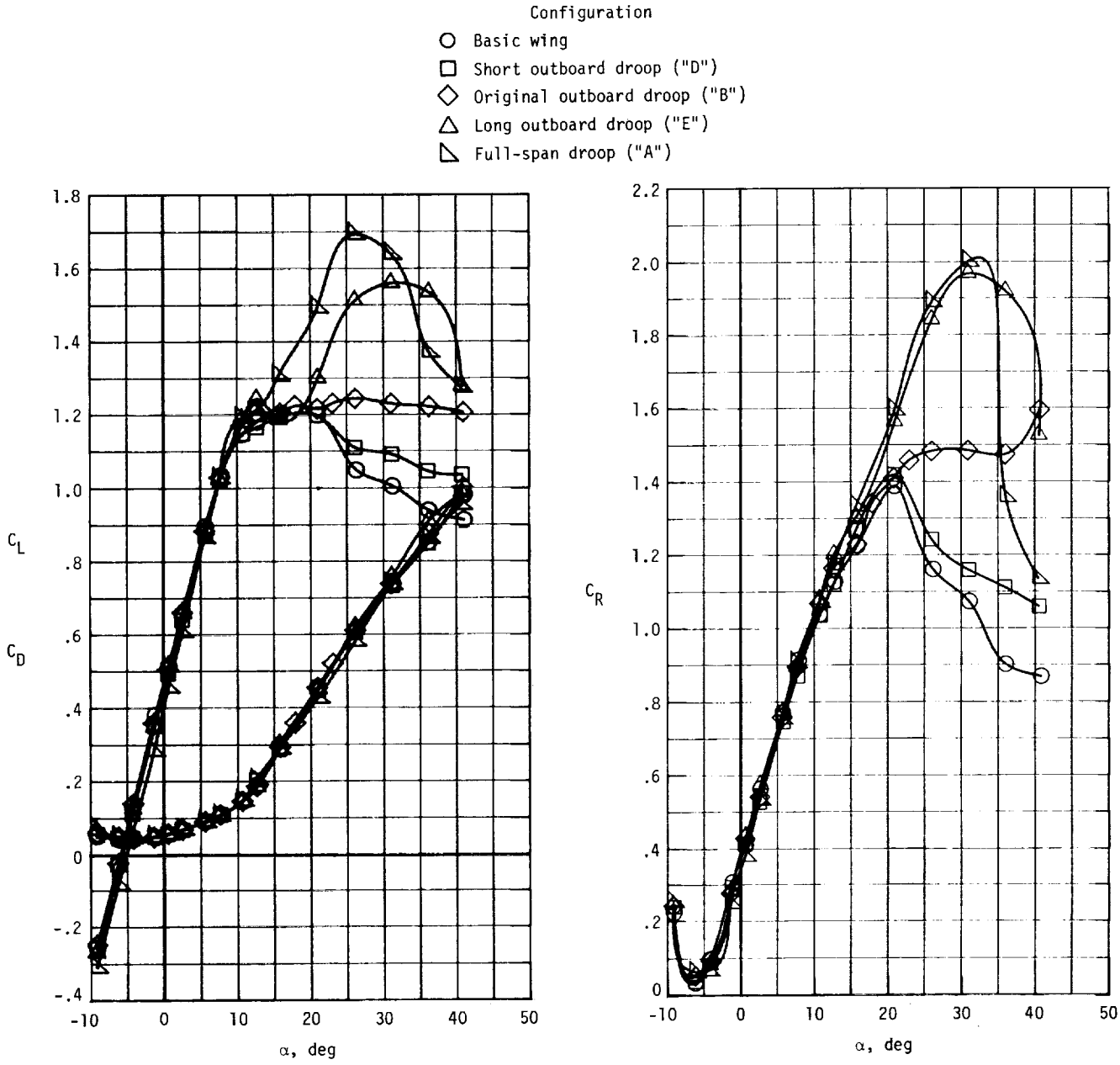

Figure 20.- Effect of variation in length of leading-edge droop on longitudinal aerodynamic characteristics of airplane. Tails off.

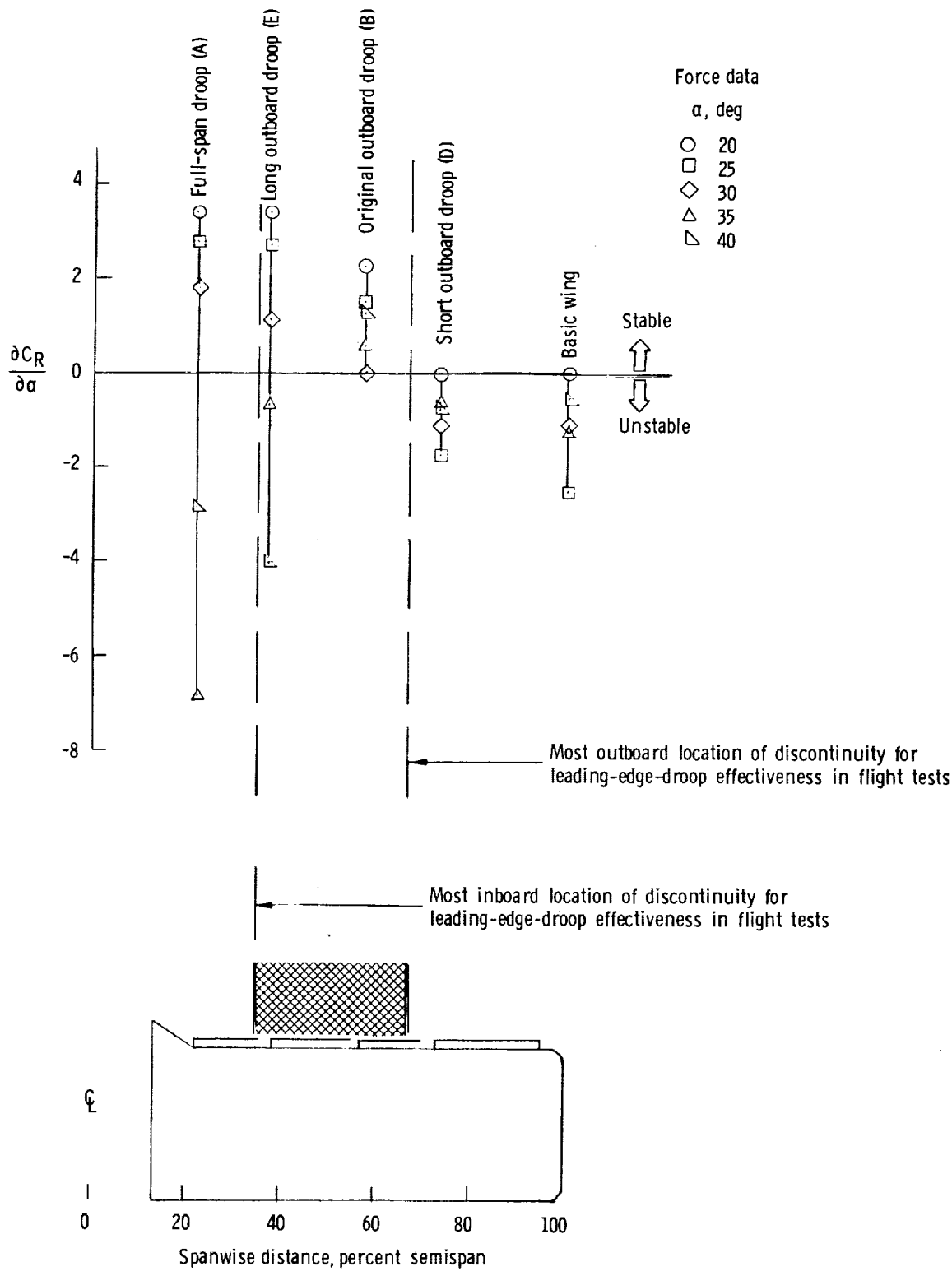

Figure 21.- Variation of autorotational stability provided by leading-edge droop as function of spanwise location of droop inboard discontinuity.

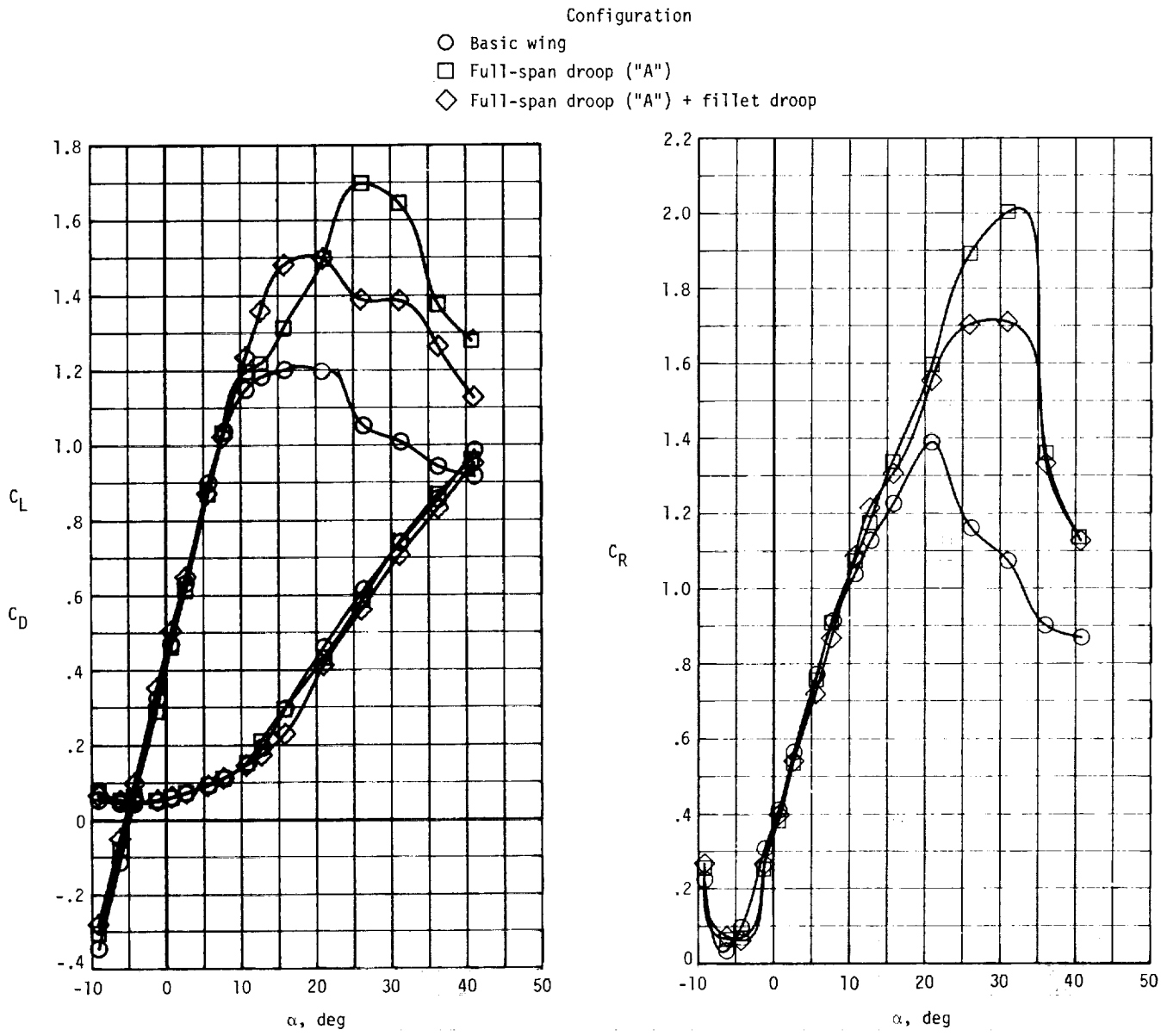

(a) Modification A.

Figure 22.- Effect of wing/fillet droop fairing on characteristics of three leading-edge configurations.

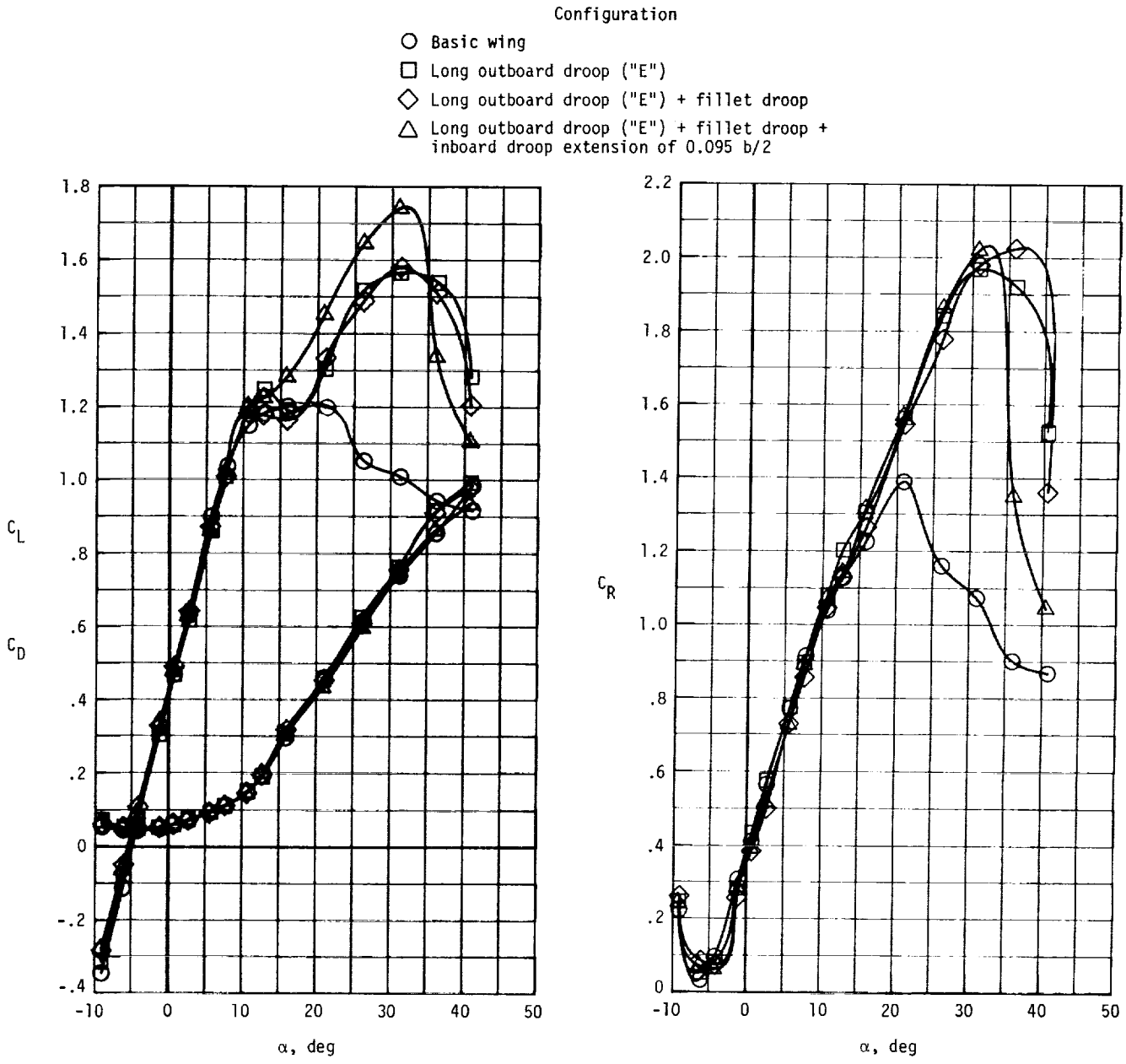

(b) Modification E.

Figure 22.- Continued.

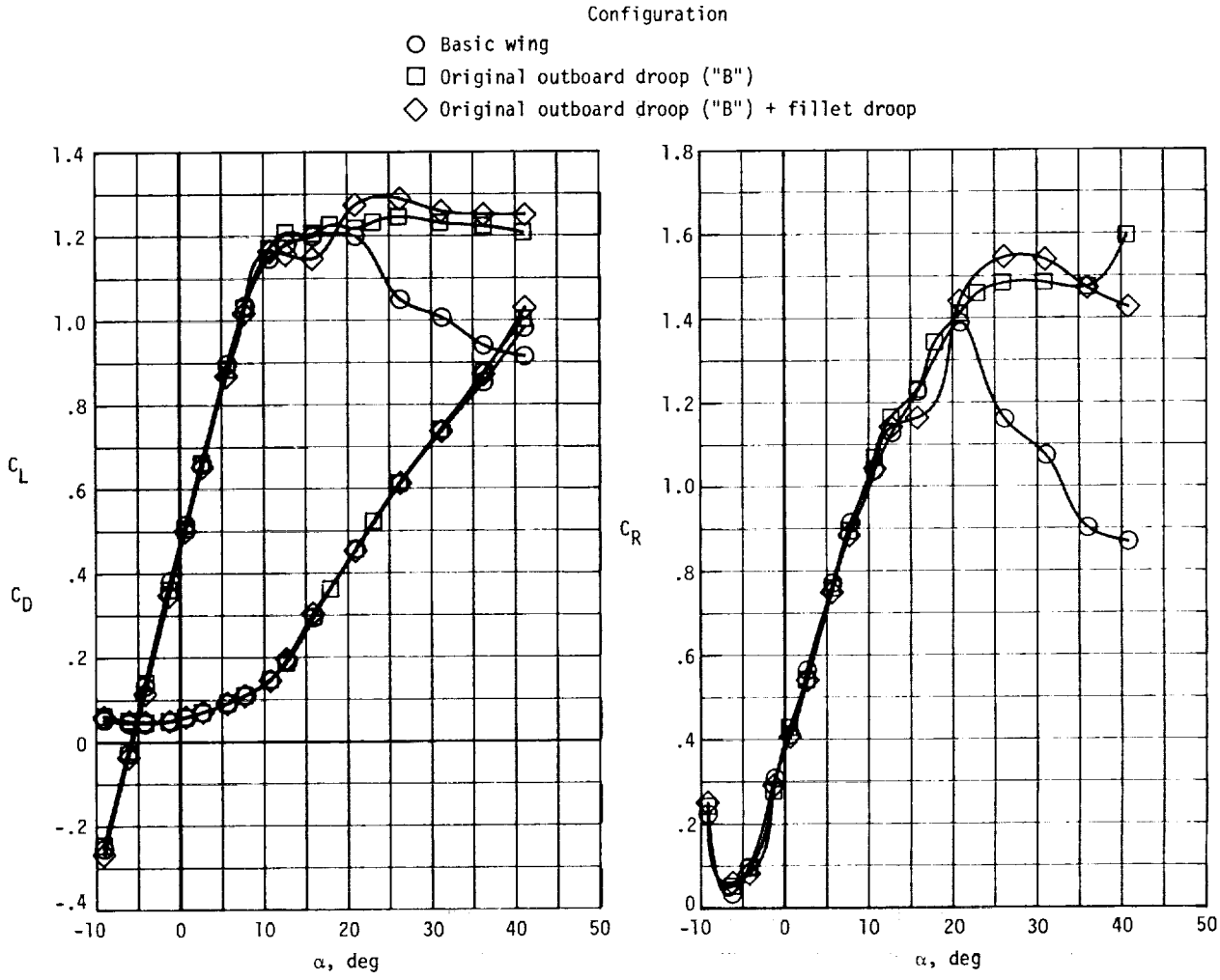

(c) Modification B.

Figure 22.- Concluded.

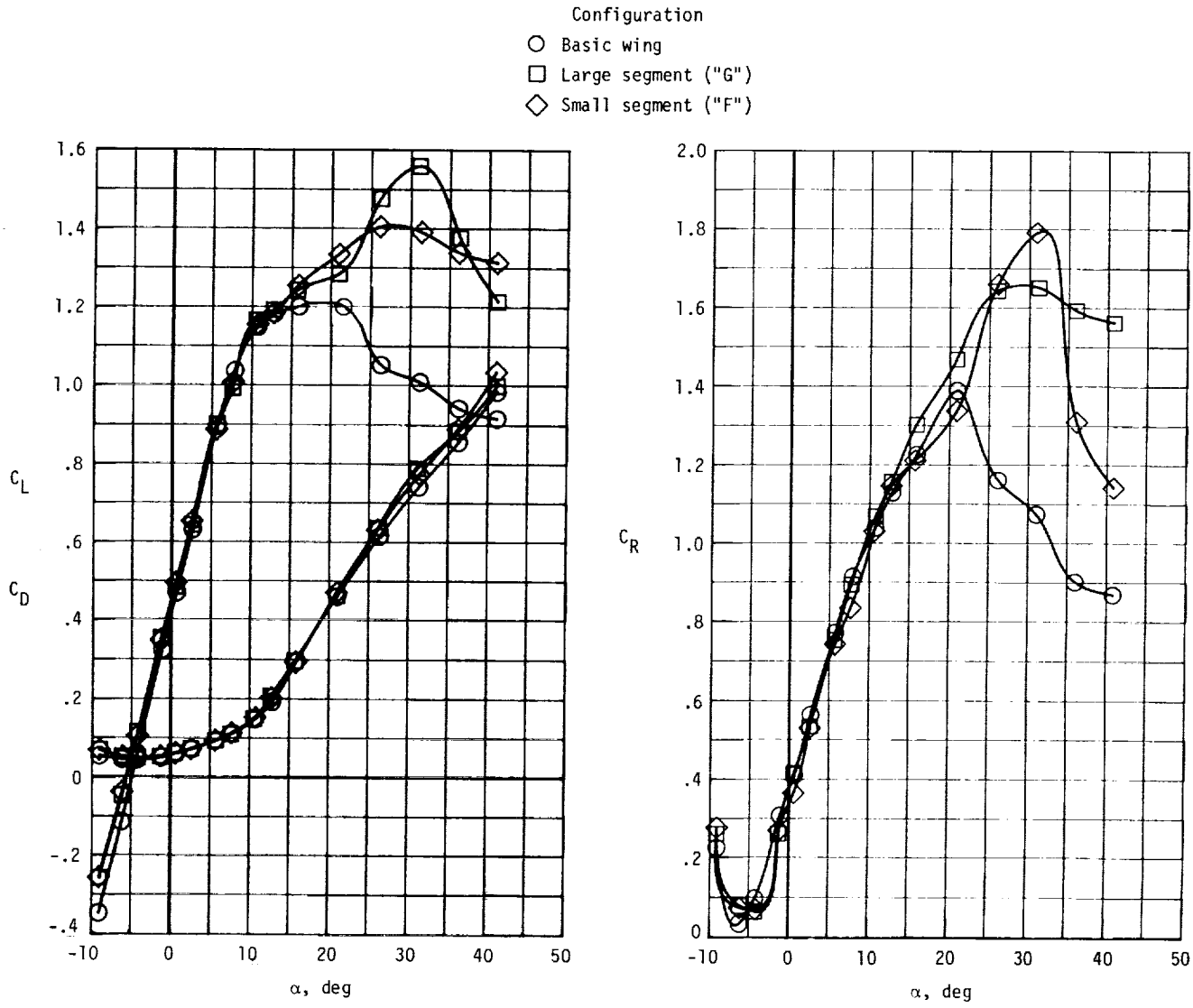

Figure 23.- Effect of segmented leading-edge droop on longitudinal aerodynamic characteristics of airplane. Tails off.

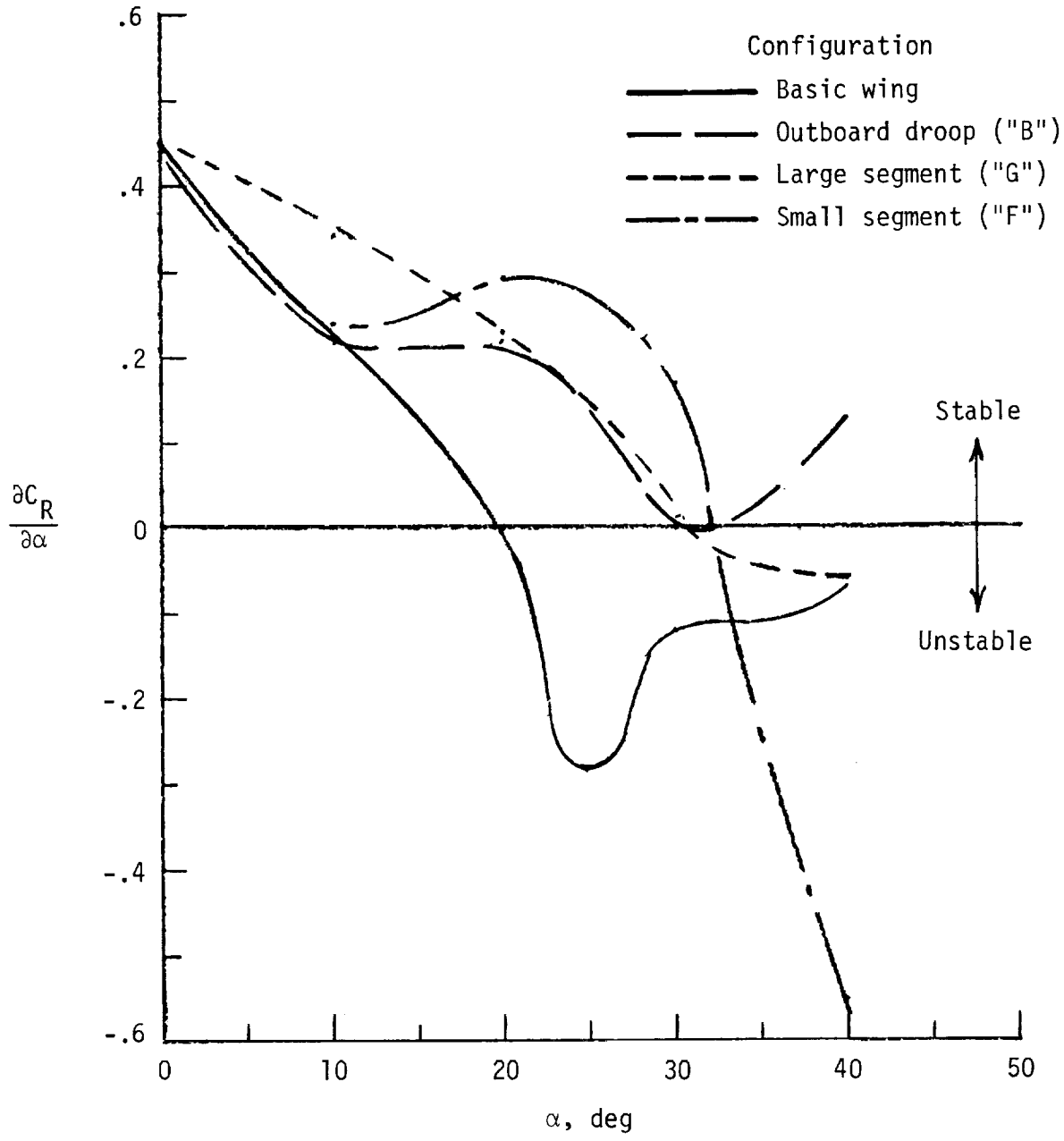

Figure 24.- Effect of segmented leading-edge droop on autorotational stability characteristics of airplane.

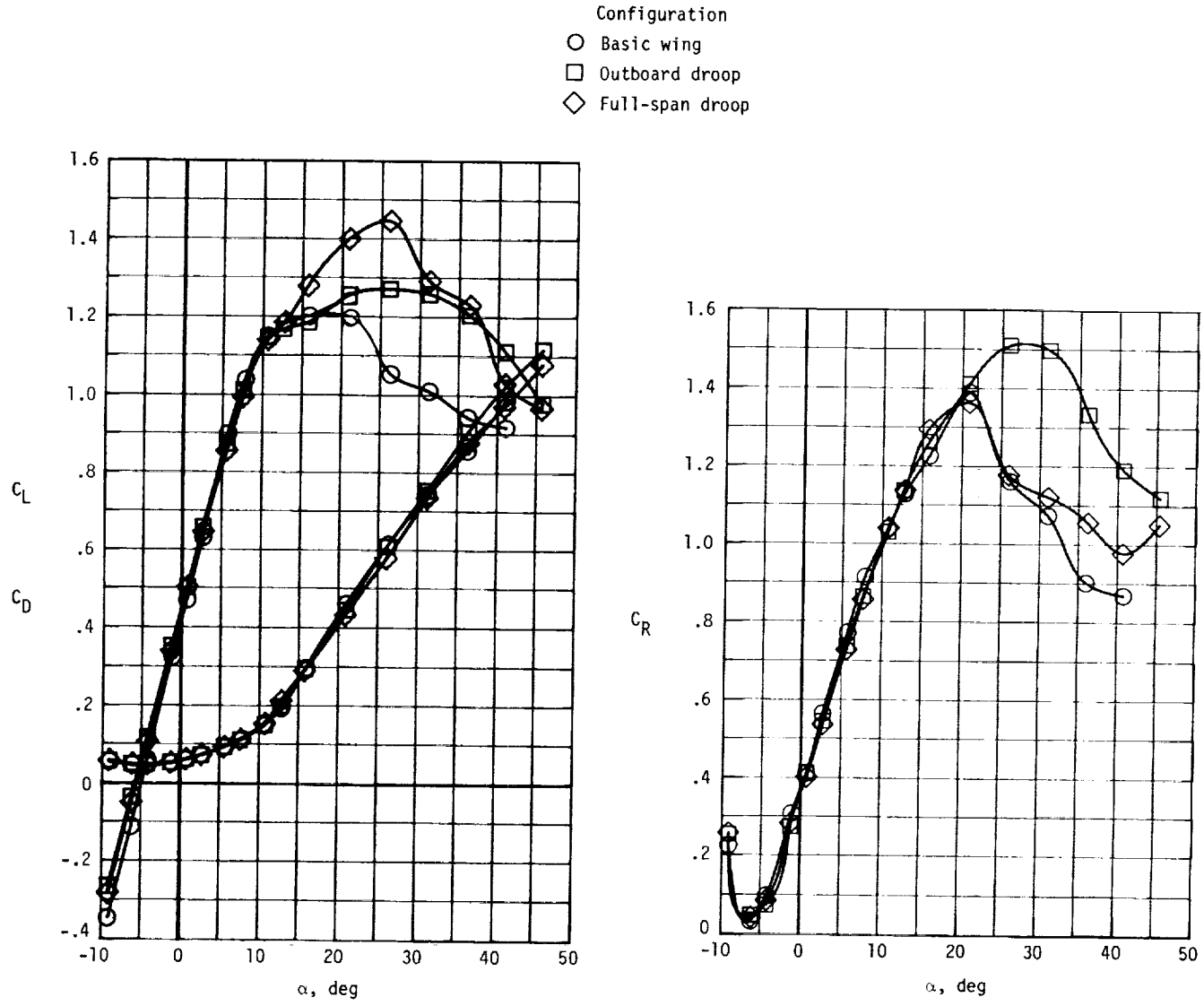

Figure 25.- Effect of LS(1)-0417 shape droop on longitudinal aerodynamic characteristics of airplane.

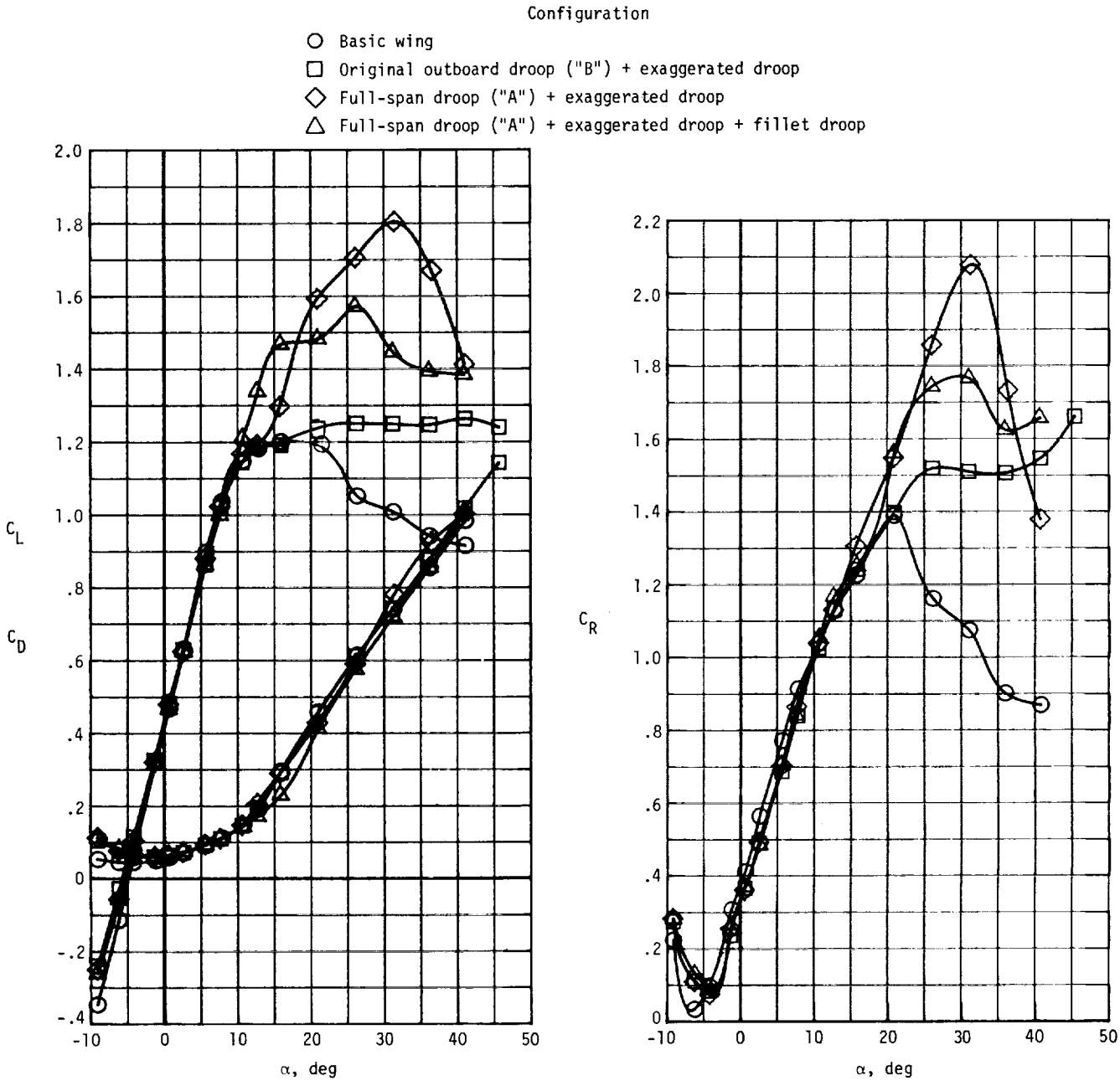

Figure 26.- Effect of exaggerated droop on leading edge of outboard wing panel.

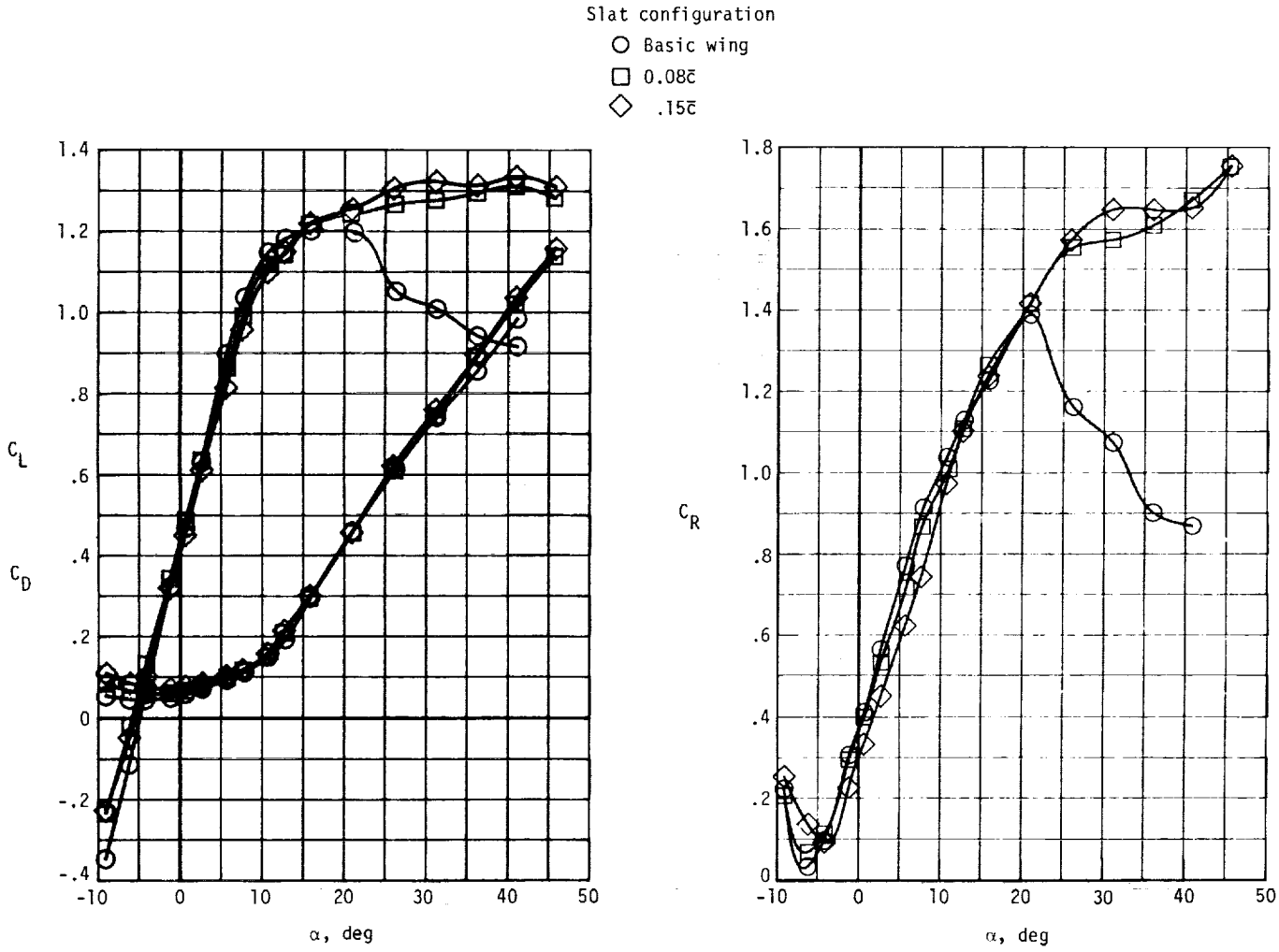

(a) Outboard slats.

Figure 27.- Effect of leading-edge slats on longitudinal aerodynamic characteristics of airplane. Tails off.

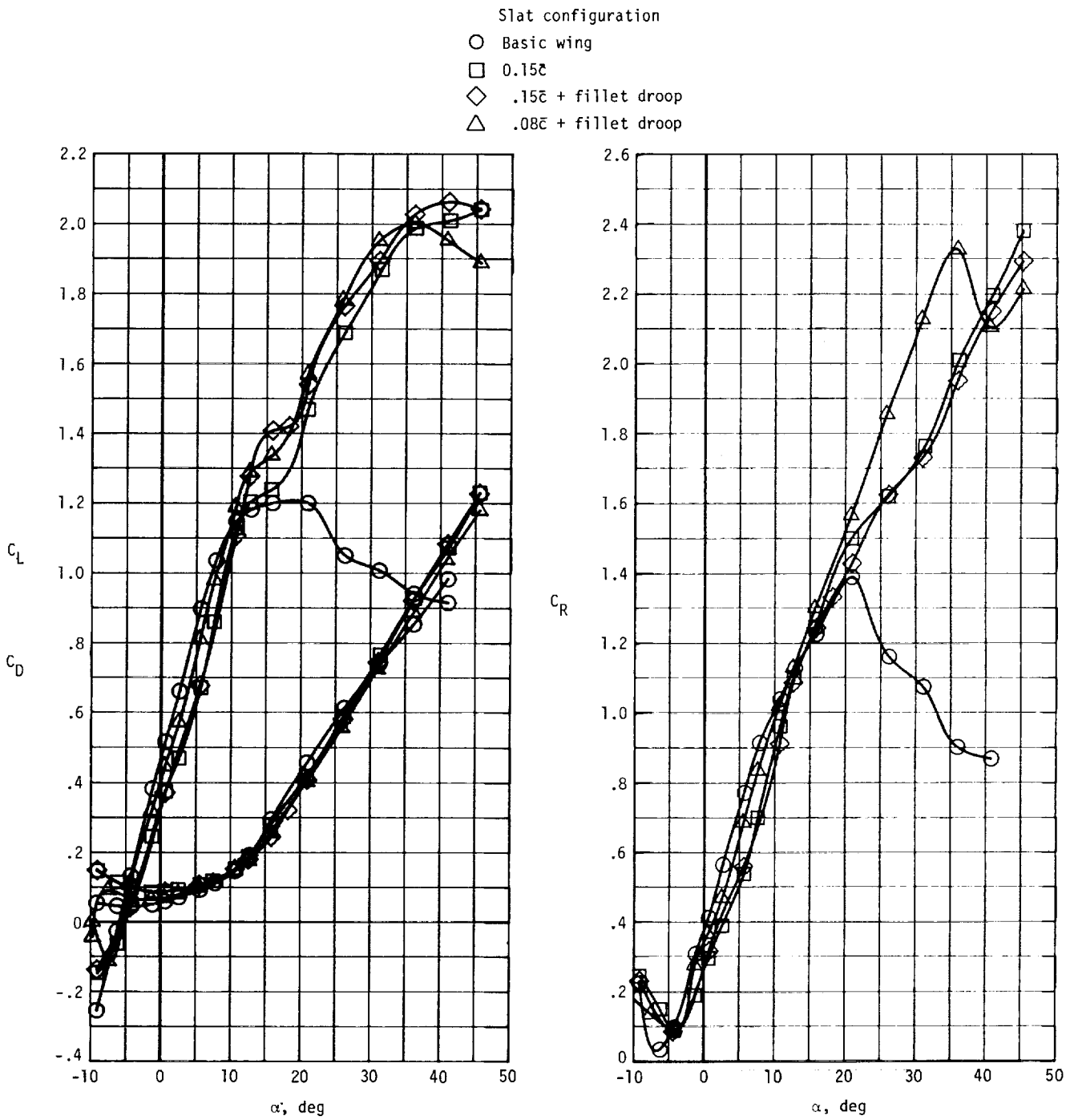

(b) Full-span slats.

Figure 27.- Concluded.

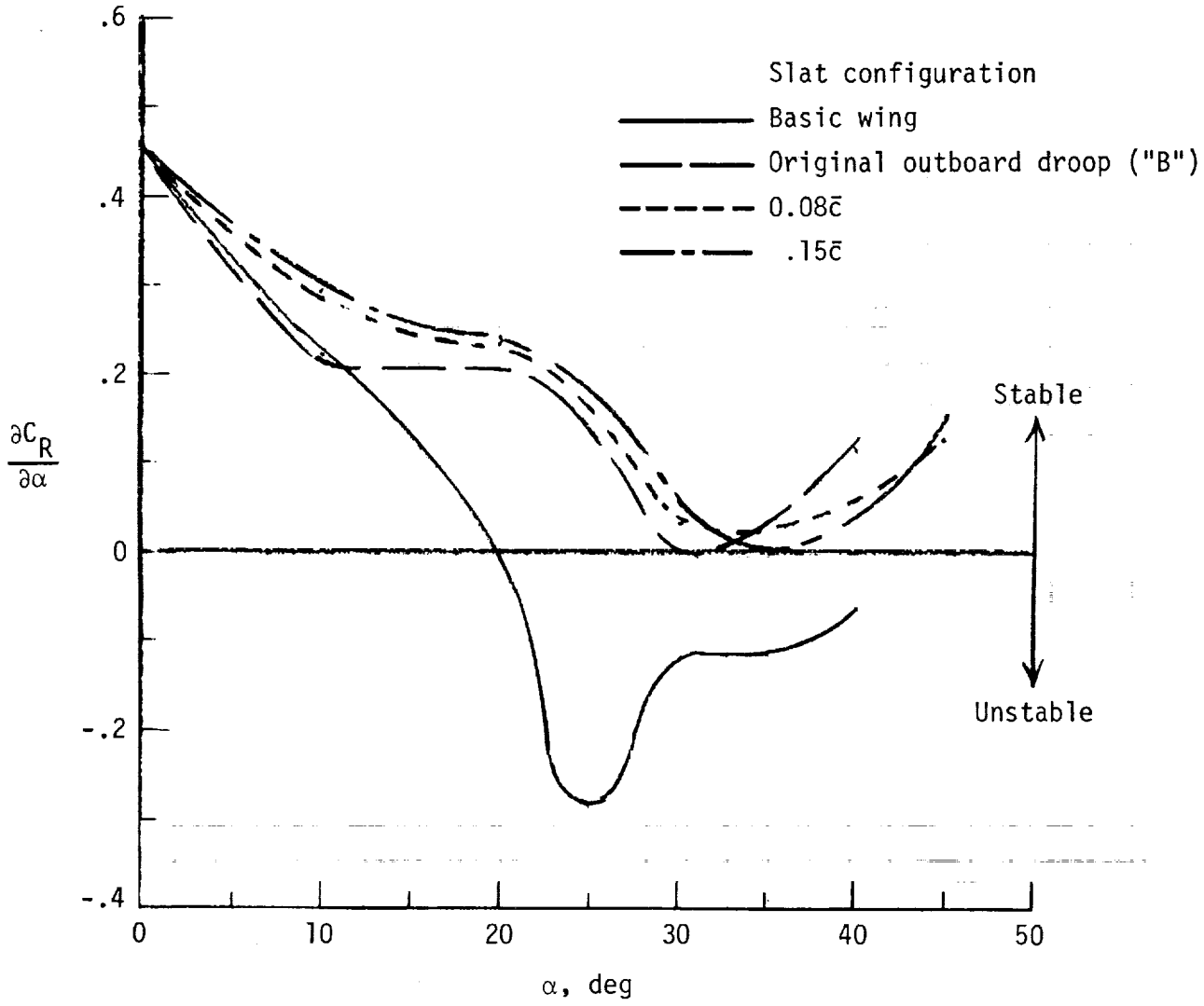

(a) Outboard slats.

Figure 28.- Effect of leading-edge slats on autorotational stability characteristics of airplane as compared to leading-edge-droop configuration.

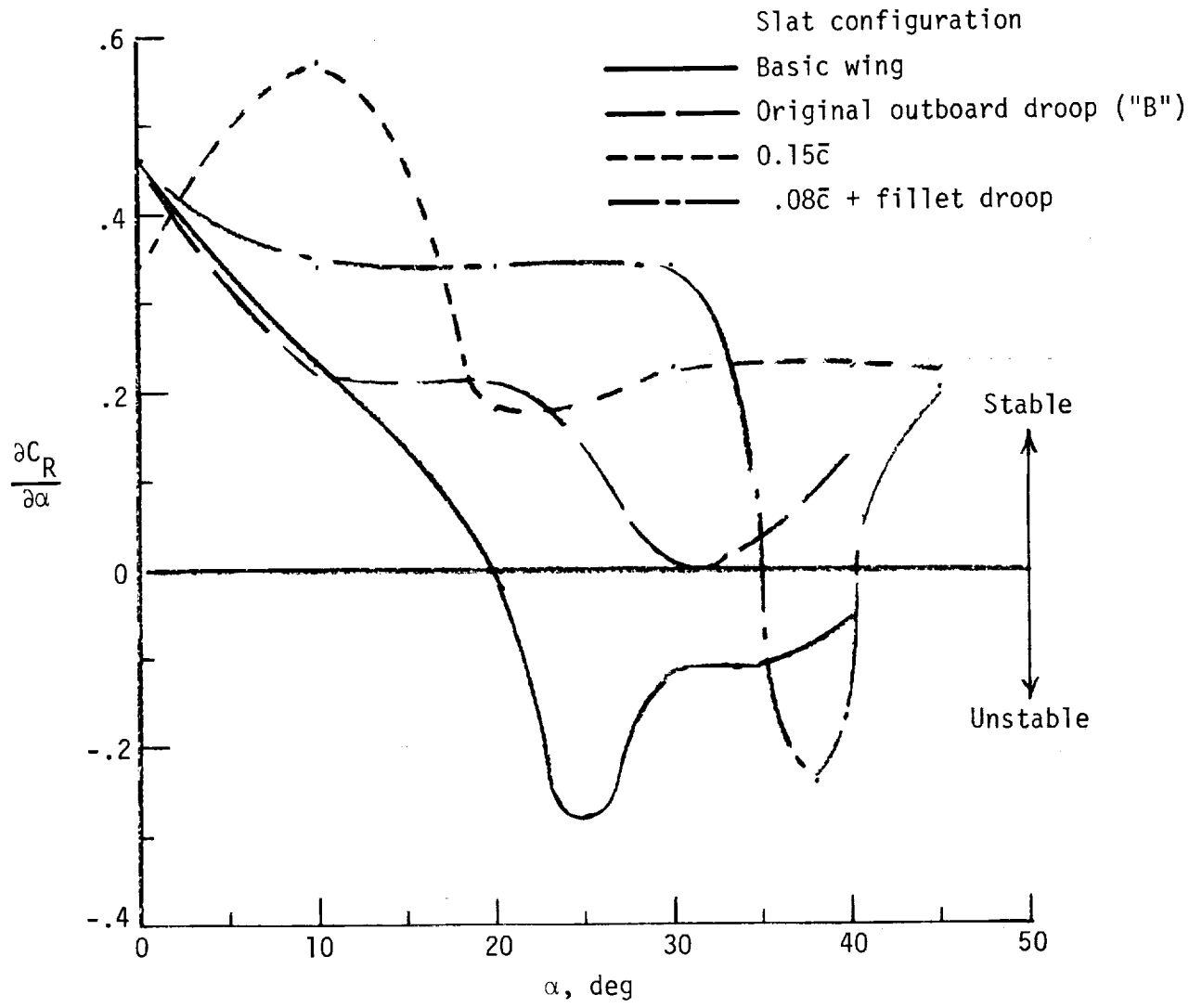

(b) Full-span slats.

Figure 28.- Concluded.

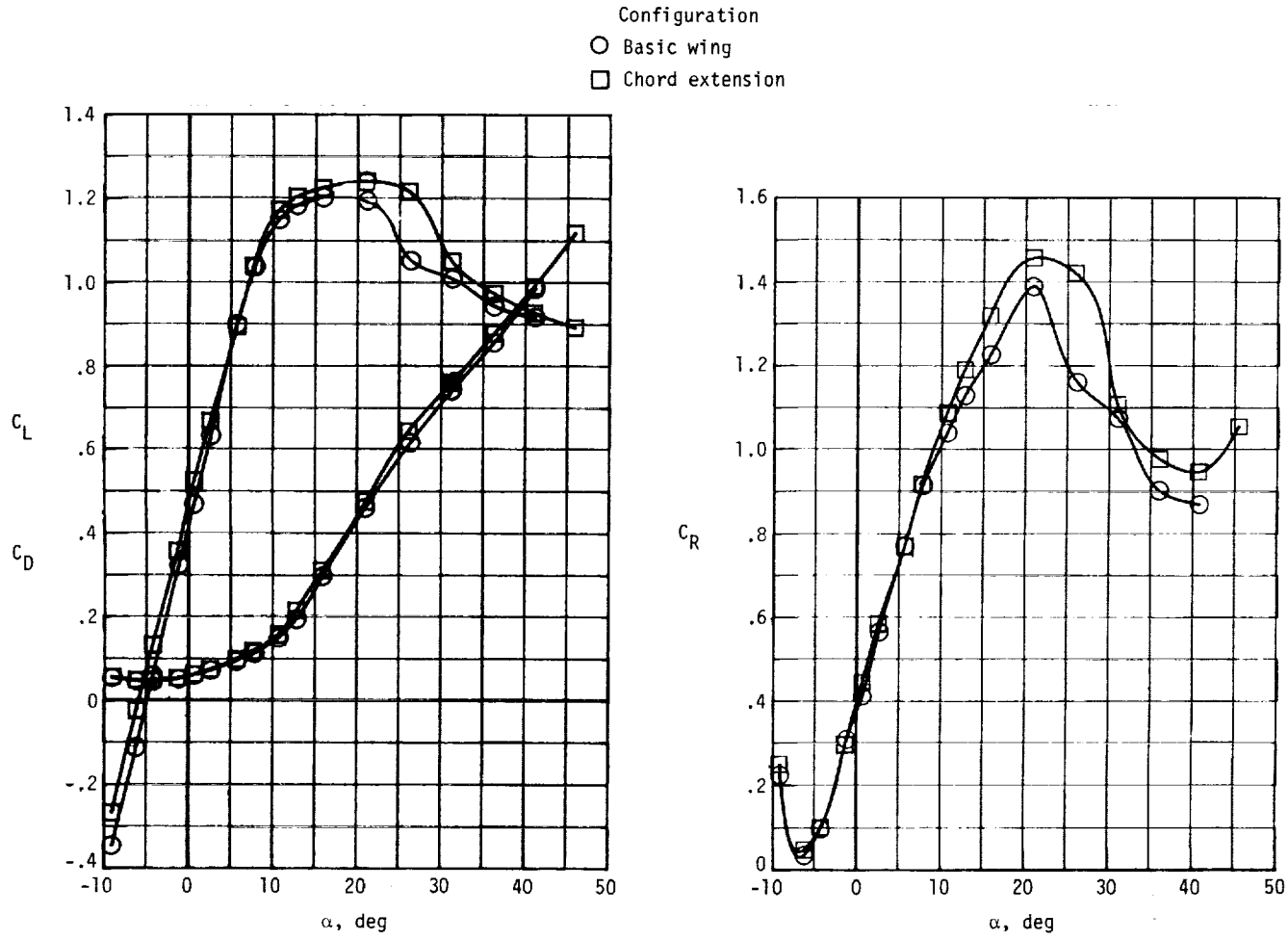

Figure 29.- Effect of extended outboard wing chord on longitudinal aerodynamic characteristics of airplane.

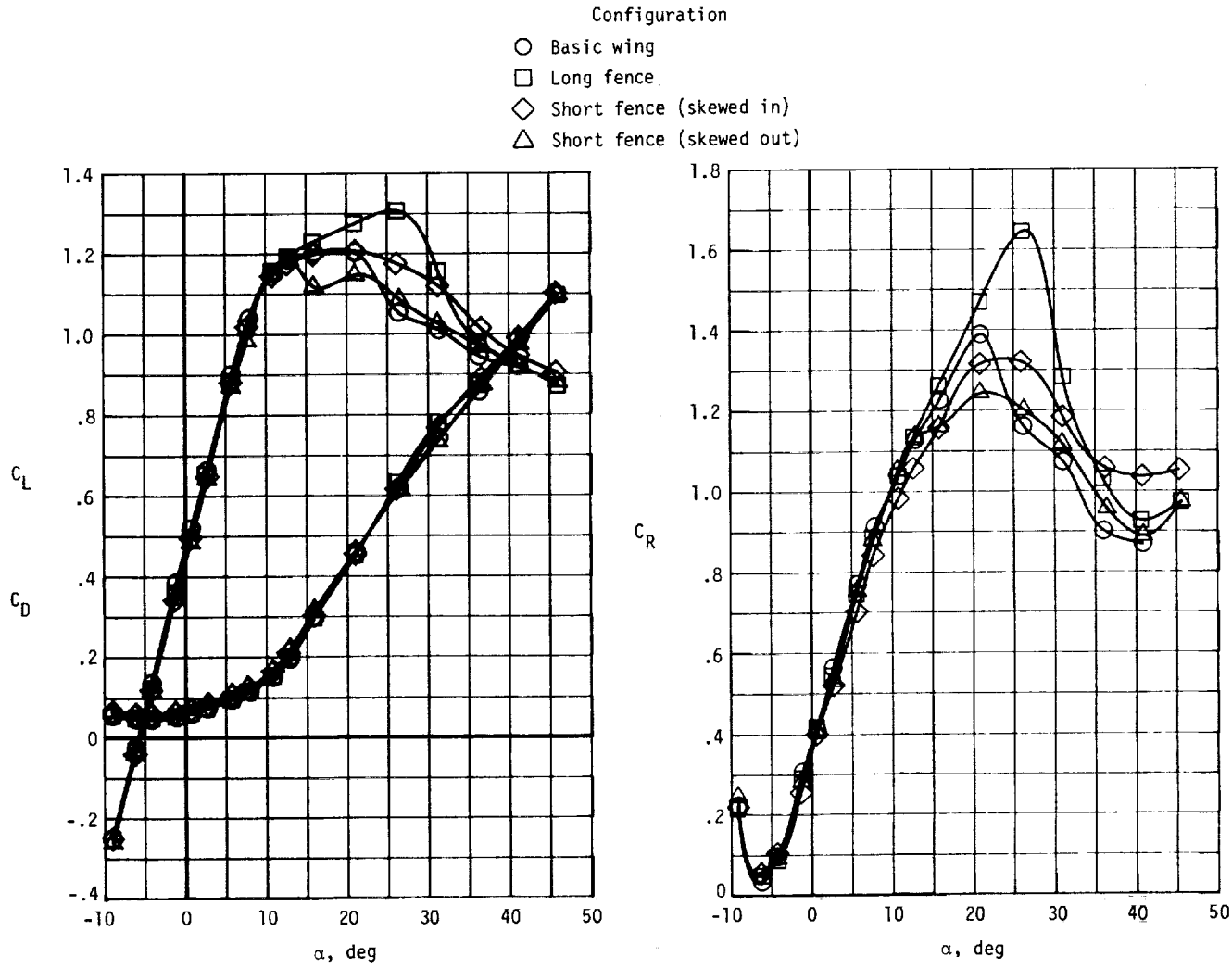

Figure 30.- Effect of wing fences on longitudinal aerodynamic characteristics of airplane.

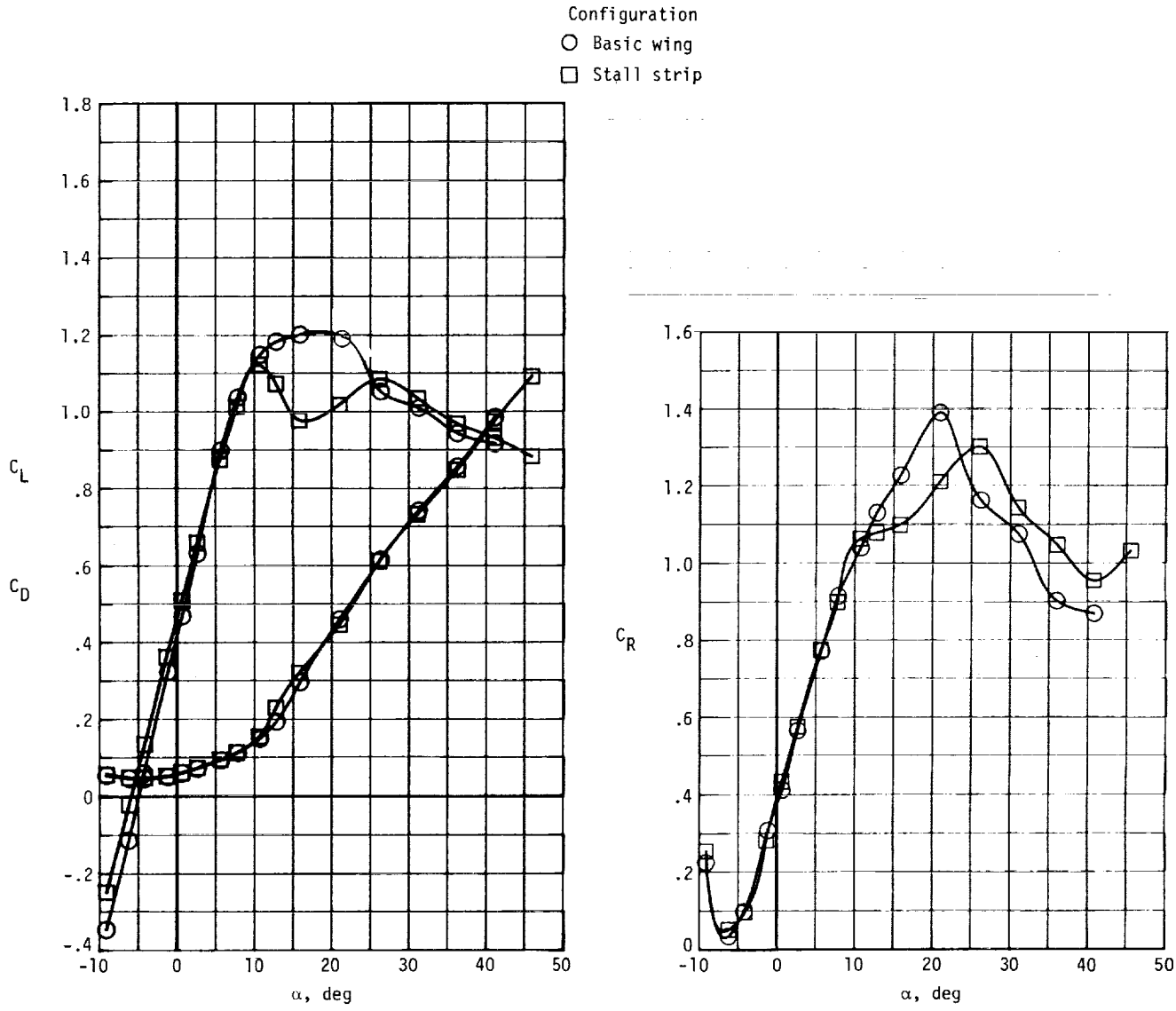

(a) Basic wing.

Figure 31.- Effect of $0.005\bar{c}$ stall strips on longitudinal aerodynamic characteristics of airplane.

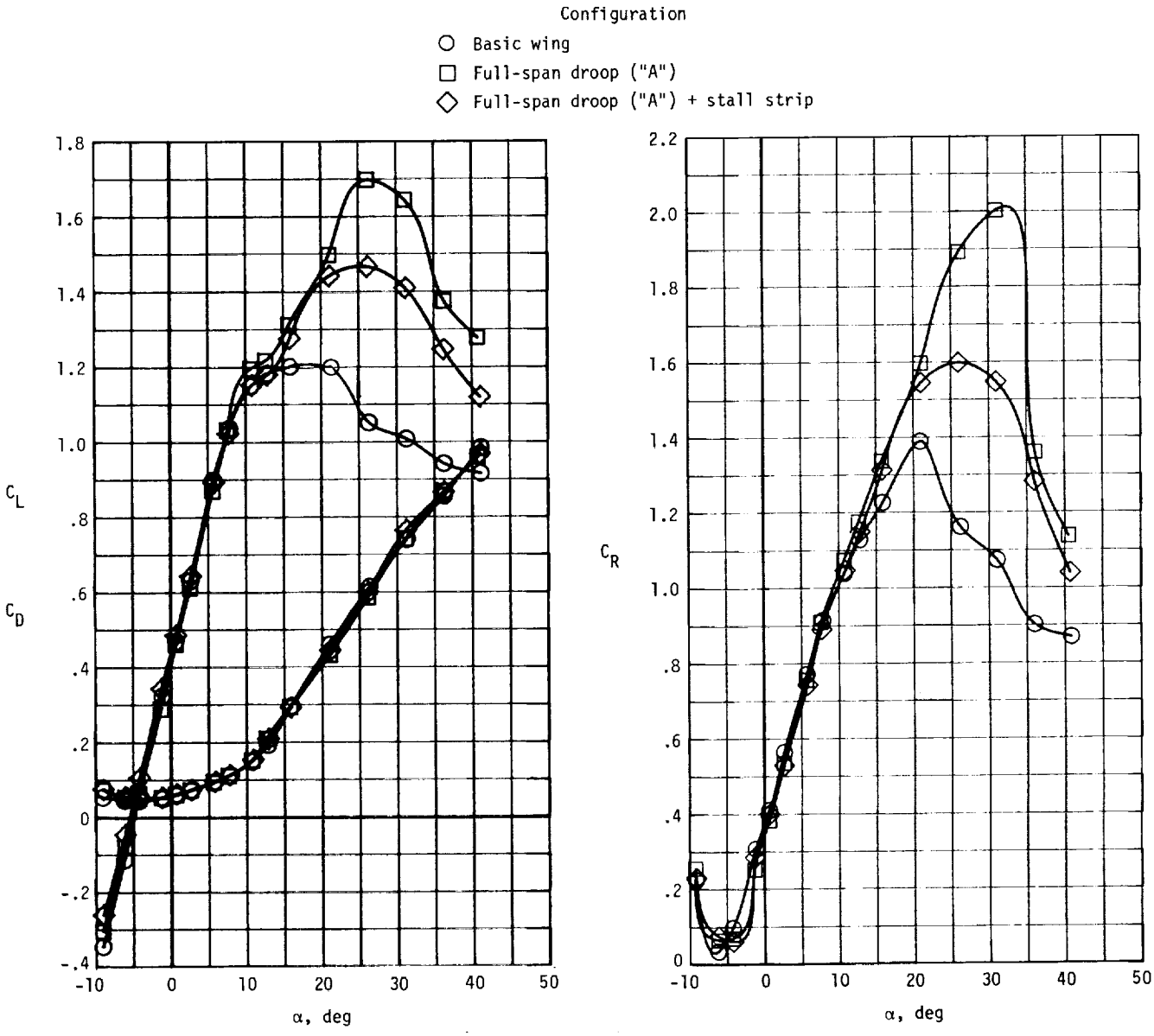

(b) Full-span droop ("A").

Figure 31.- Concluded.

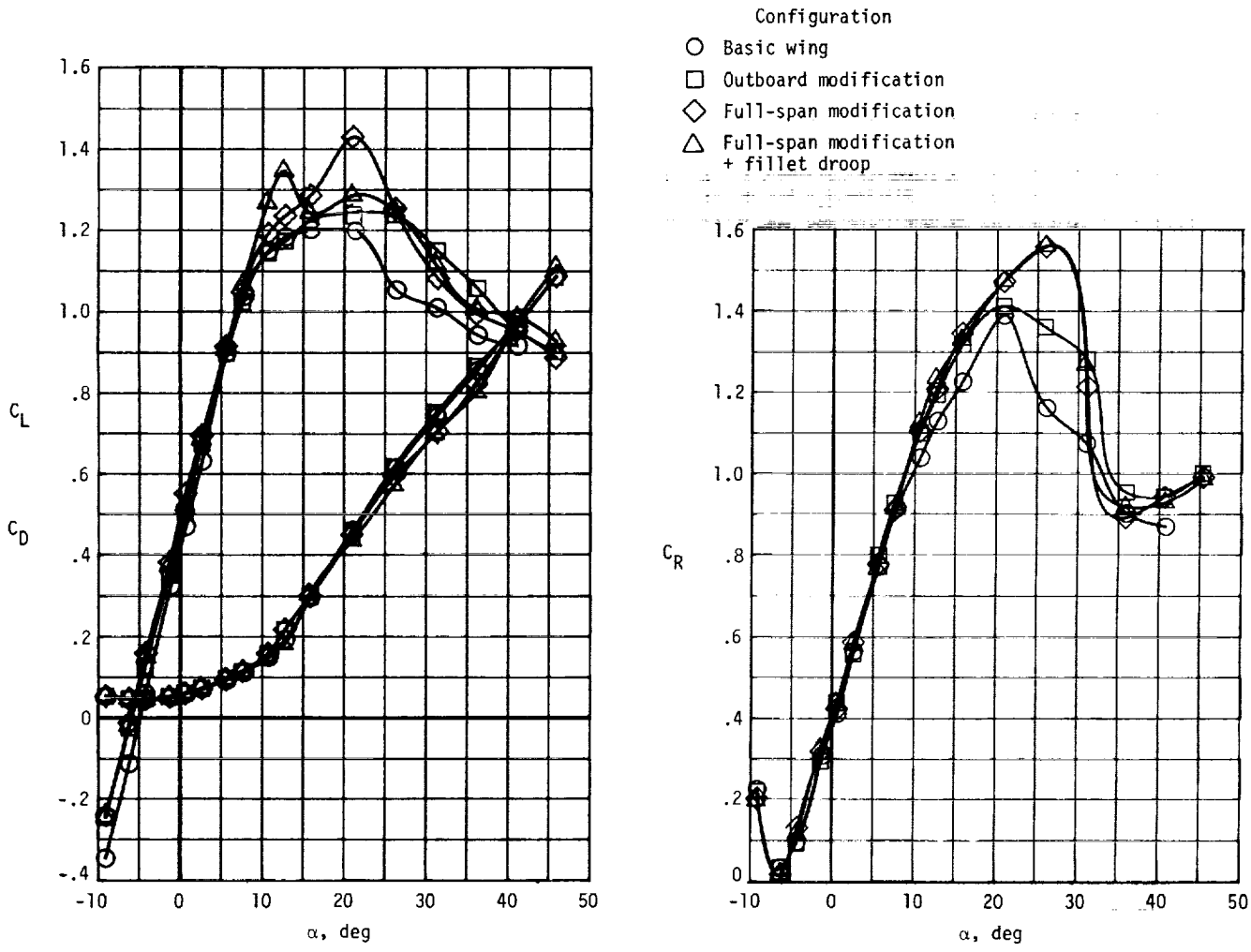

Figure 32.- Effect of airfoil upper-surface modification on longitudinal aerodynamic characteristics of airplane.

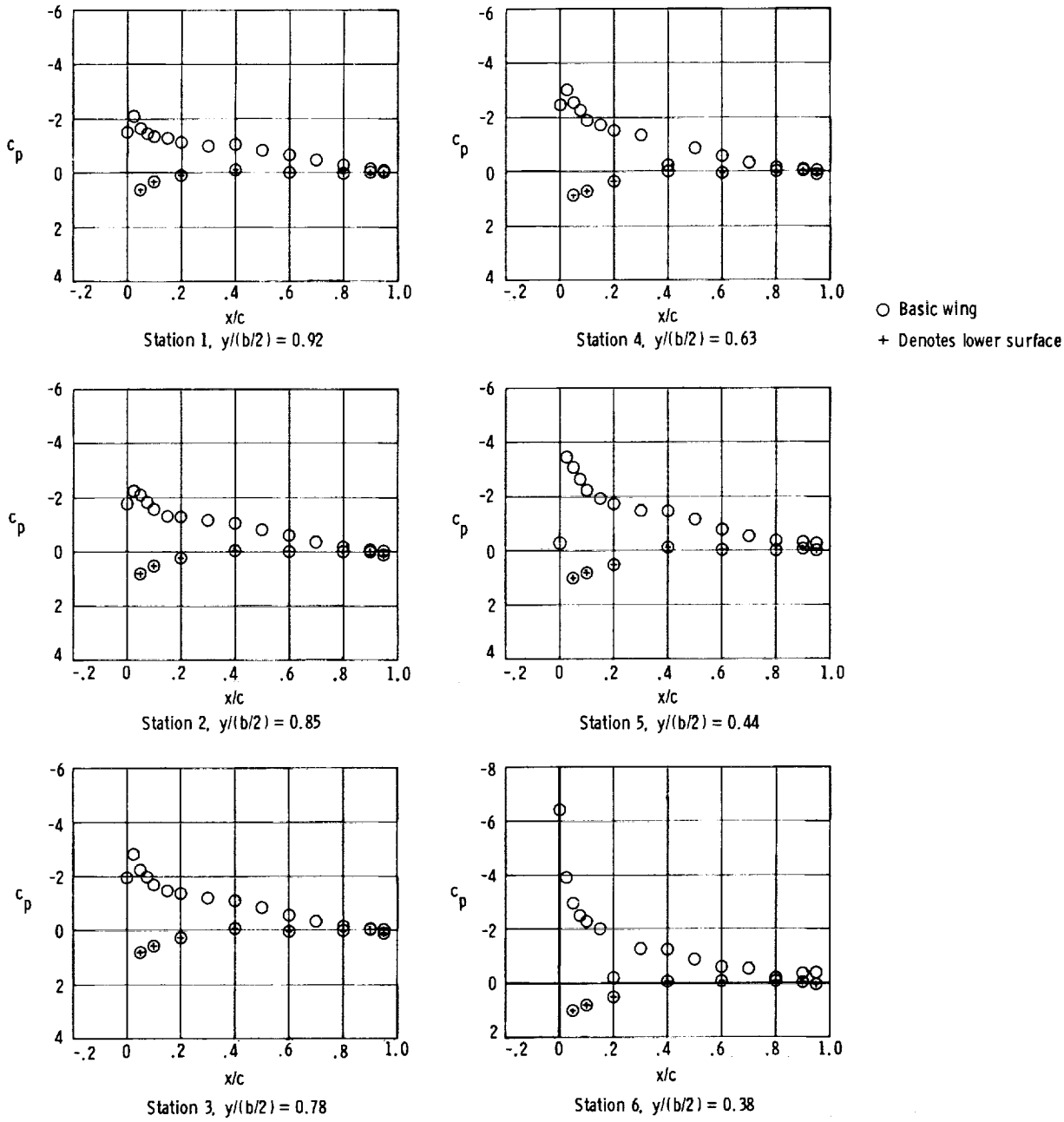

(a) $\alpha = 11.2°$.

Figure 33.- Chordwise pressure coefficients for basic wing.

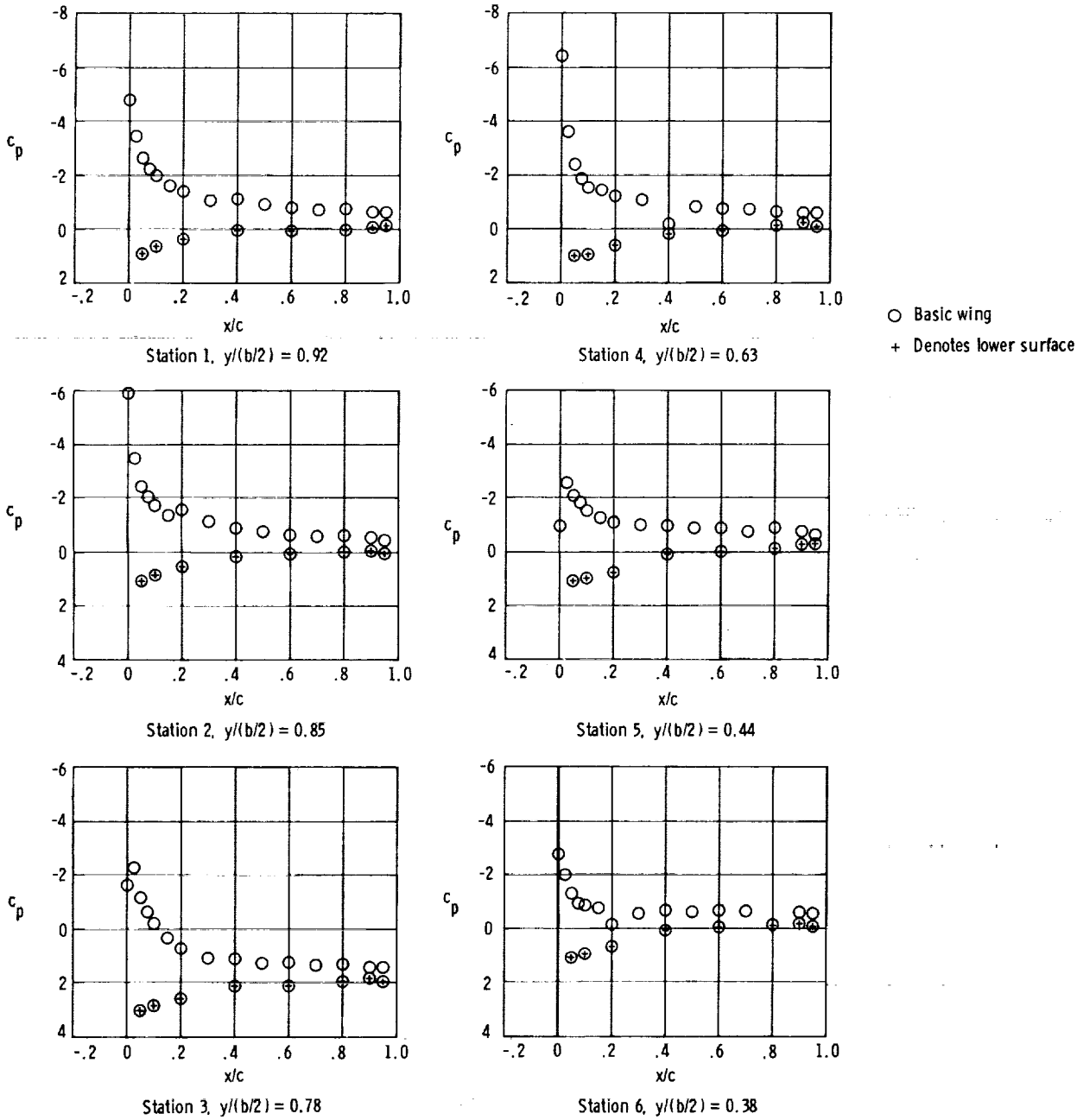

(b) $\alpha = 21.6°$.

Figure 33.- Continued.

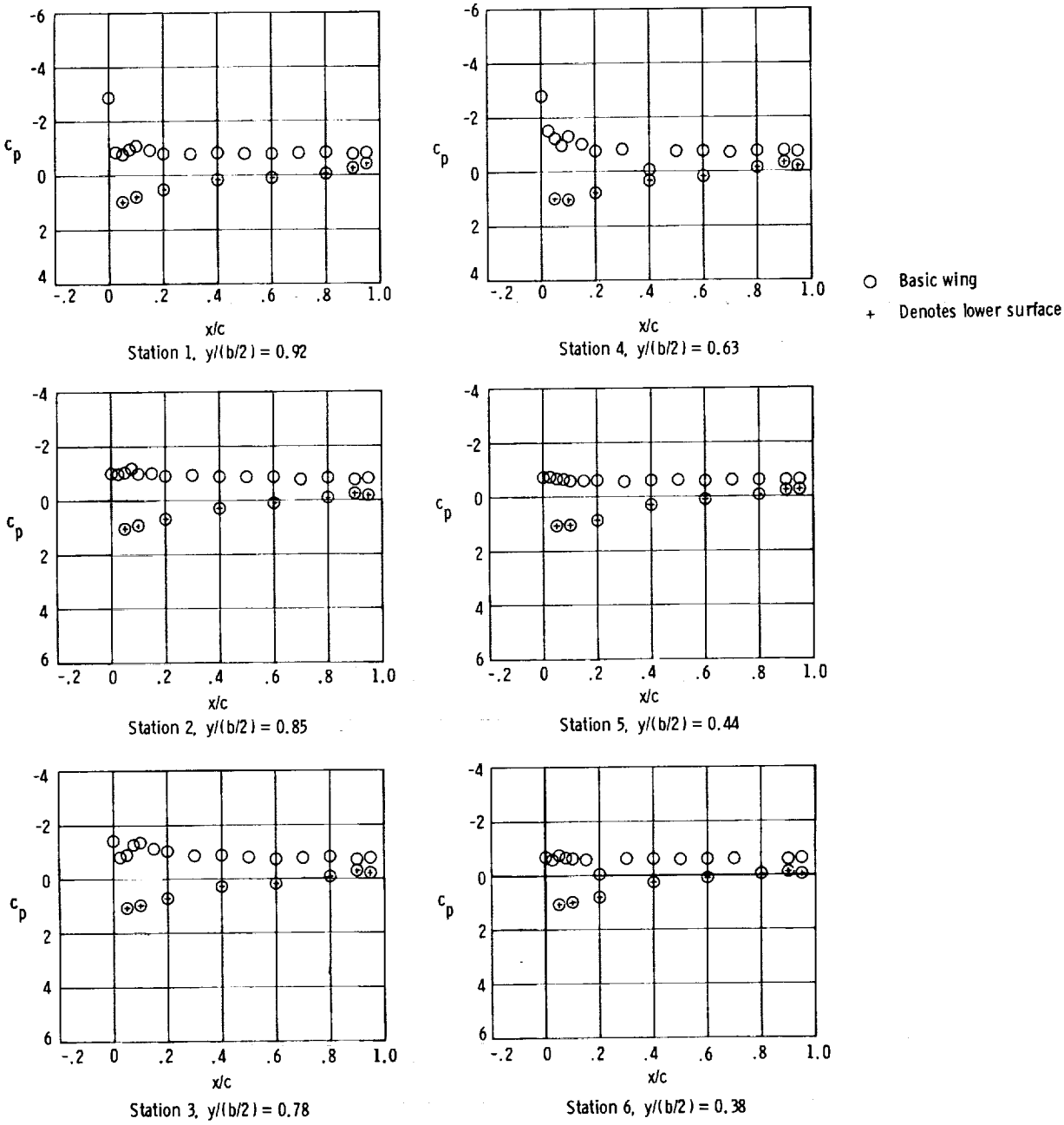

(c) $\alpha = 31.9°$.

Figure 33.- Continued.

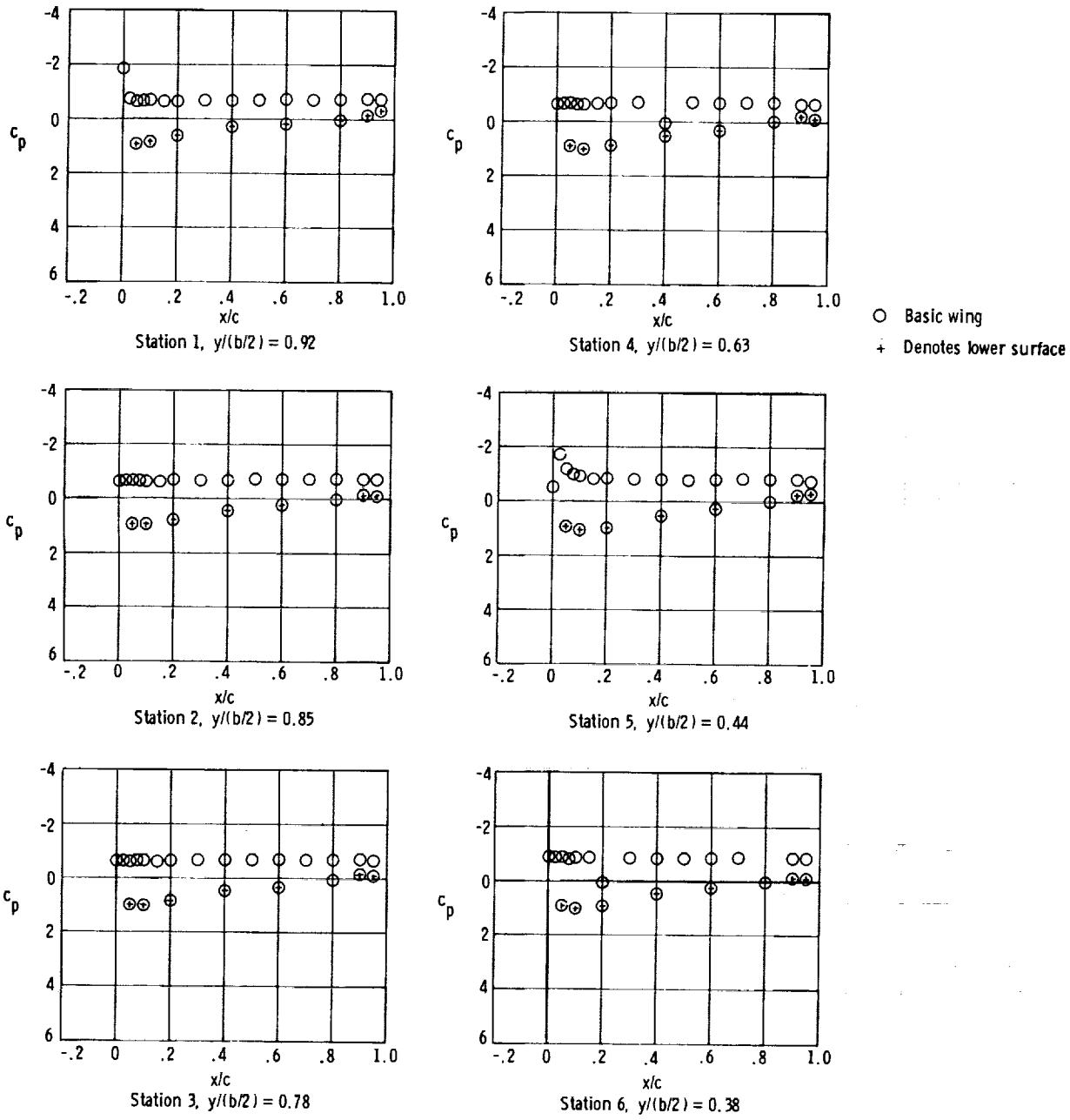

(d) $\alpha = 41.5°$.

Figure 33.- Concluded.

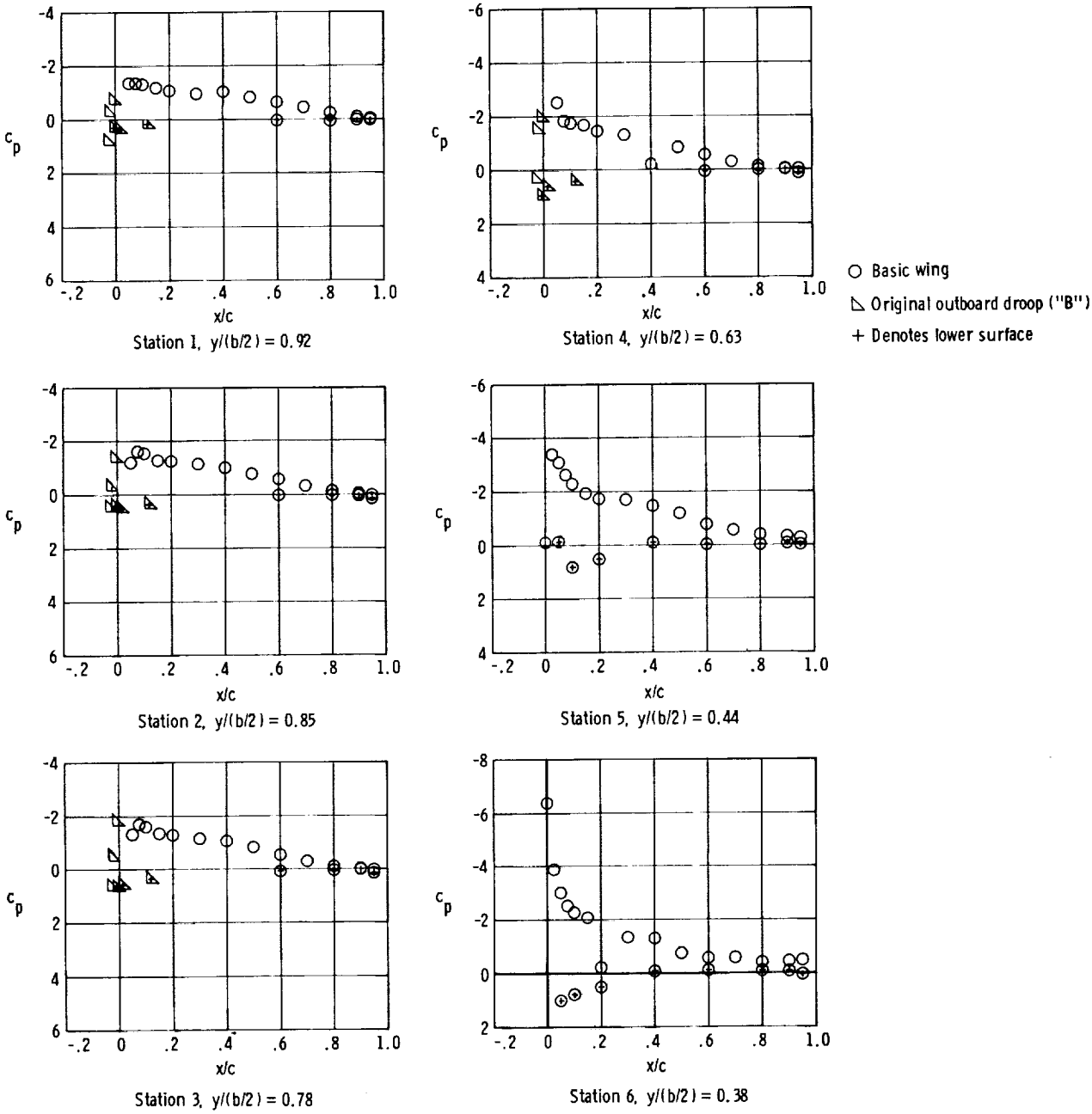

(a) $\alpha = 11.2°$.

Figure 34.- Chordwise pressure coefficients for wing with modification B.

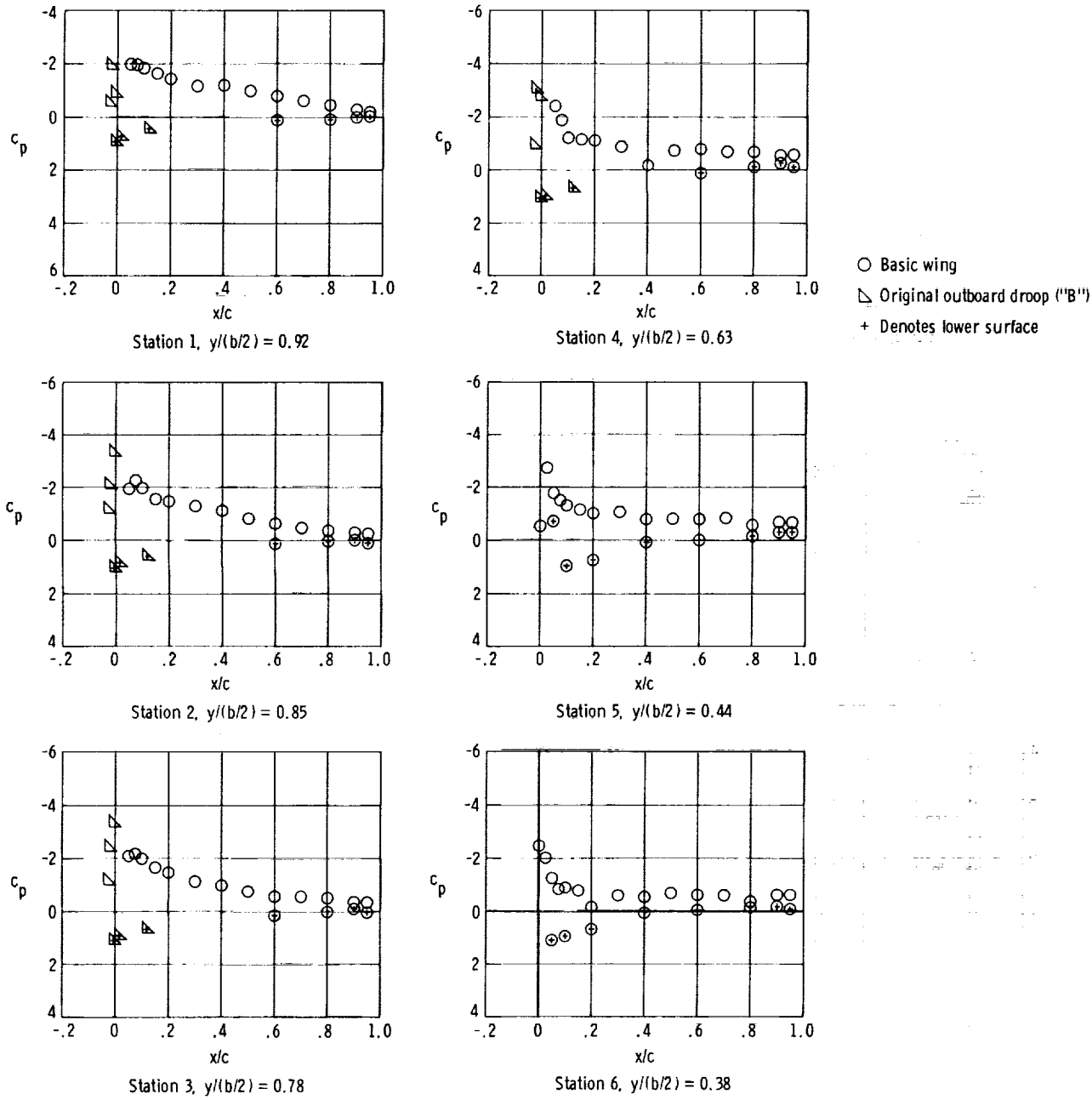

(b) $\alpha = 21.6°$.

Figure 34.- Continued.

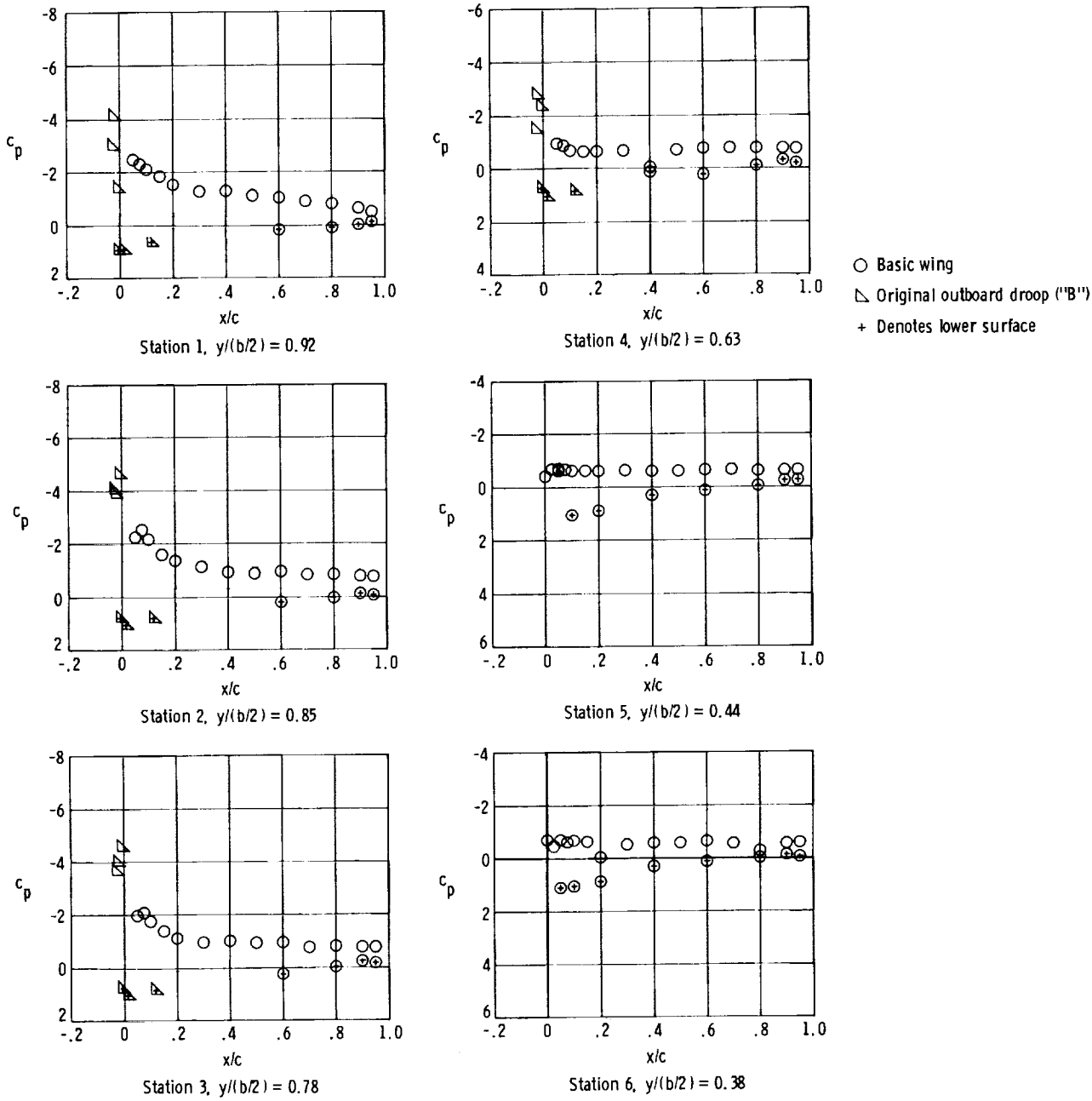

(c) $\alpha = 31.9°$.

Figure 34.- Continued.

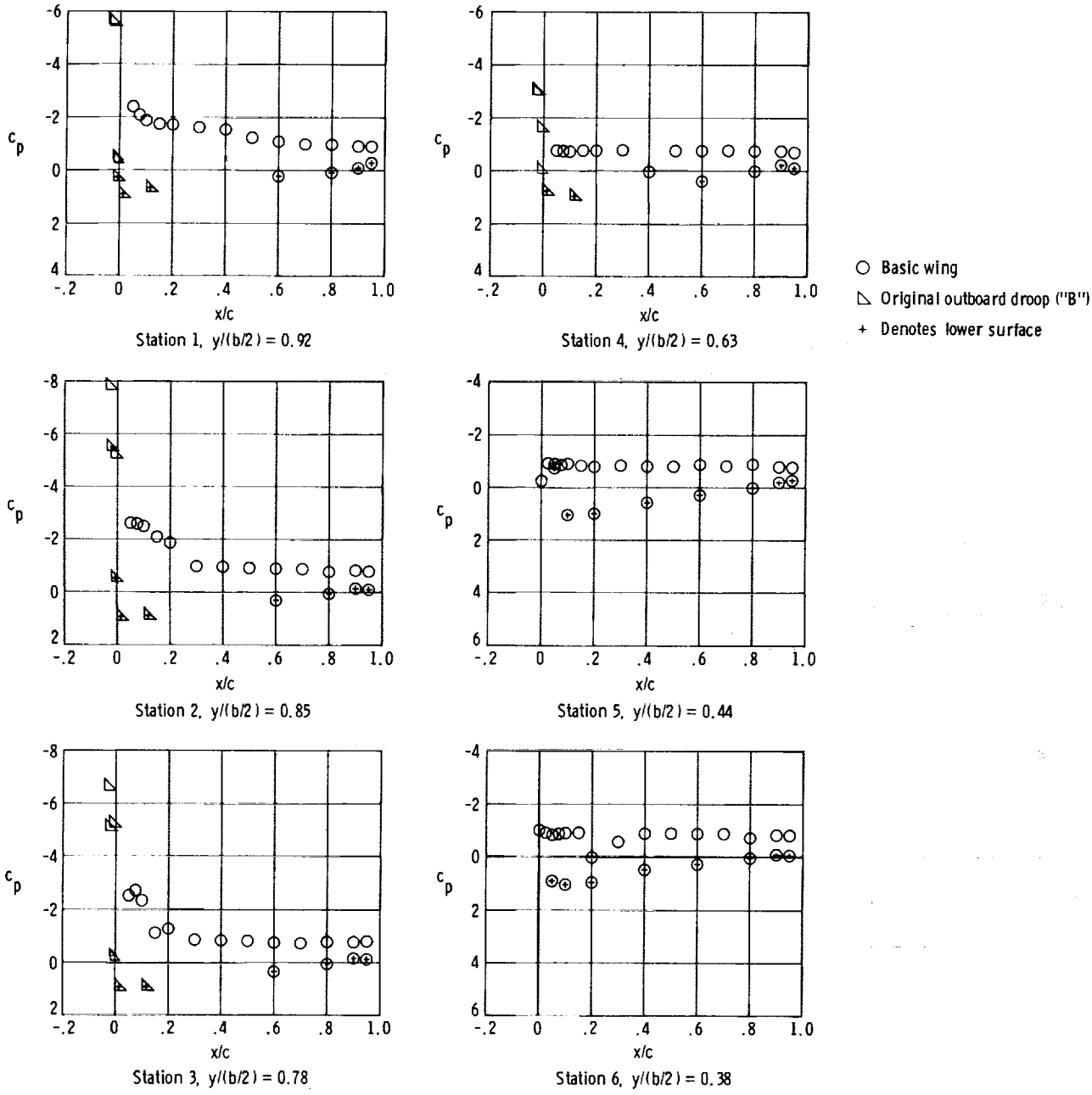

(d) $\alpha = 41.5°$.

Figure 34.- Concluded.

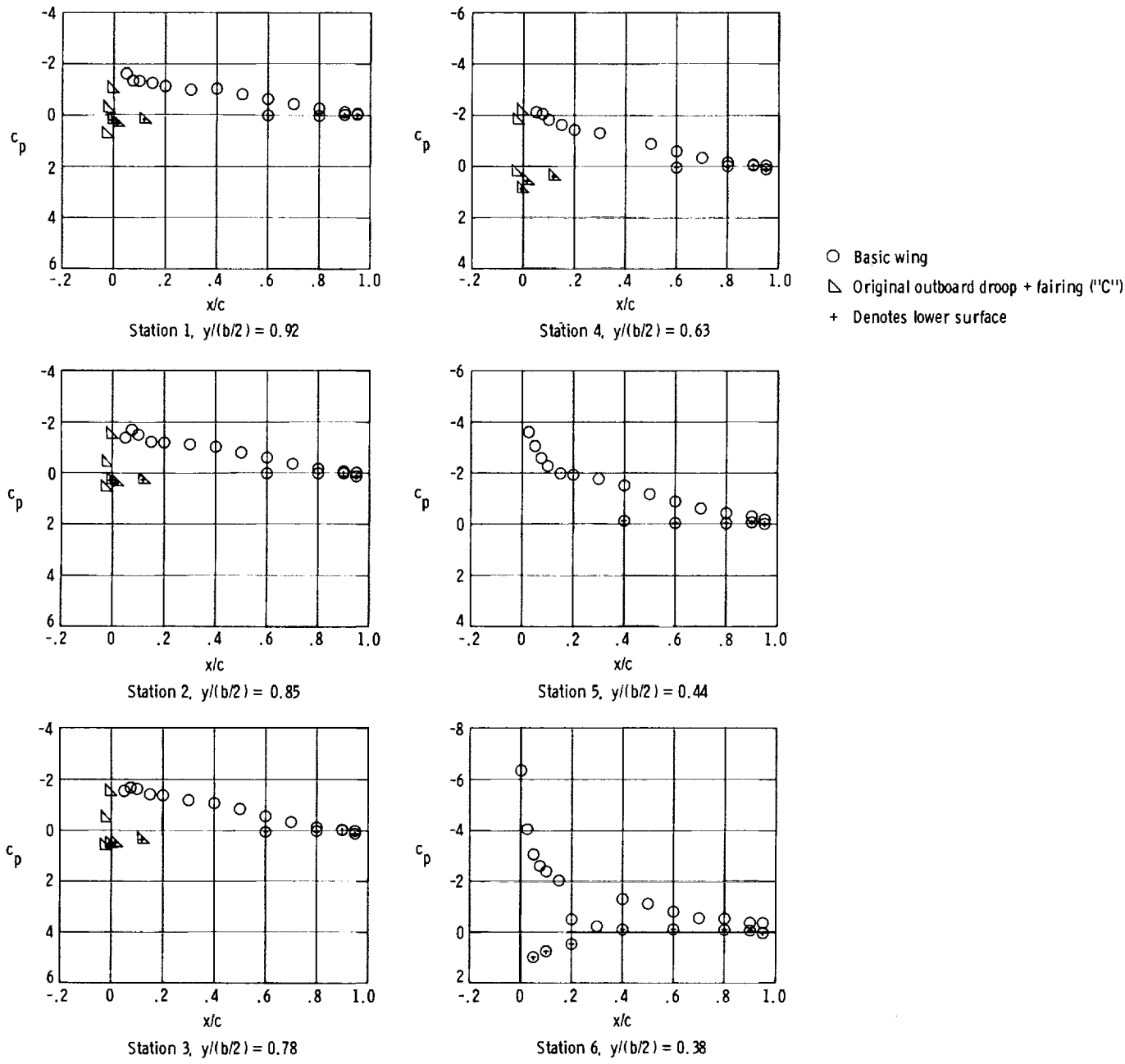

(a) $\alpha = 11.2°$.

Figure 35.- Chordwise pressure coefficient for wing with modification C.

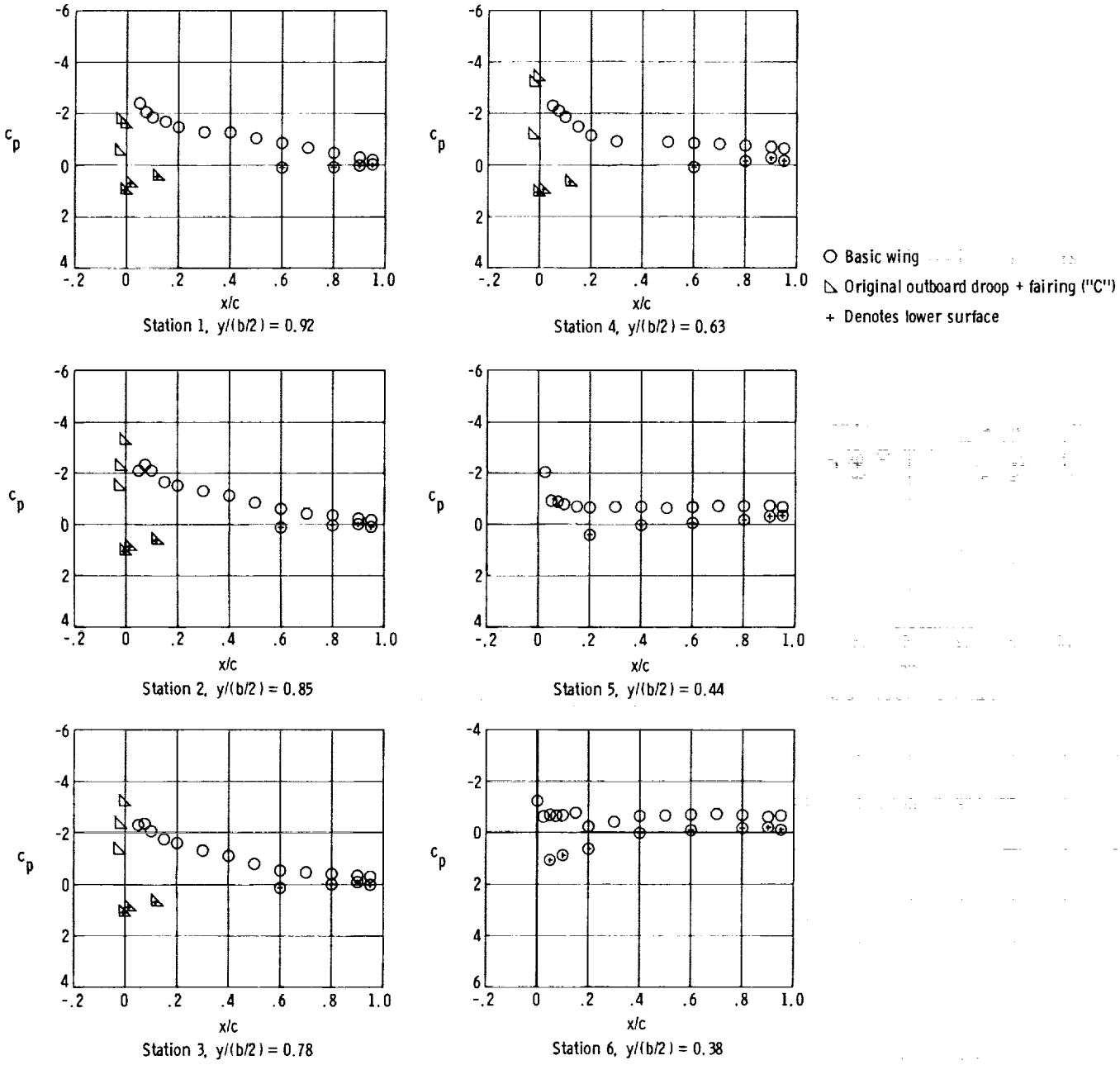

(b) $\alpha = 21.6°$.

Figure 35.- Continued.

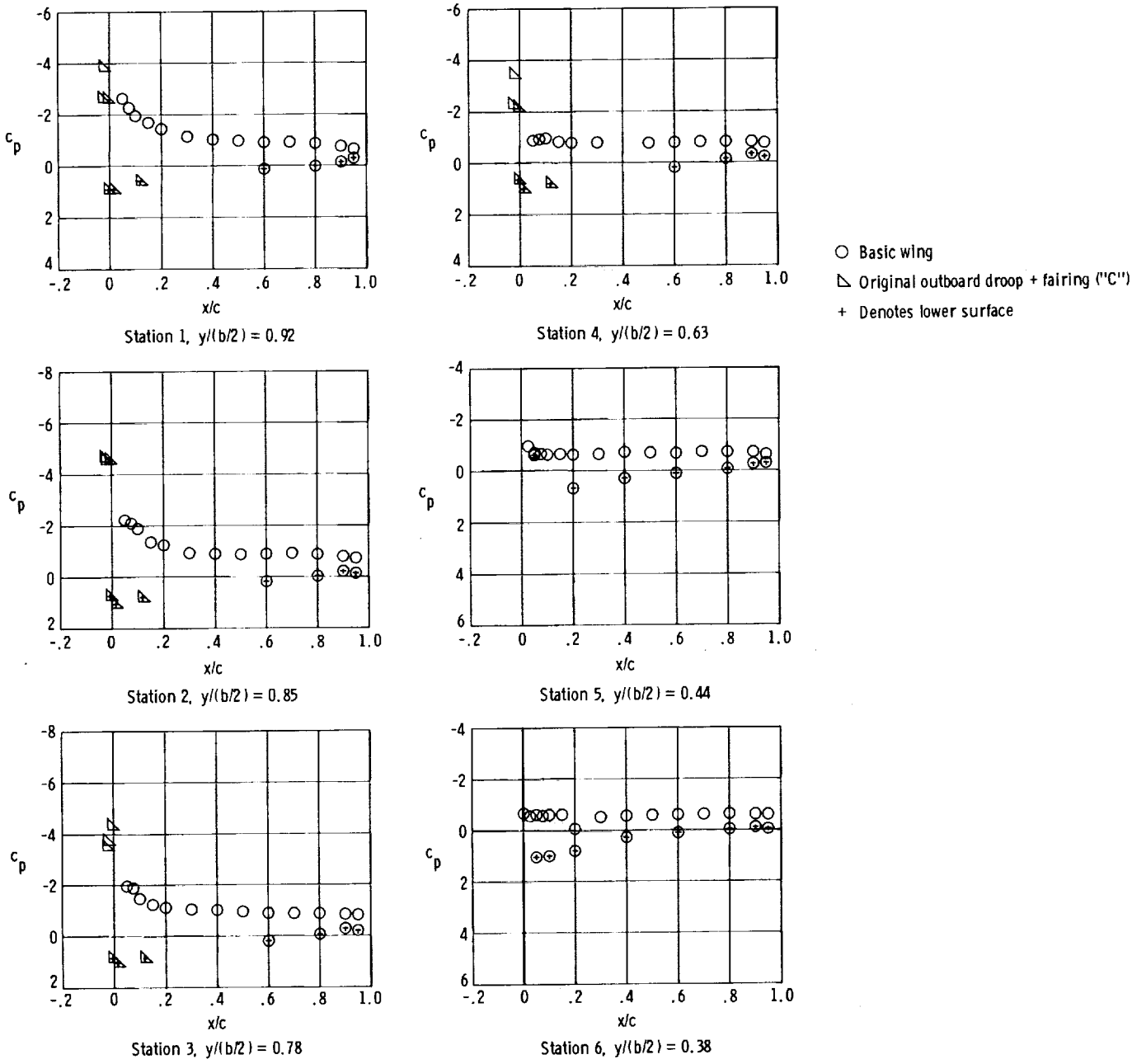

(c) $\alpha = 31.7°$.

Figure 35.- Continued.

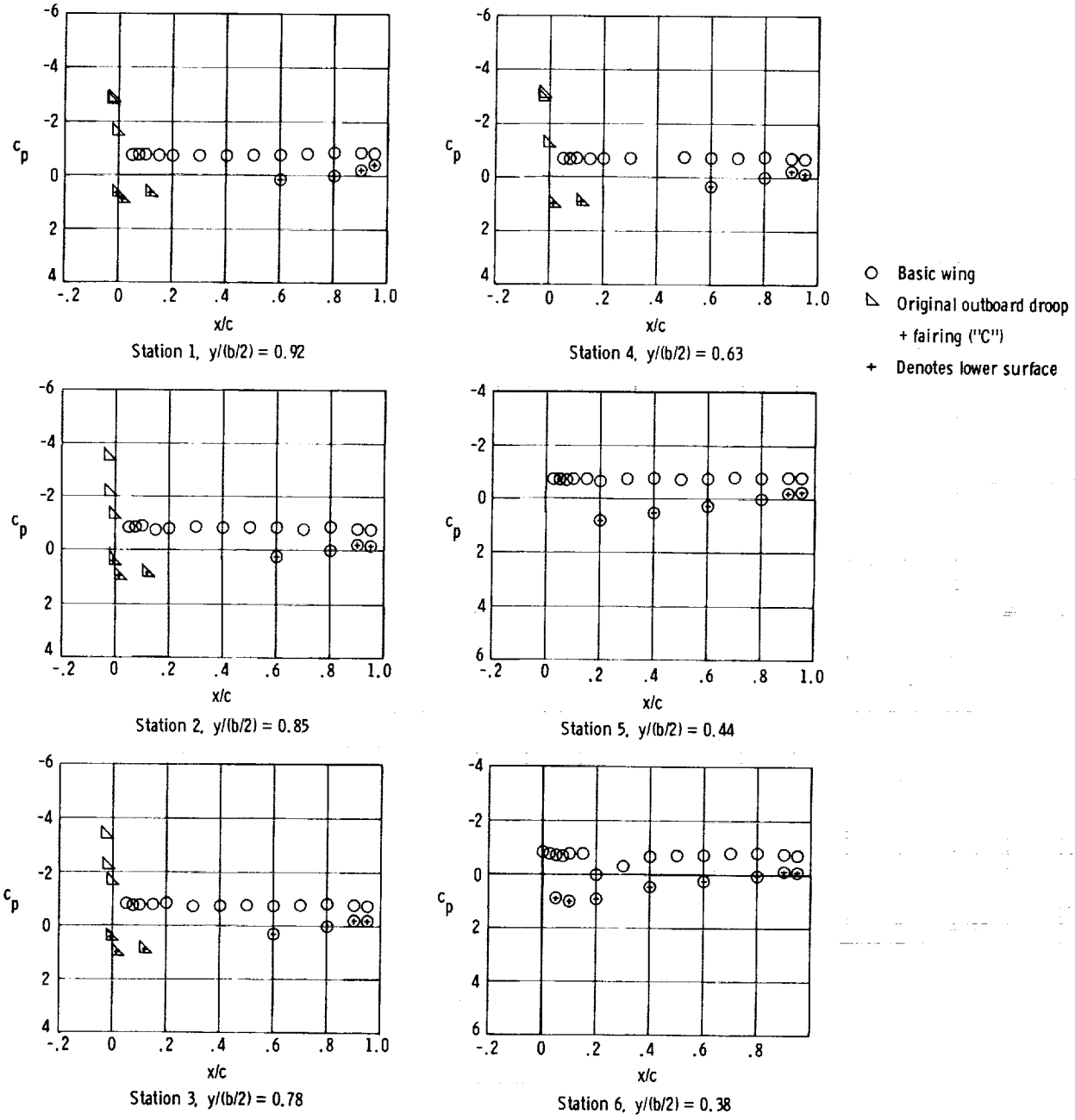

(d) $\alpha = 41.5°$.

Figure 35.- Concluded.

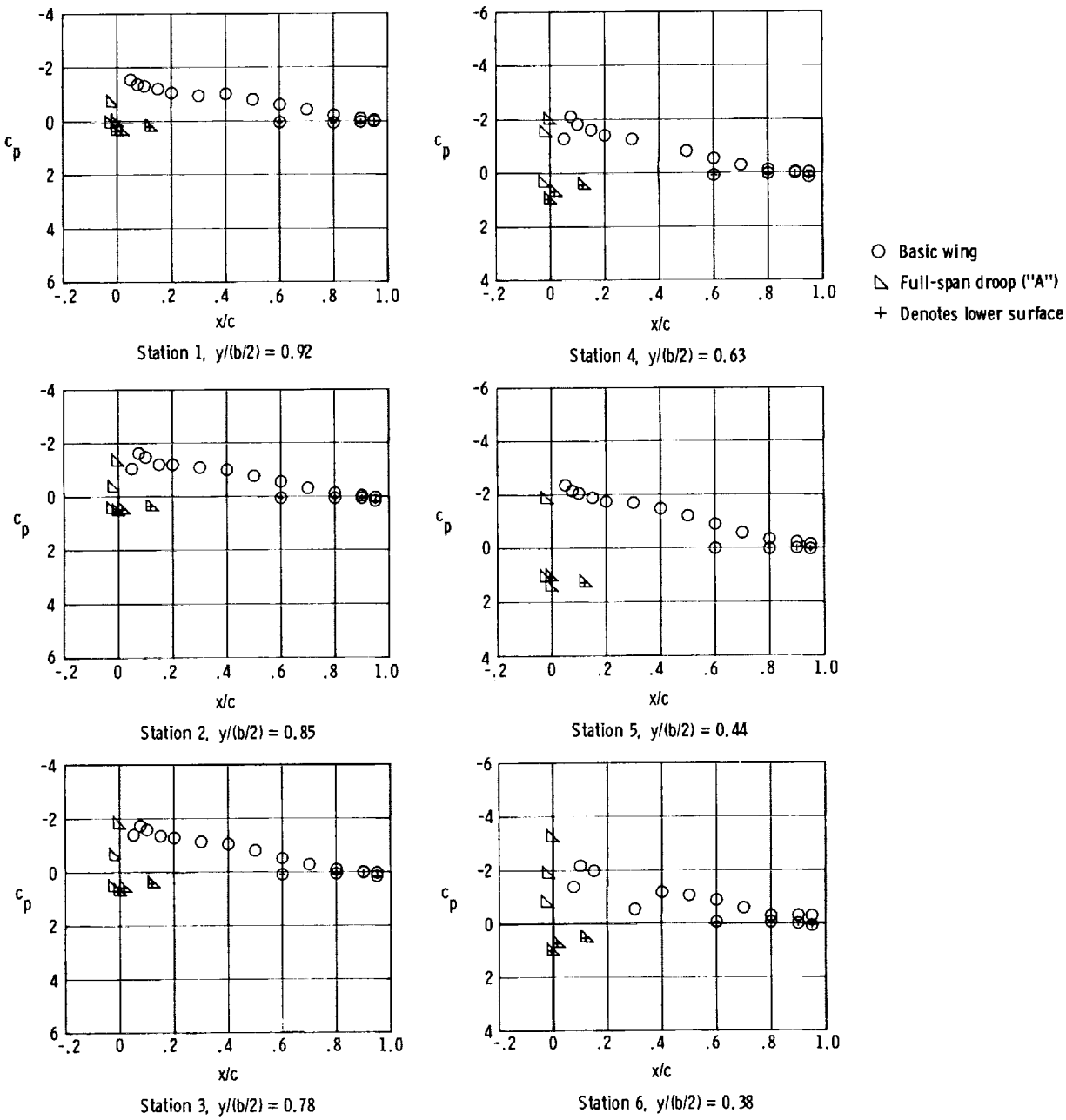

(a) $\alpha = 11.4°$.

Figure 36.- Chordwise pressure coefficients for wing with modification A.

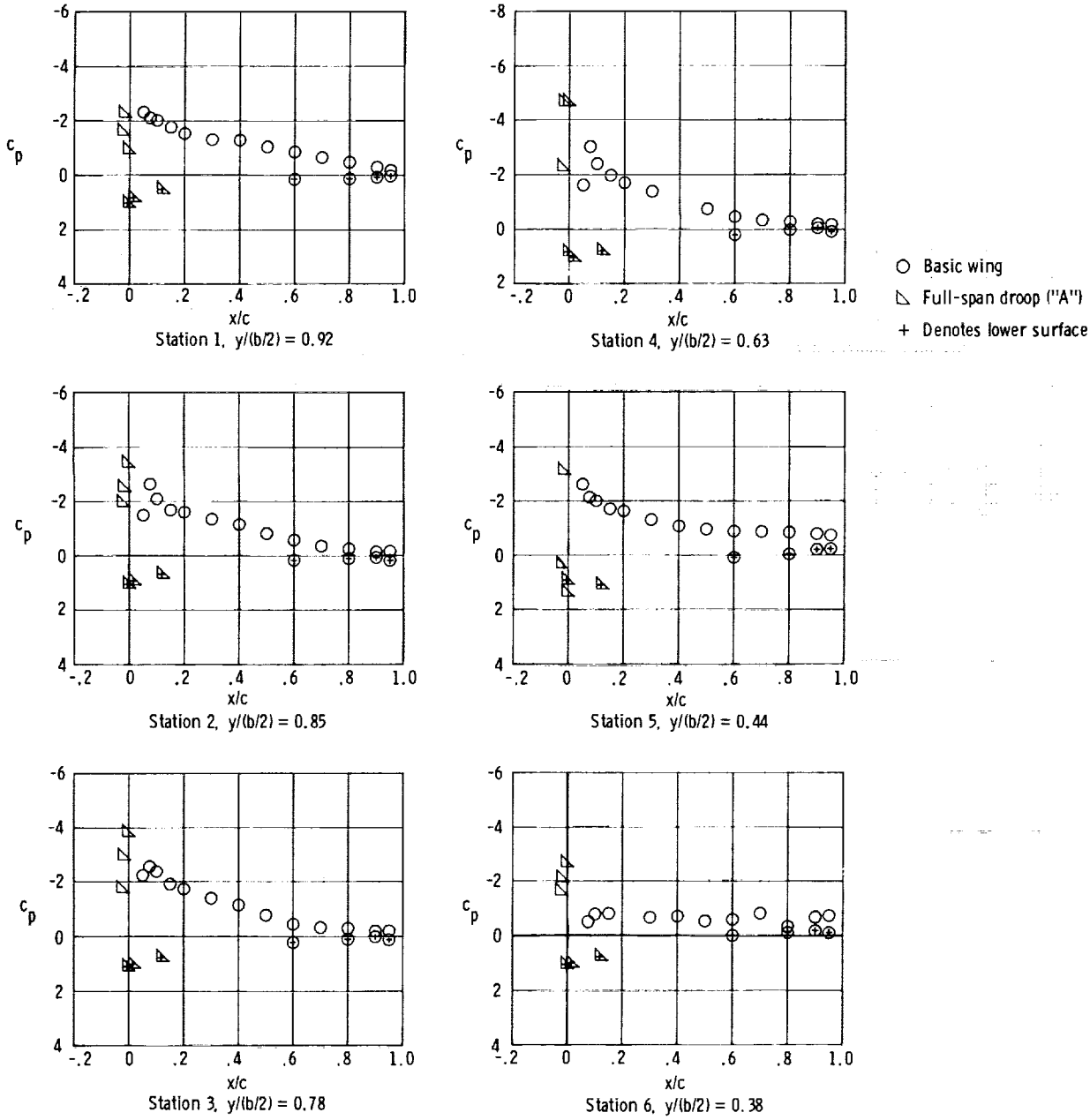

(b) $\alpha = 21.5°$.

Figure 36.- Continued.

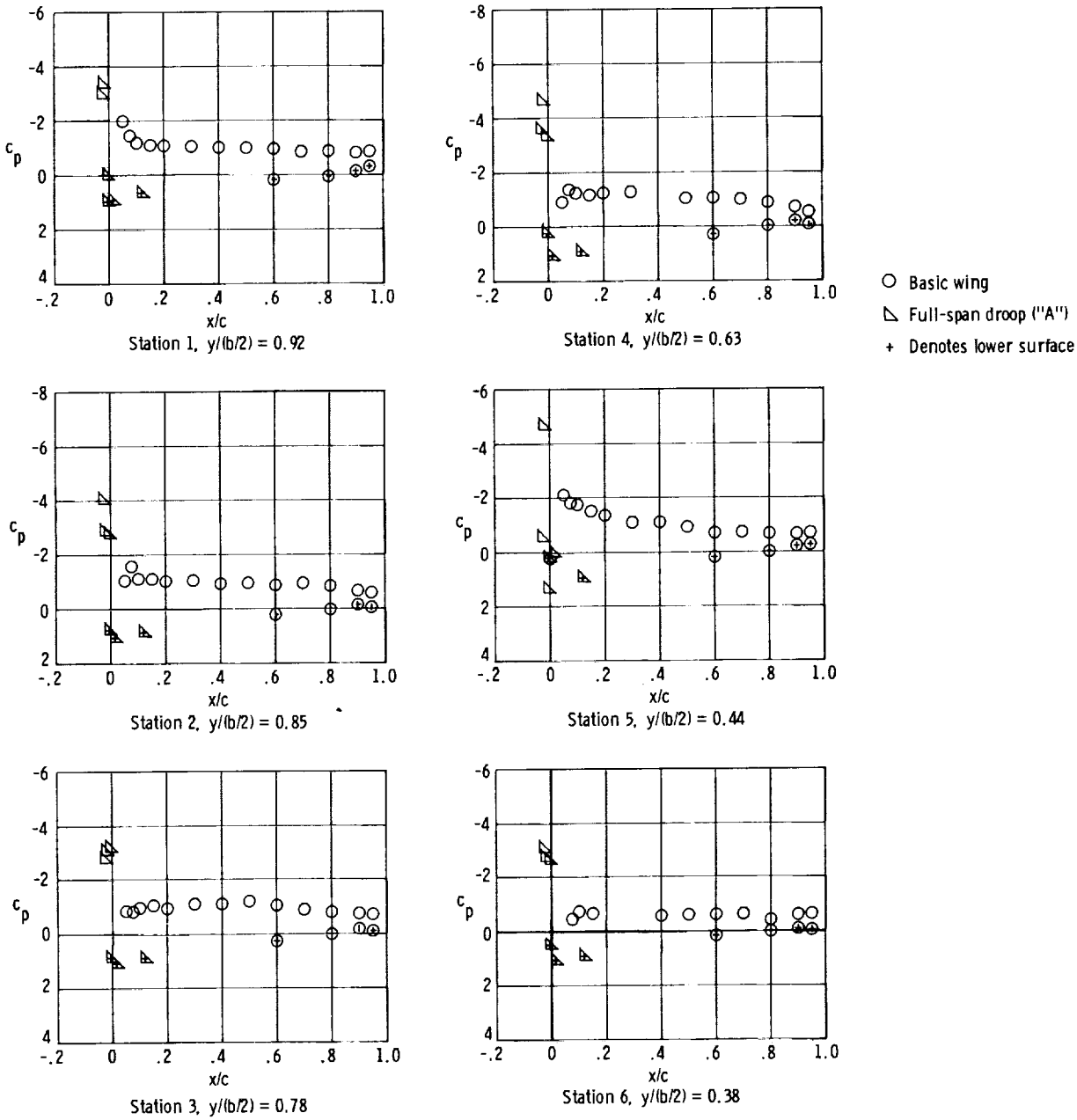

(c) $\alpha = 31.7°$.

Figure 36.- Continued.

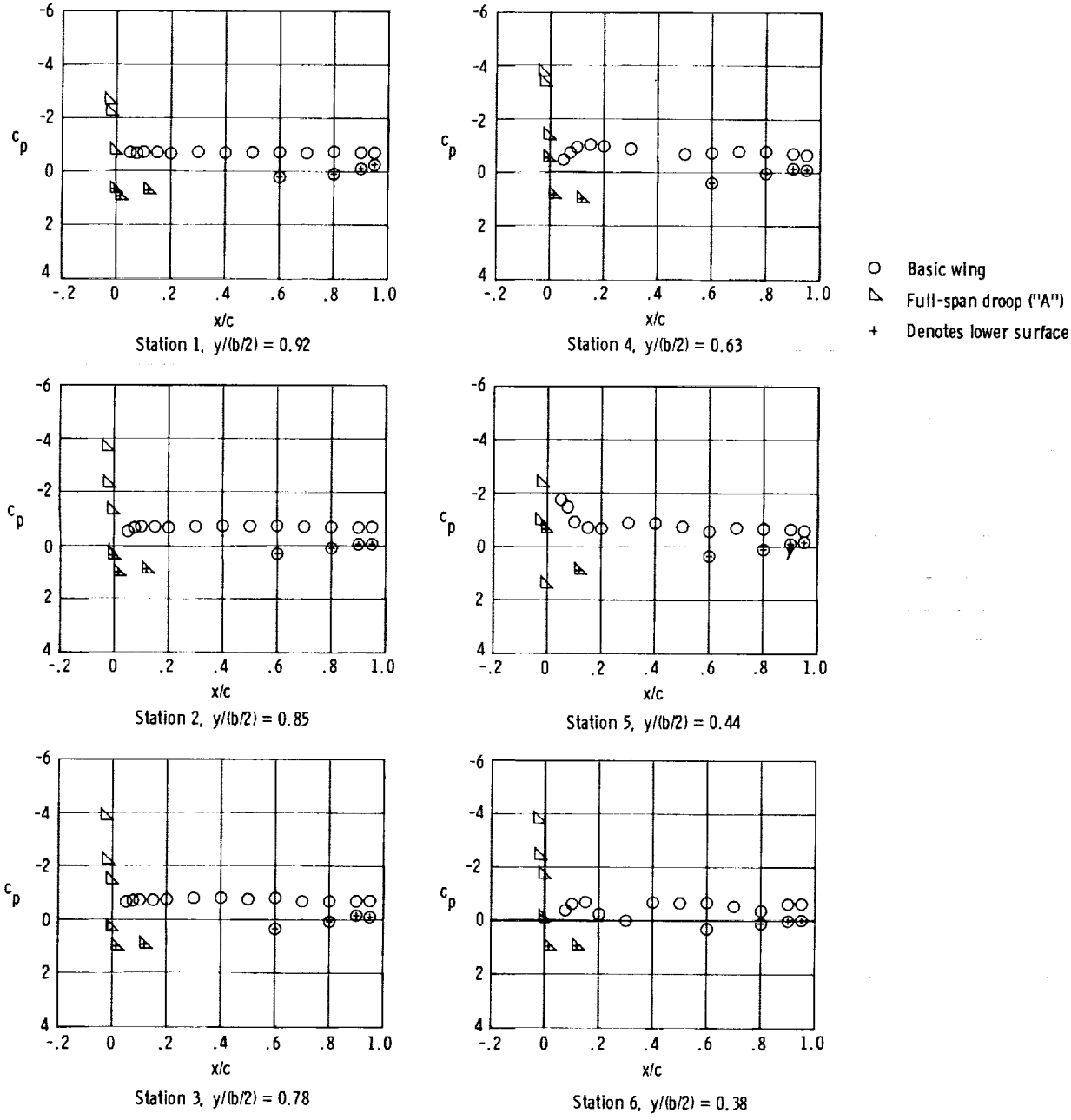

(d) $\alpha = 41.8°$.

Figure 36.- Concluded.

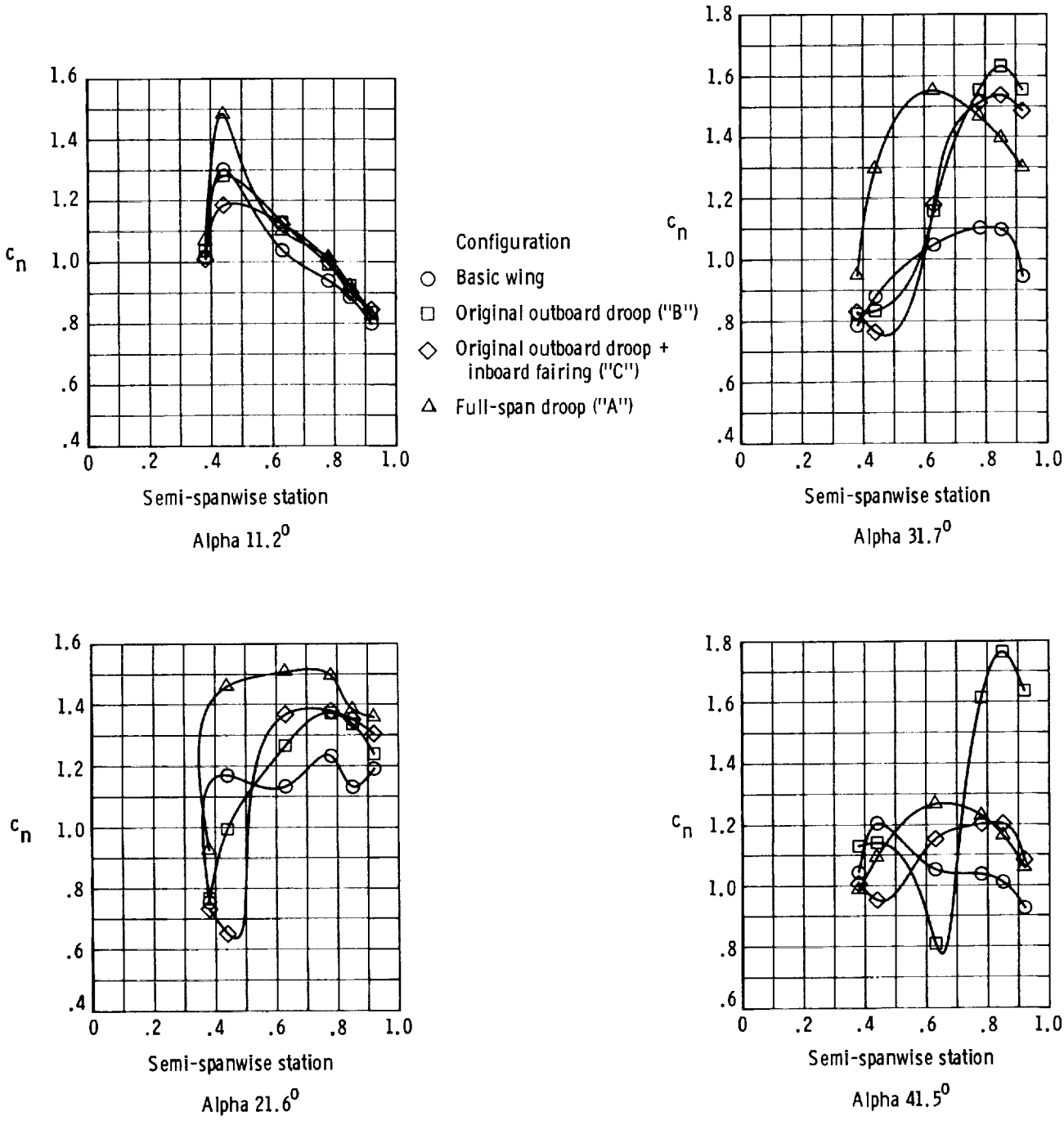

Figure 37.- Spanwise pressure distributions for airplane with several leading-edge-droop configurations.

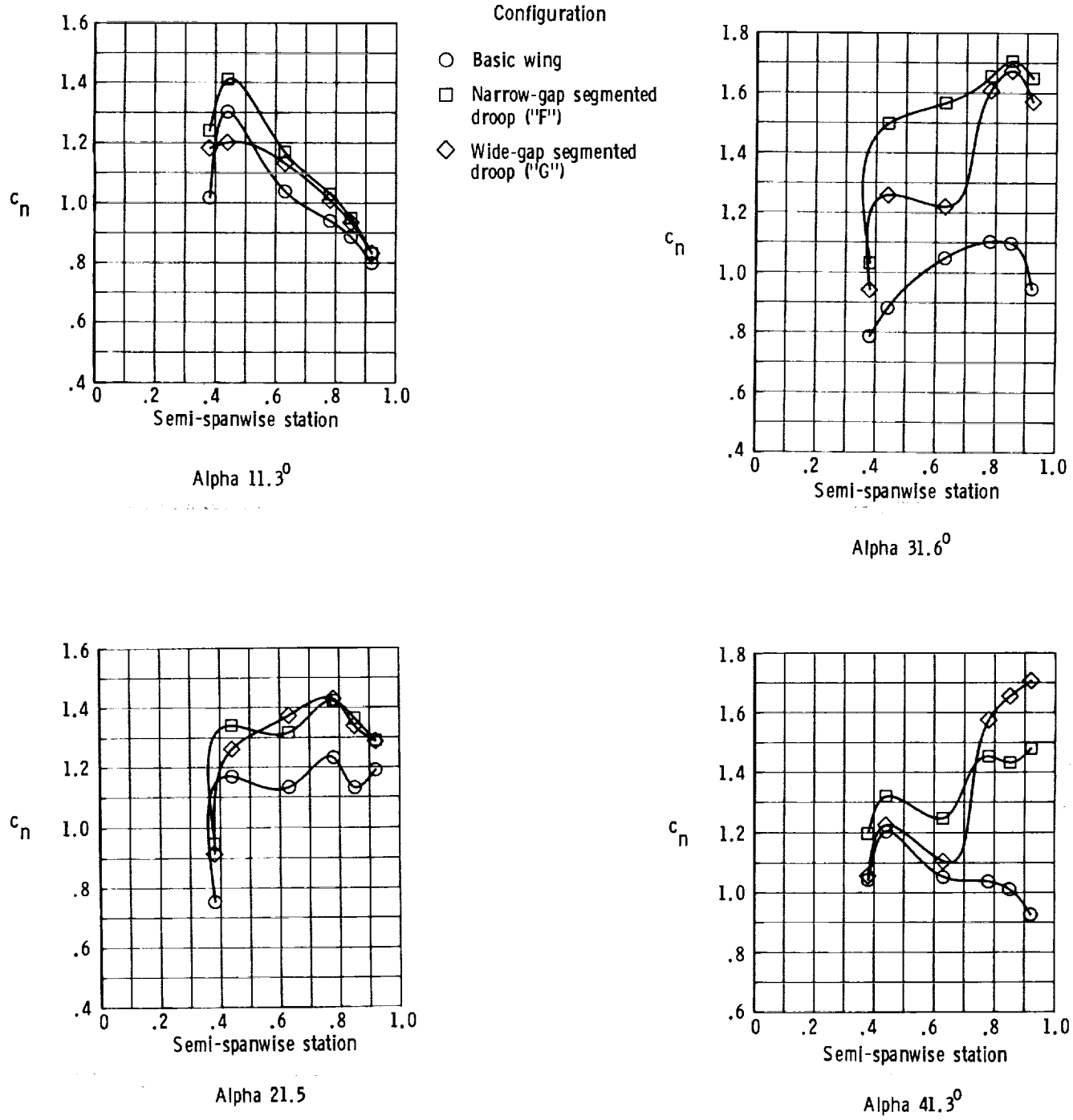

Figure 38.- Spanwise pressure distributions for airplane with segmented leading-edge droop.

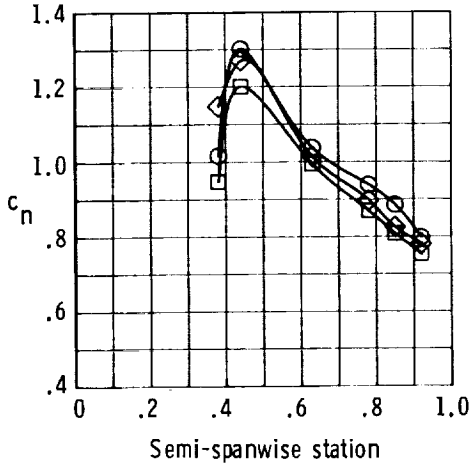

Alpha 11.2°

Configuration
○ Basic wing
□ Outboard slat
◇ Full-span slat + fillet droop

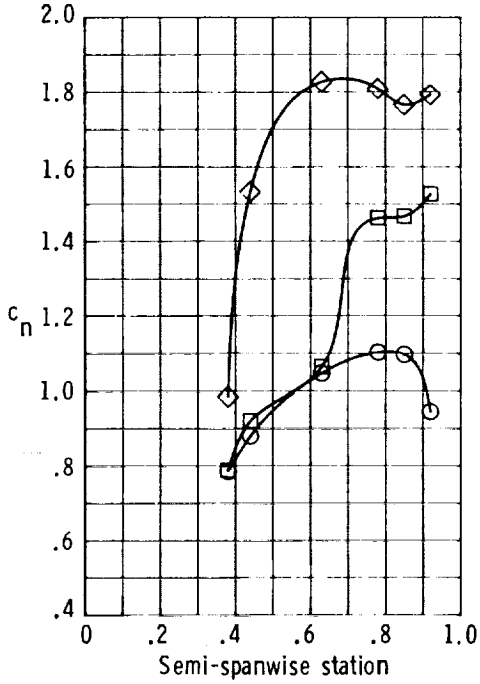

Alpha 31.7°

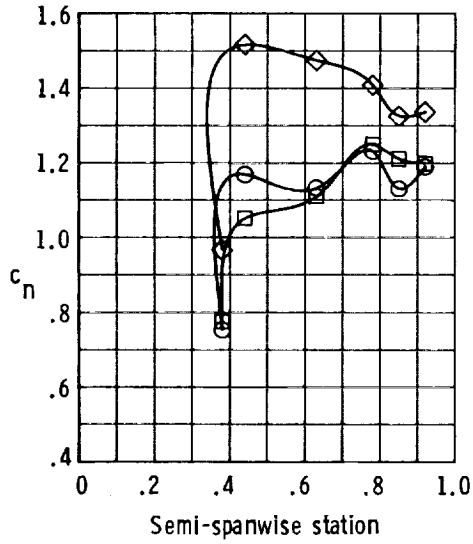

Alpha 21.5°

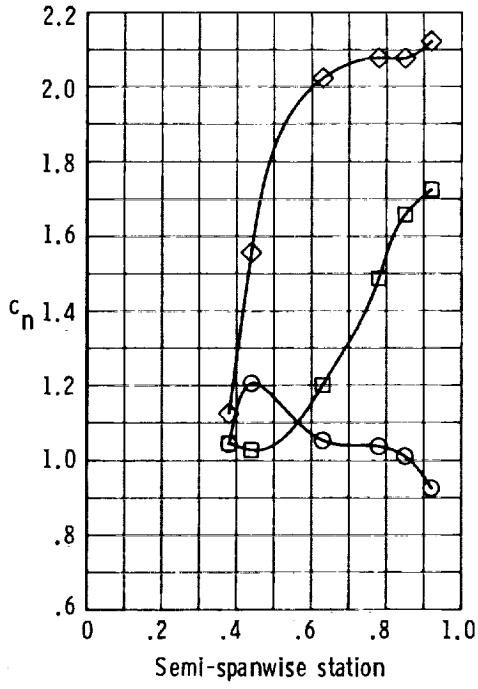

Alpha 41.4°

Figure 39.- Spanwise pressure distributions for airplane with $0.08\bar{c}$ leading-edge slat.

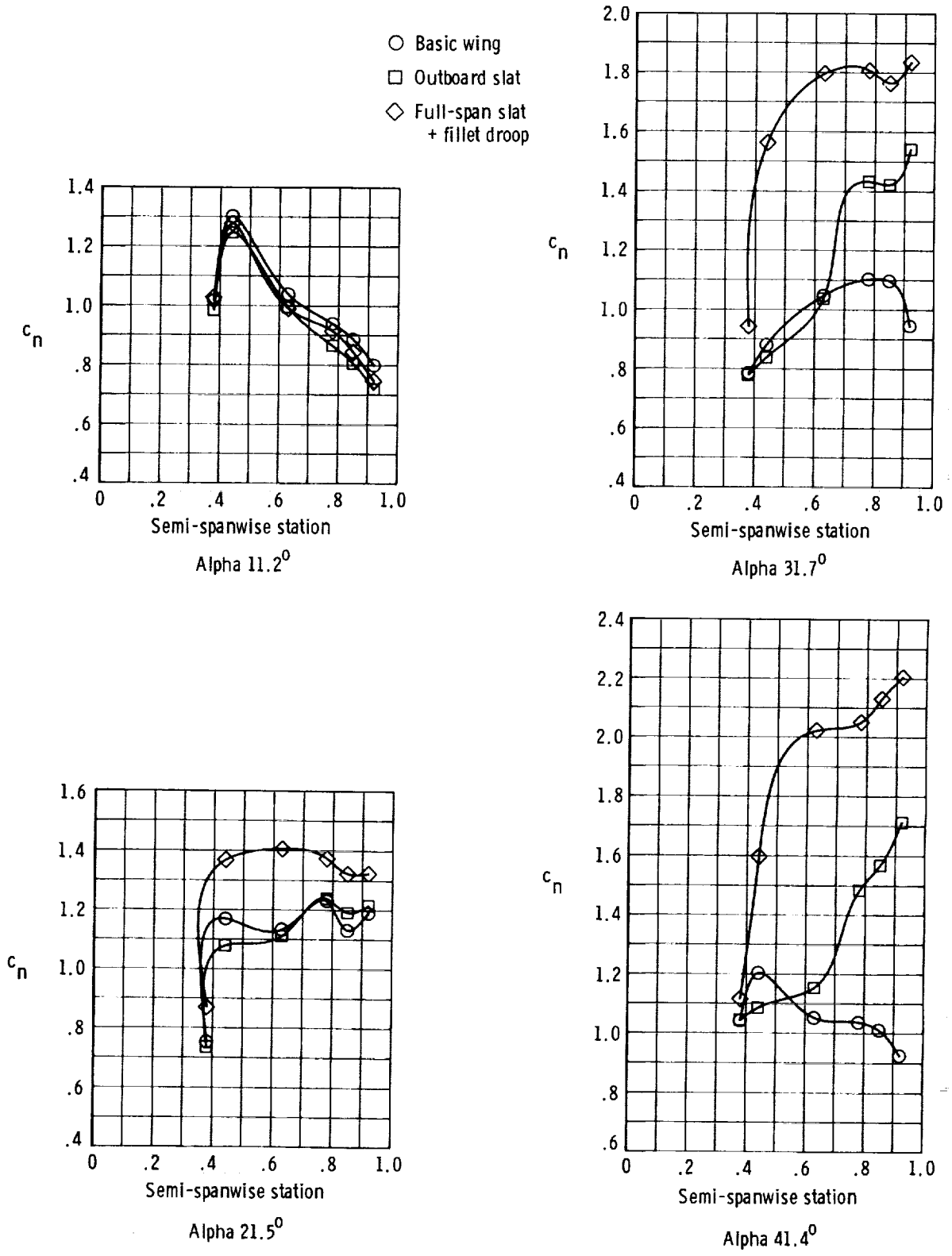

Figure 40.- Spanwise pressure distributions for airplane with 0.15$\bar{c}$ leading-edge slat.

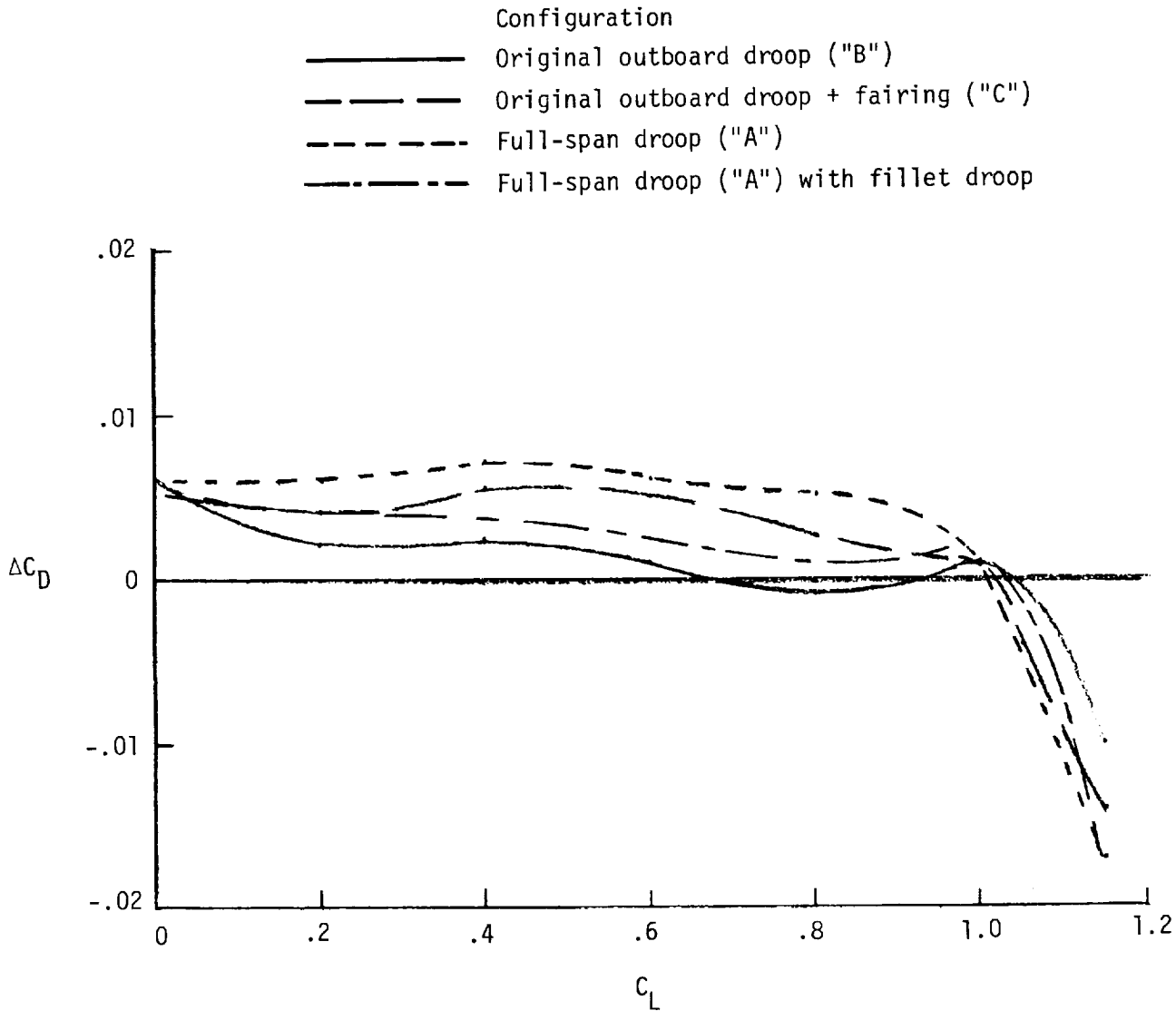

Figure 41.- Incremental values of drag coefficient for airplane with several wing-leading-edge configurations.

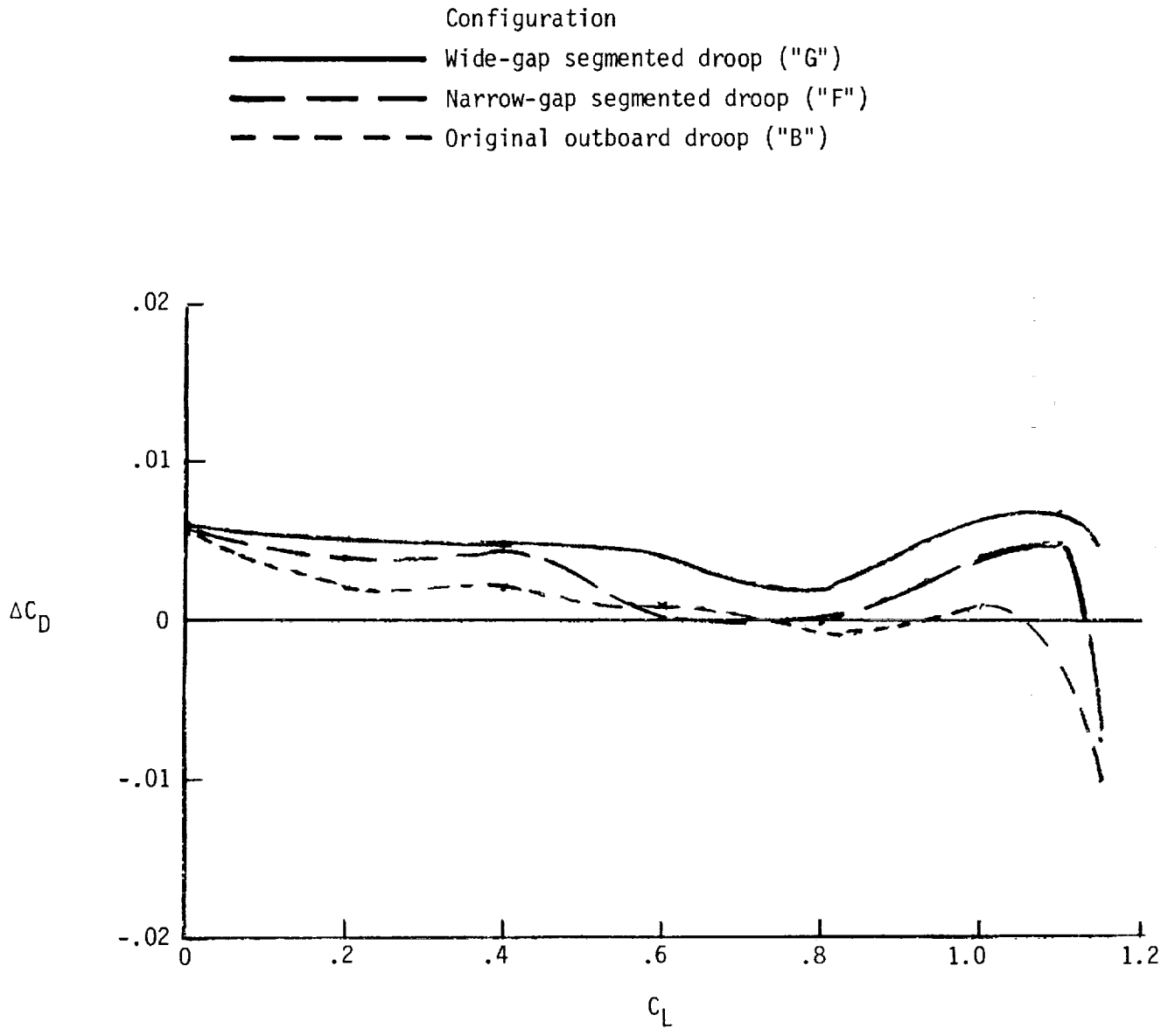

Figure 42.- Values of incremental drag coefficient for airplane with segmented leading-edge droop.

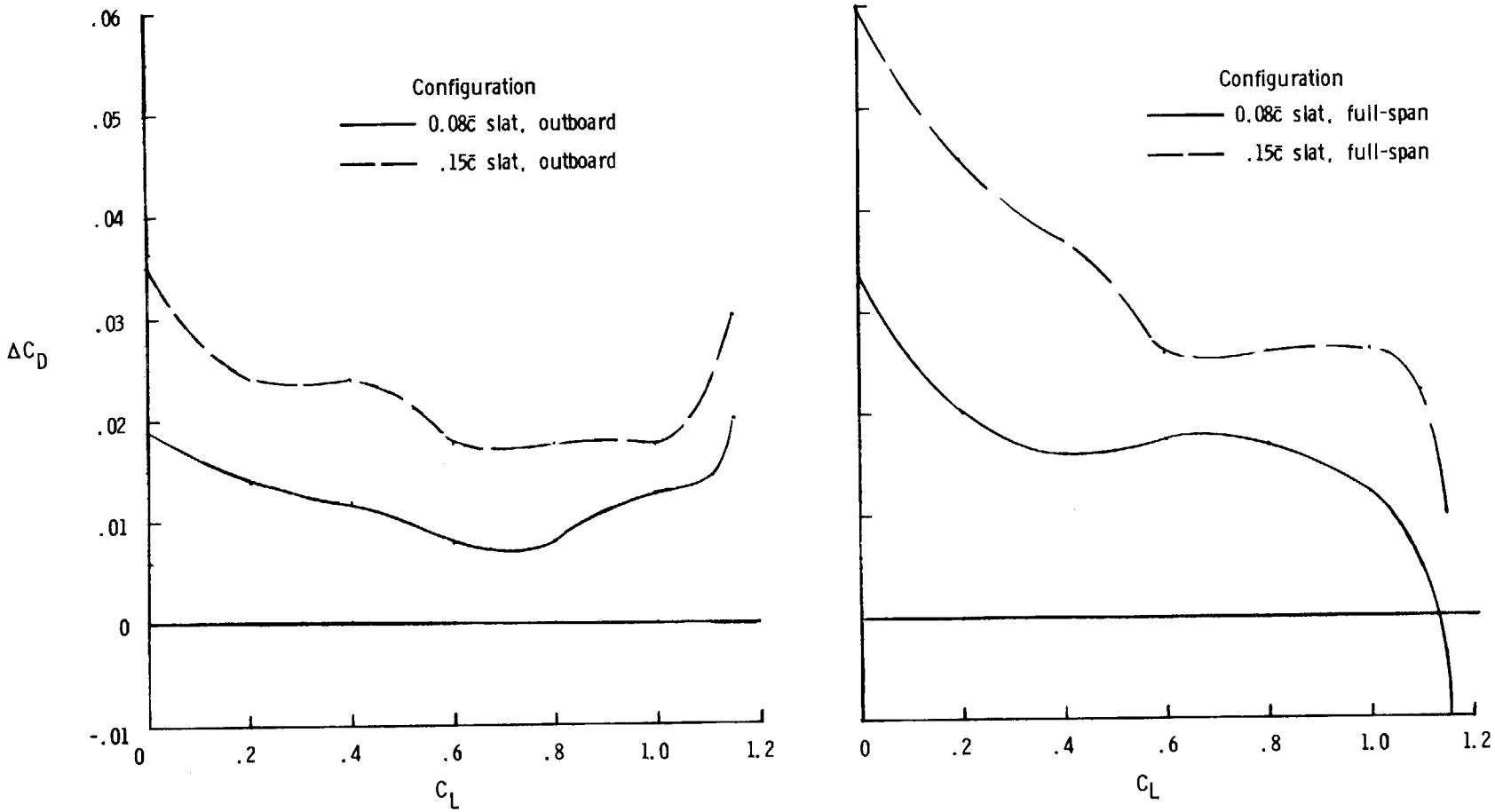

Figure 43.- Values of incremental drag coefficient for leading-edge-slat configurations with reference to basic wing configuration.

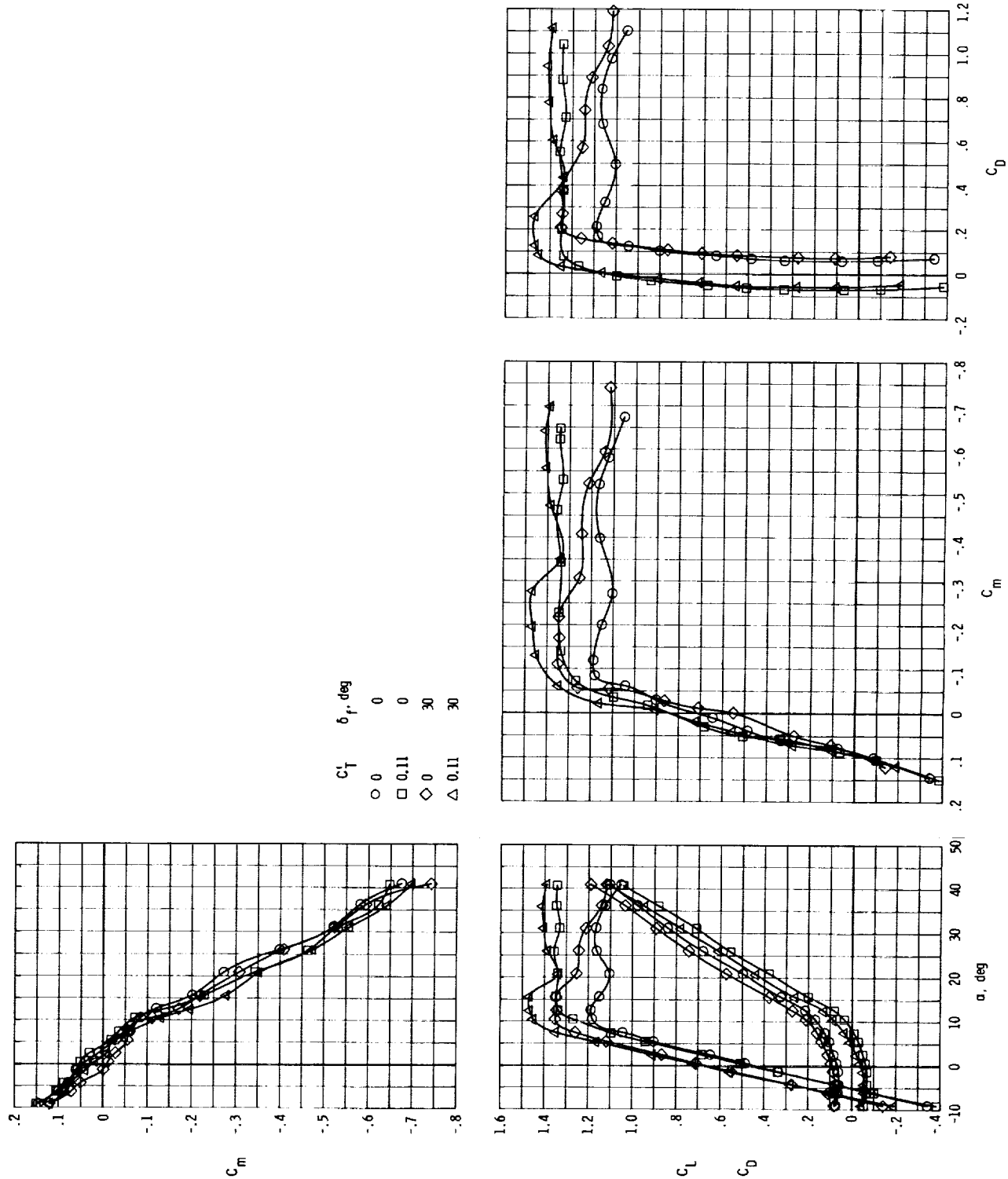

Figure 44.- Effects of power and flap deflection on longitudinal aerodynamic characteristics of complete basic airplane.

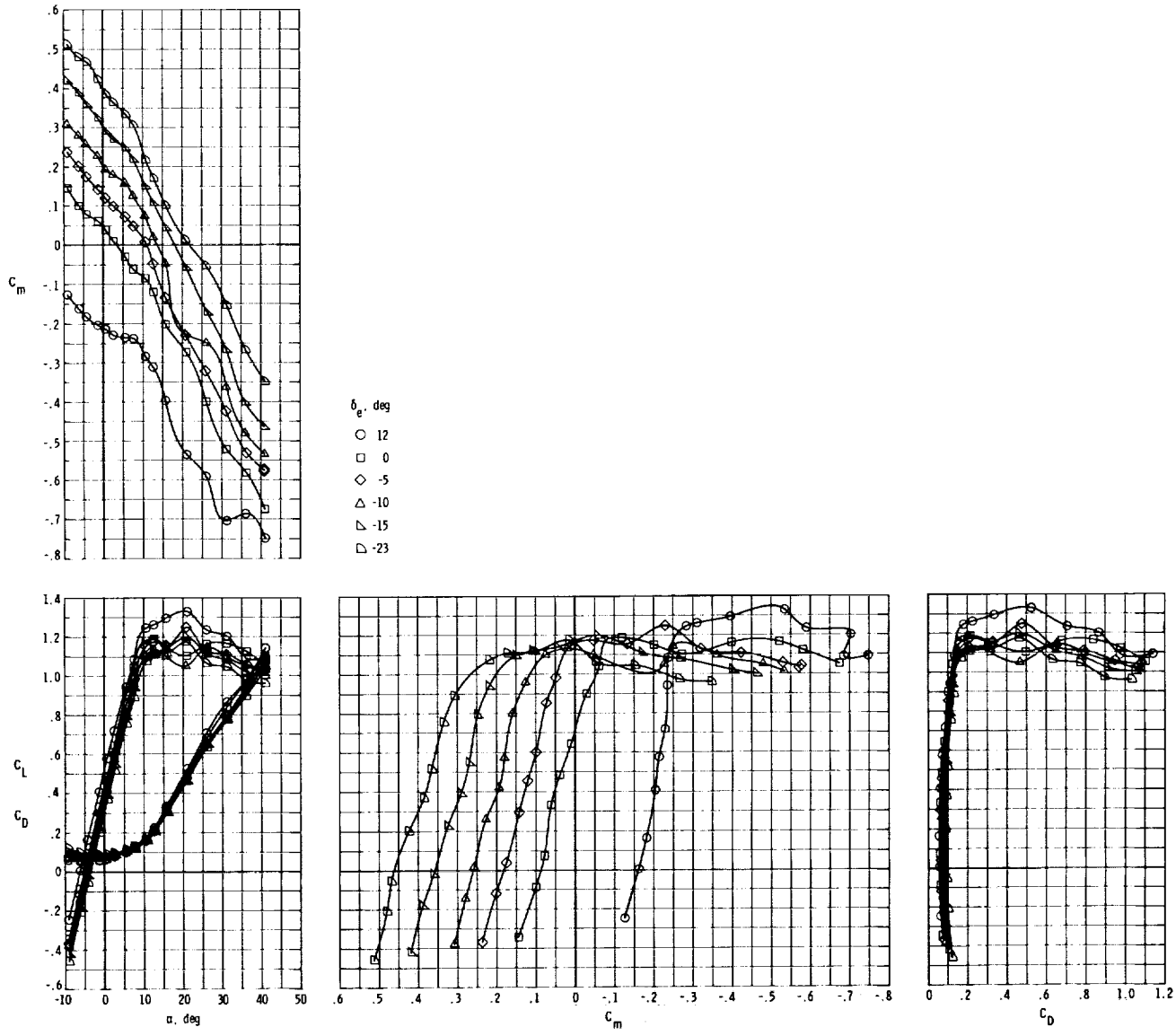

(a) $C_T' = 0.$

Figure 45.- Effect of elevator deflection on longitudinal aerodynamic characteristics of complete basic airplane.

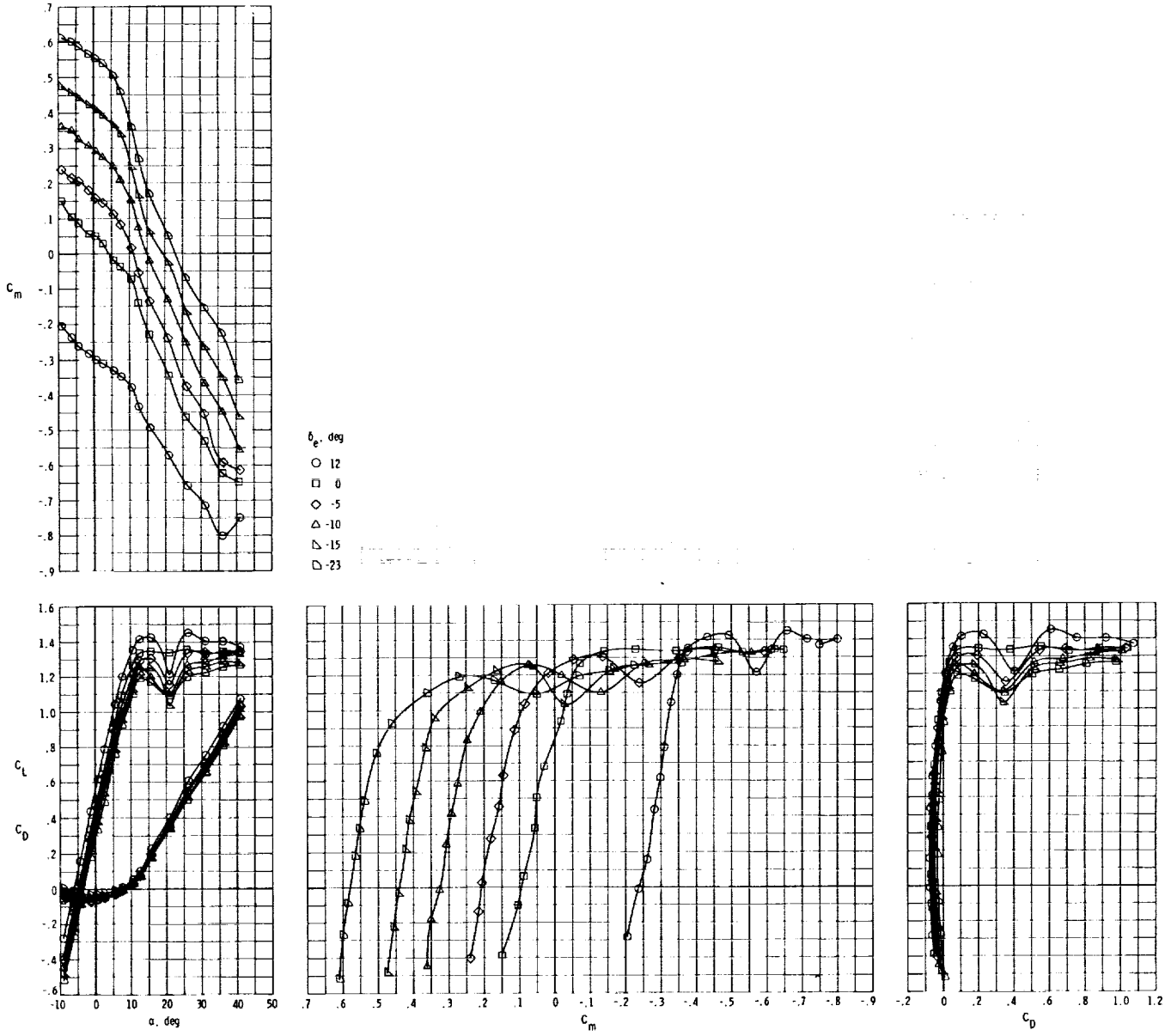

(b) $C_T' = 0.11$.

Figure 45.- Concluded.

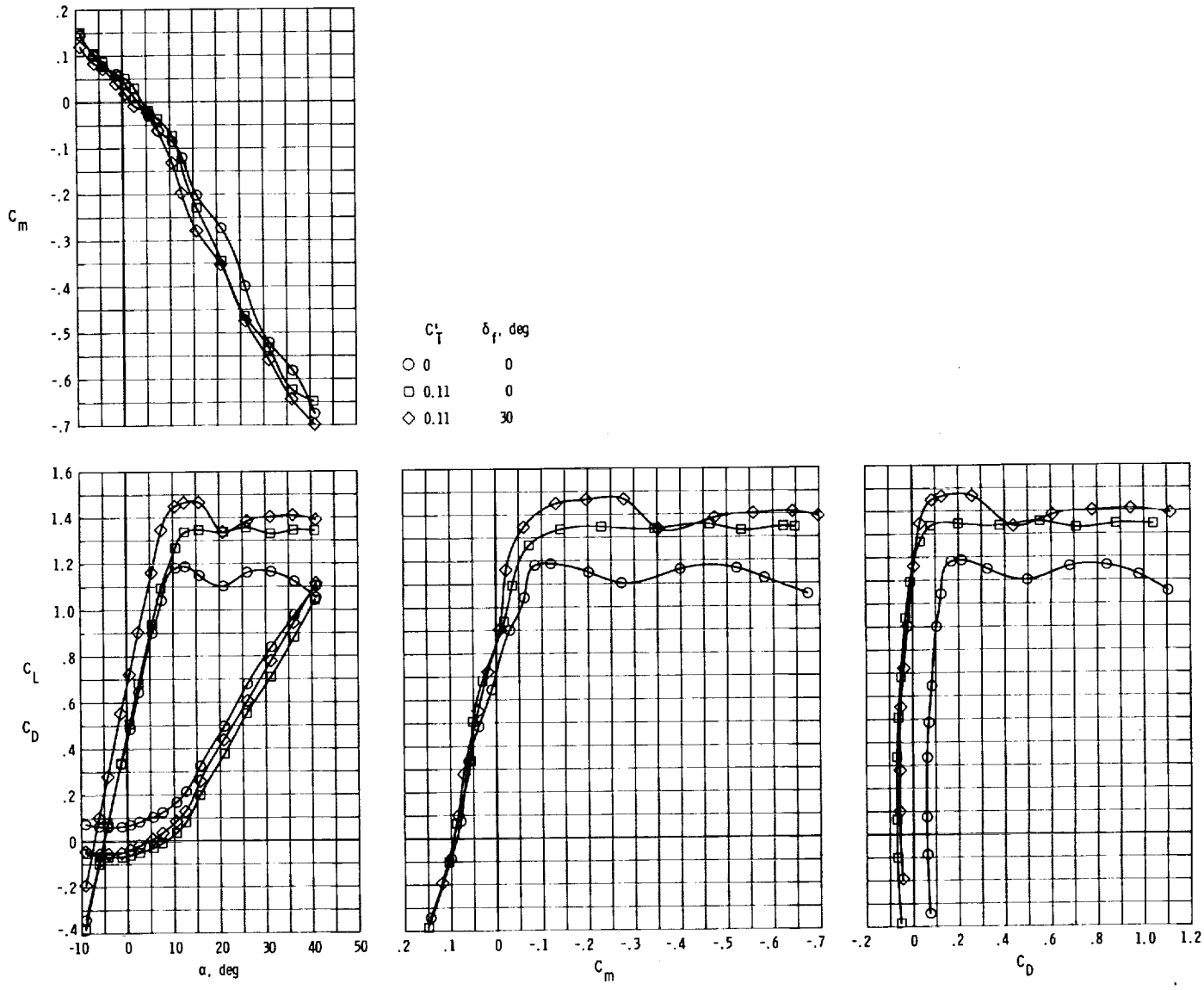

(a) Tail on.

Figure 46.- Effect of horizontal tail on longitudinal aerodynamic characteristics of complete basic airplane.

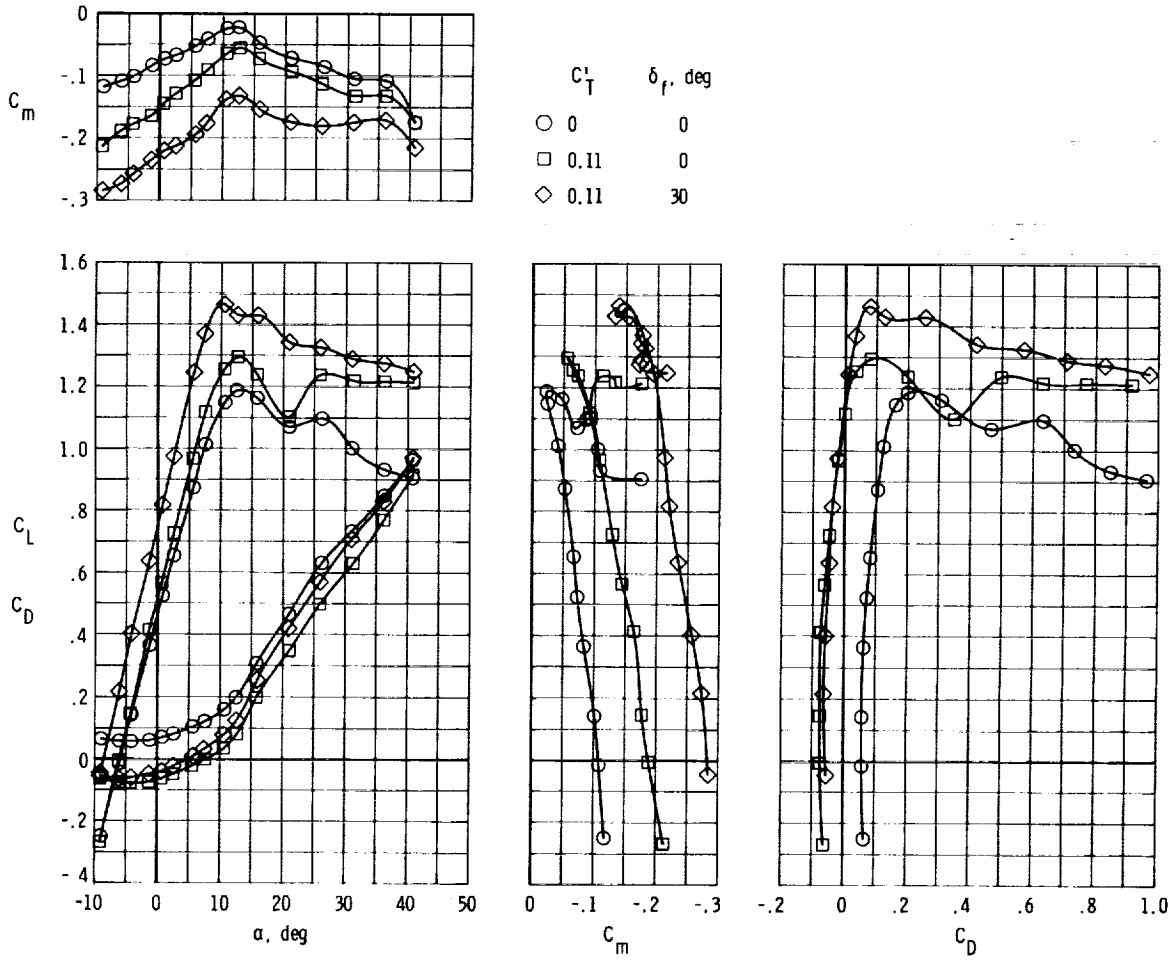

(b) Tail off.

Figure 46.- Concluded.

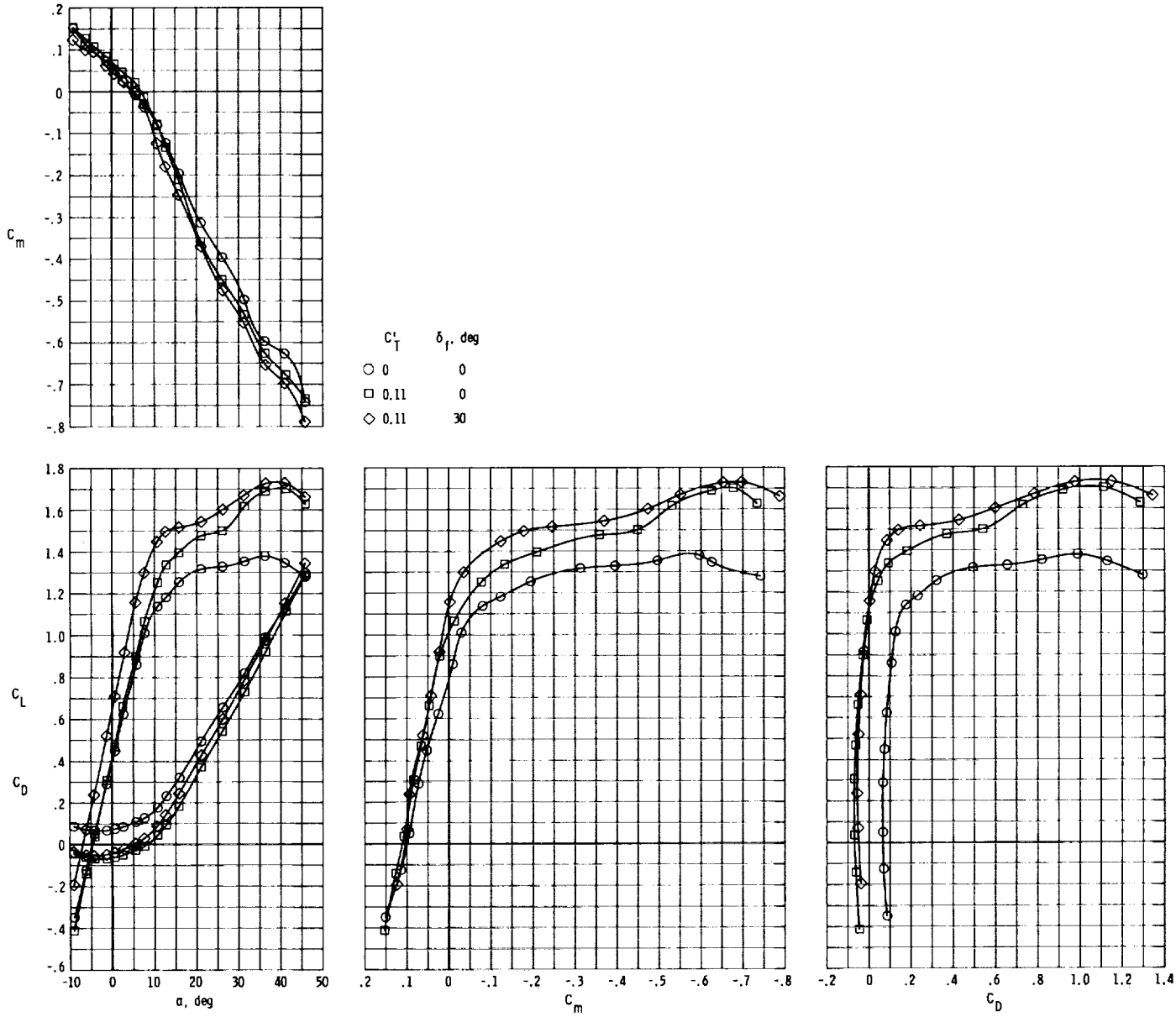

Figure 47.- Longitudinal characteristics of complete airplane with modification B wing. (See fig. 5(b).)

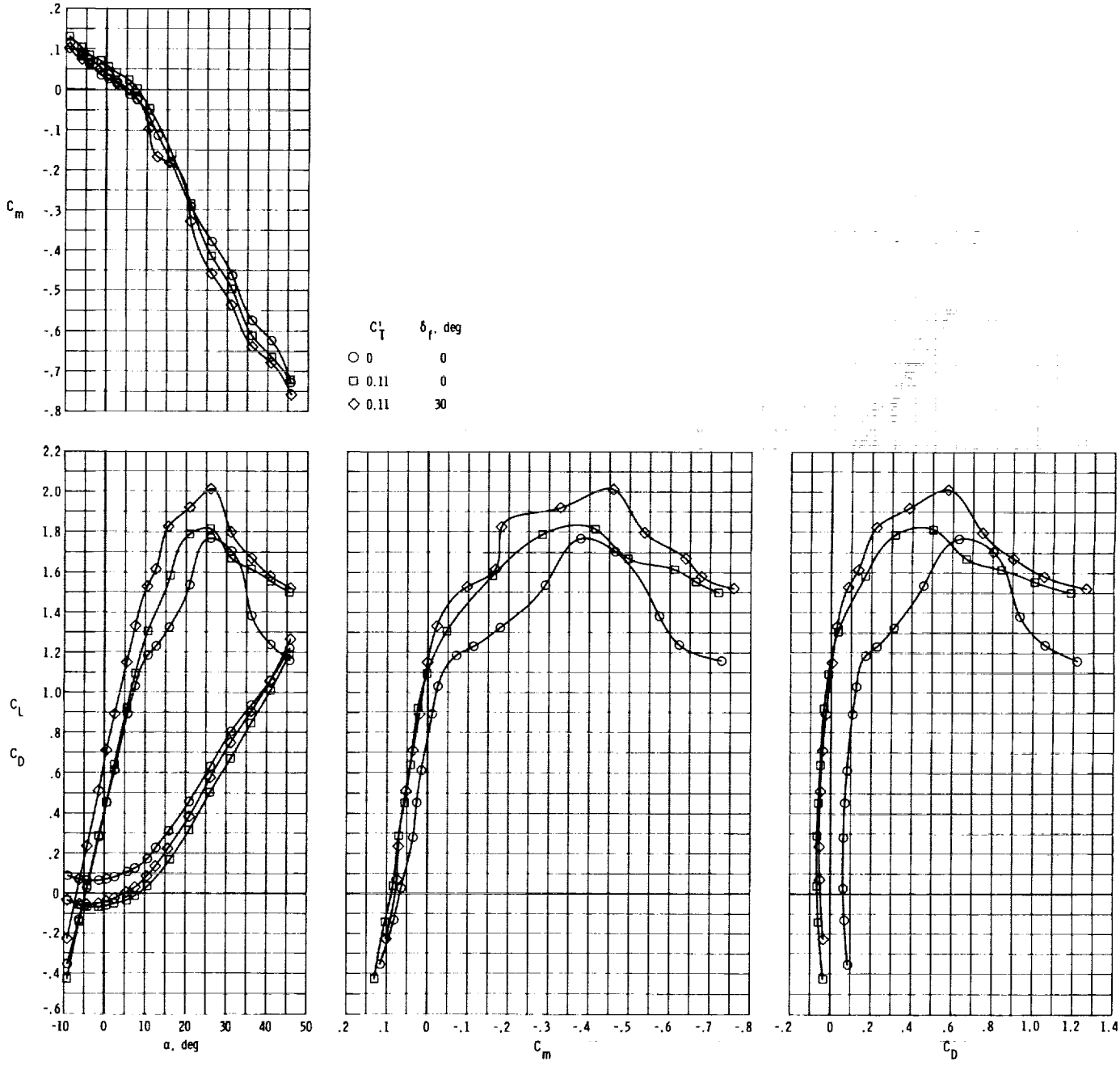

Figure 48.- Longitudinal aerodynamic characteristics of complete airplane with modification A wing. (See fig. 5(a).)

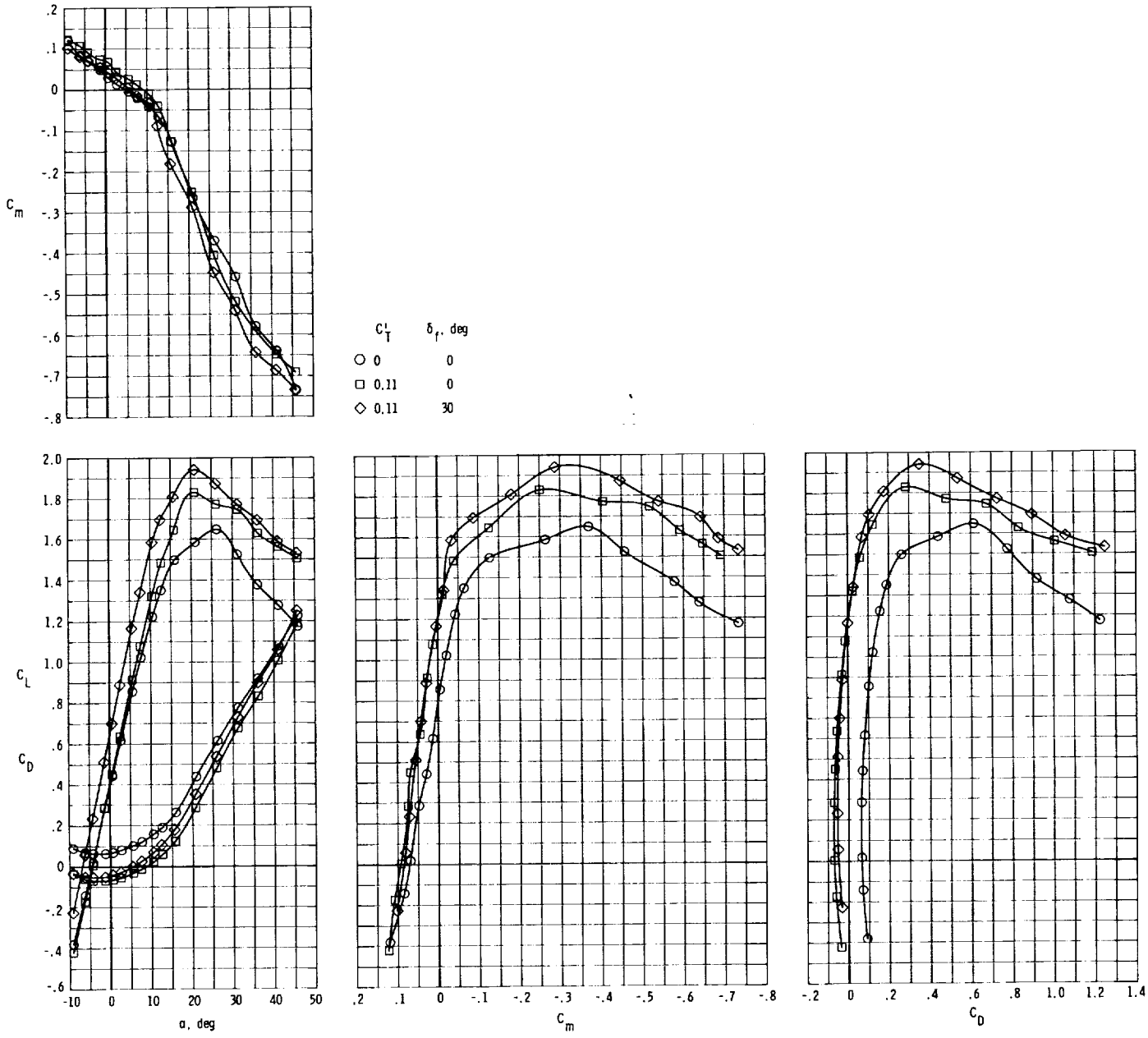

Figure 49.- Longitudinal aerodynamic characteristics of complete airplane with modification A wing and fillet droop. (See figs. 5(a) and 12(d).)

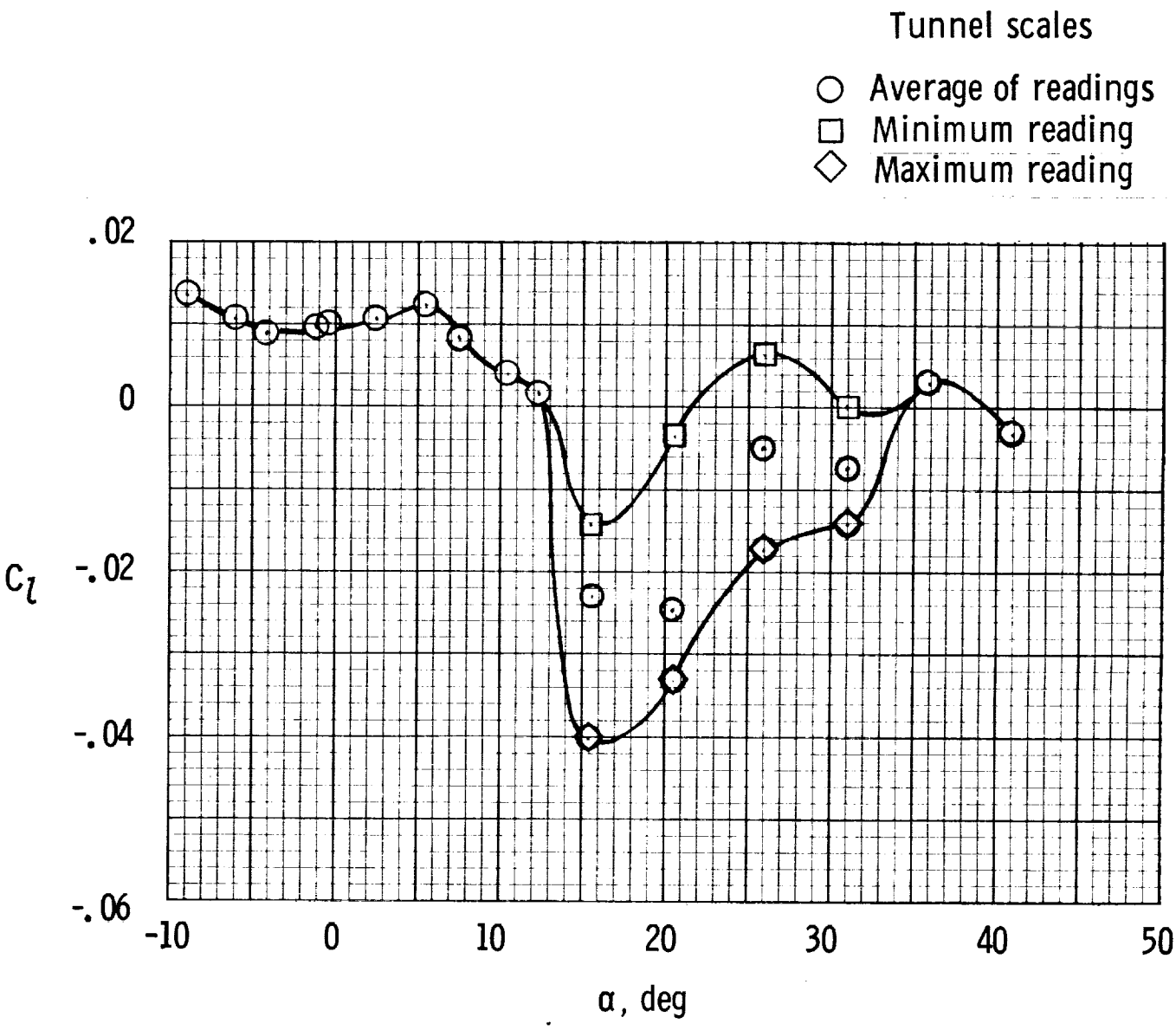

Figure 50.- Rolling moment on complete airplane showing fluctuations at high angles of attack.

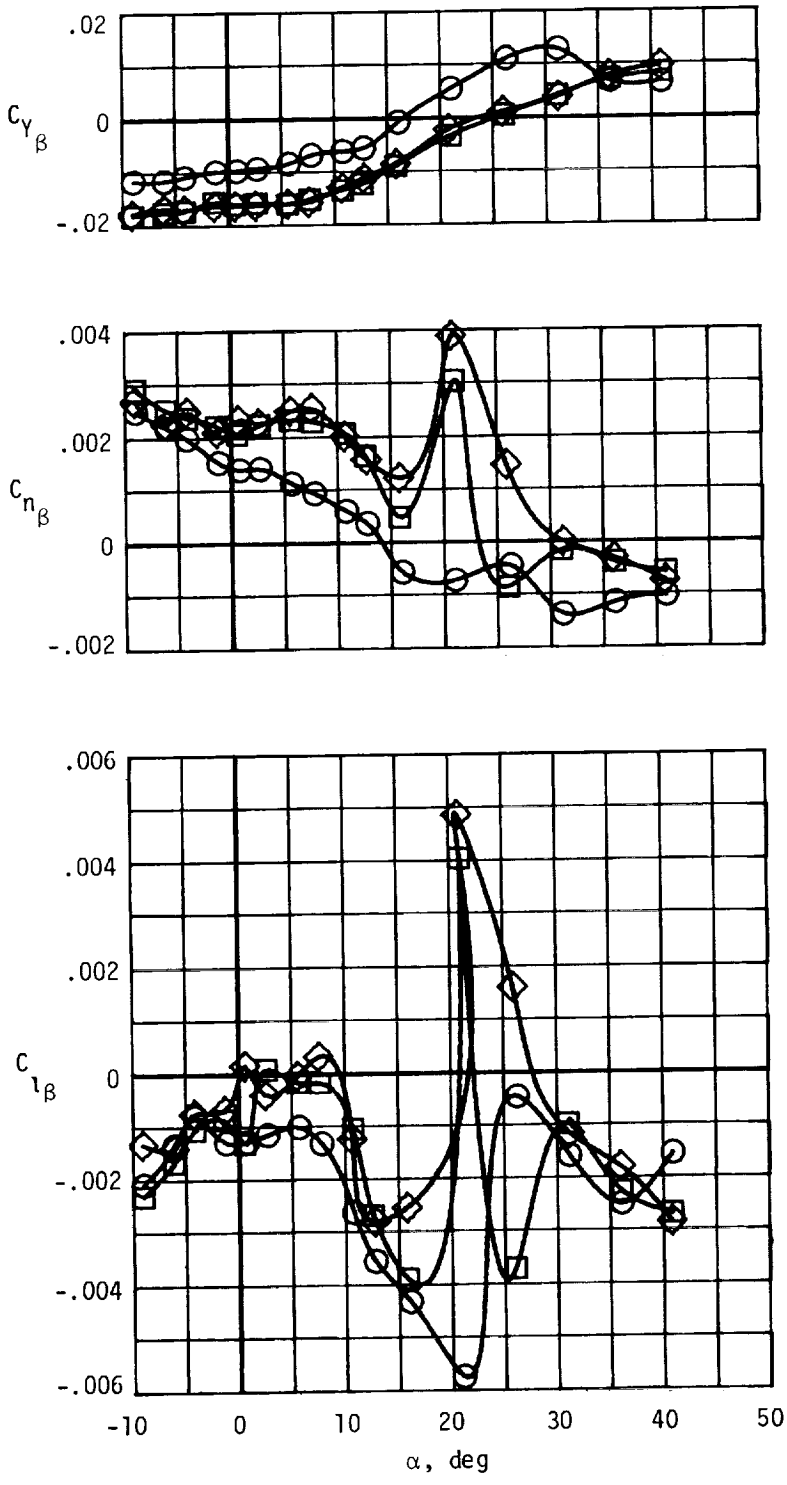

(a) Tail on.

Figure 51.- Effect of vertical tail on static-lateral-stability characteristics of complete basic airplane.

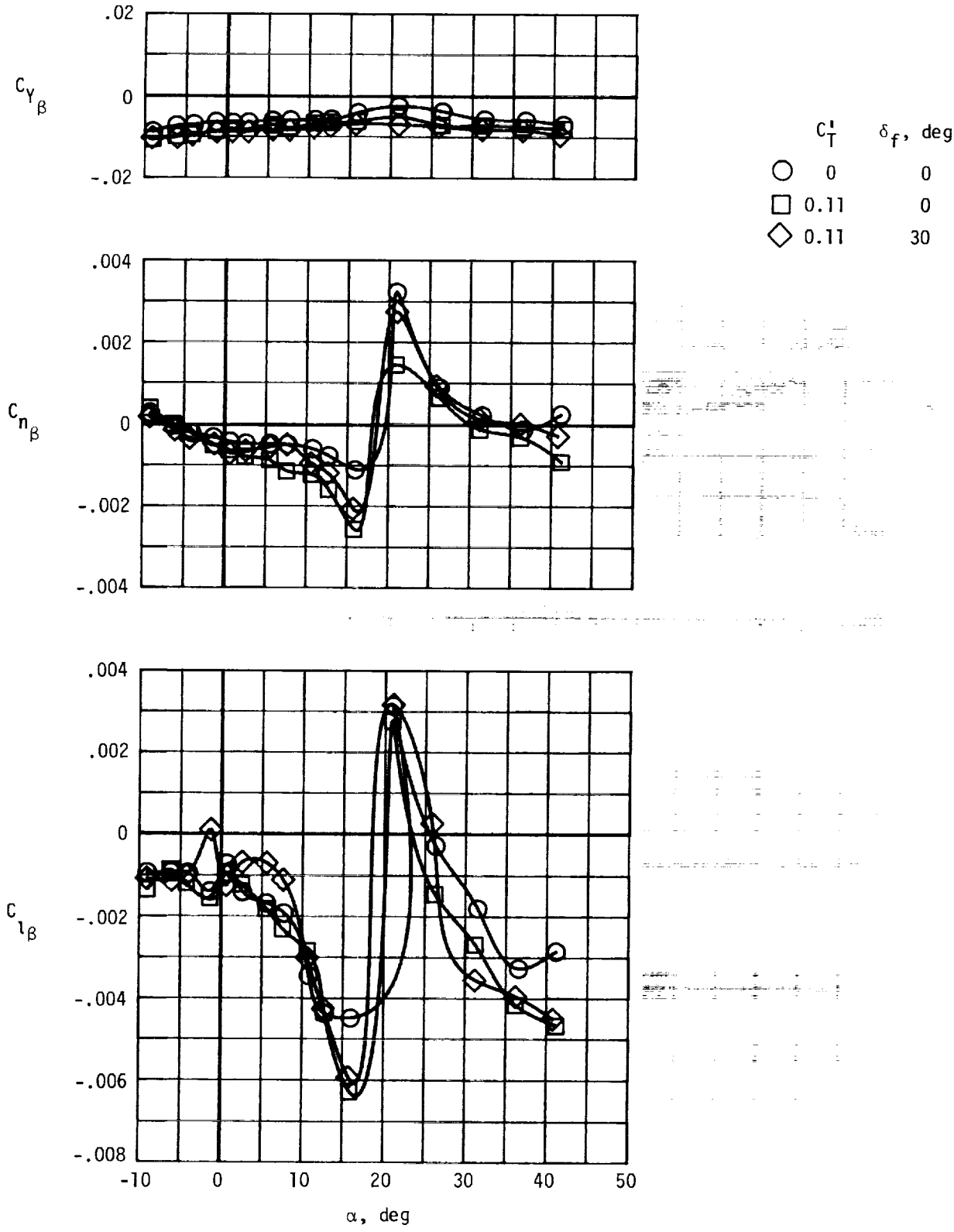

(b) Tail off.

Figure 51.- Concluded.

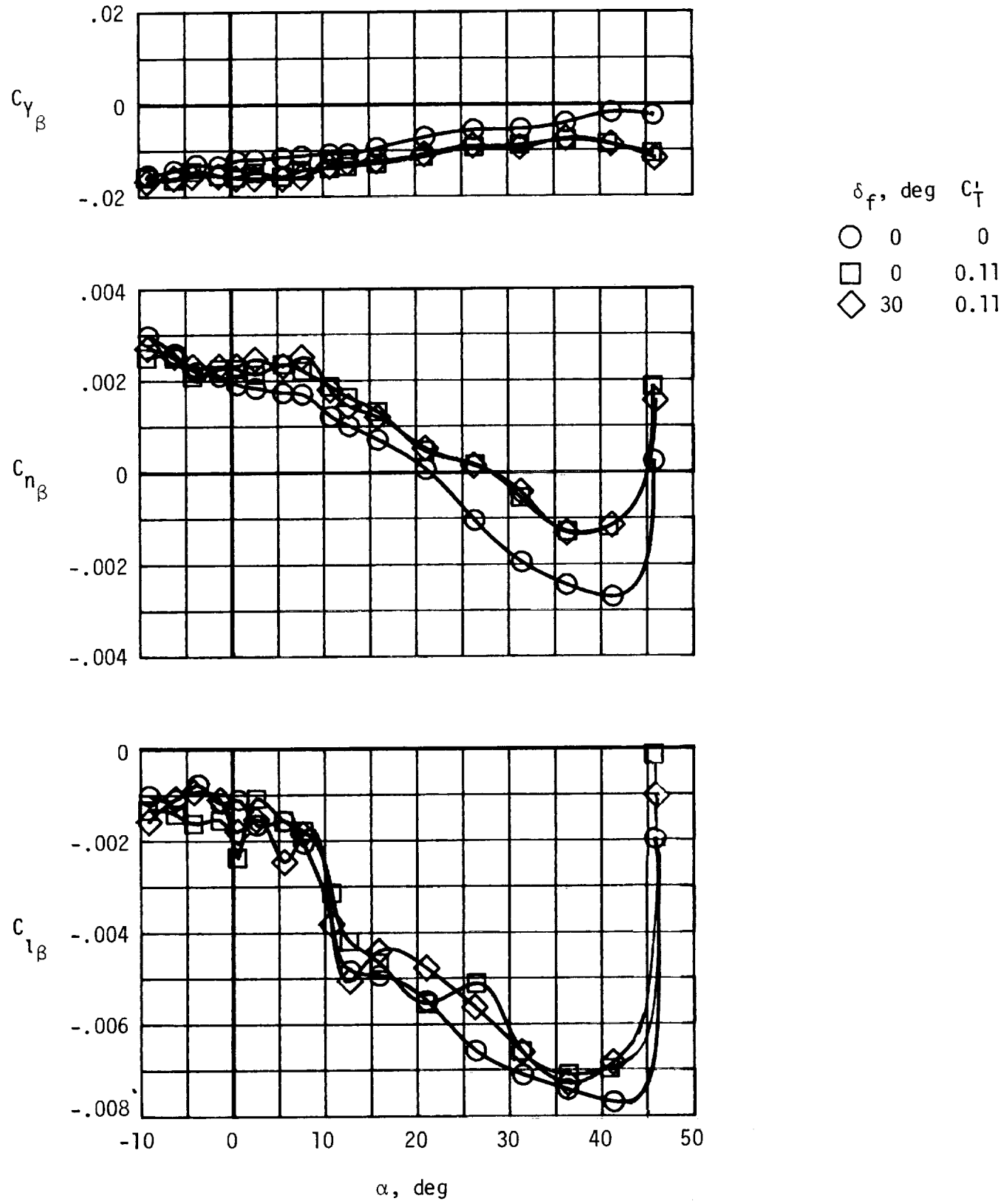

Figure 52.- Lateral-directional characteristics of complete airplane with modification B wing. (See fig. 5(b).)

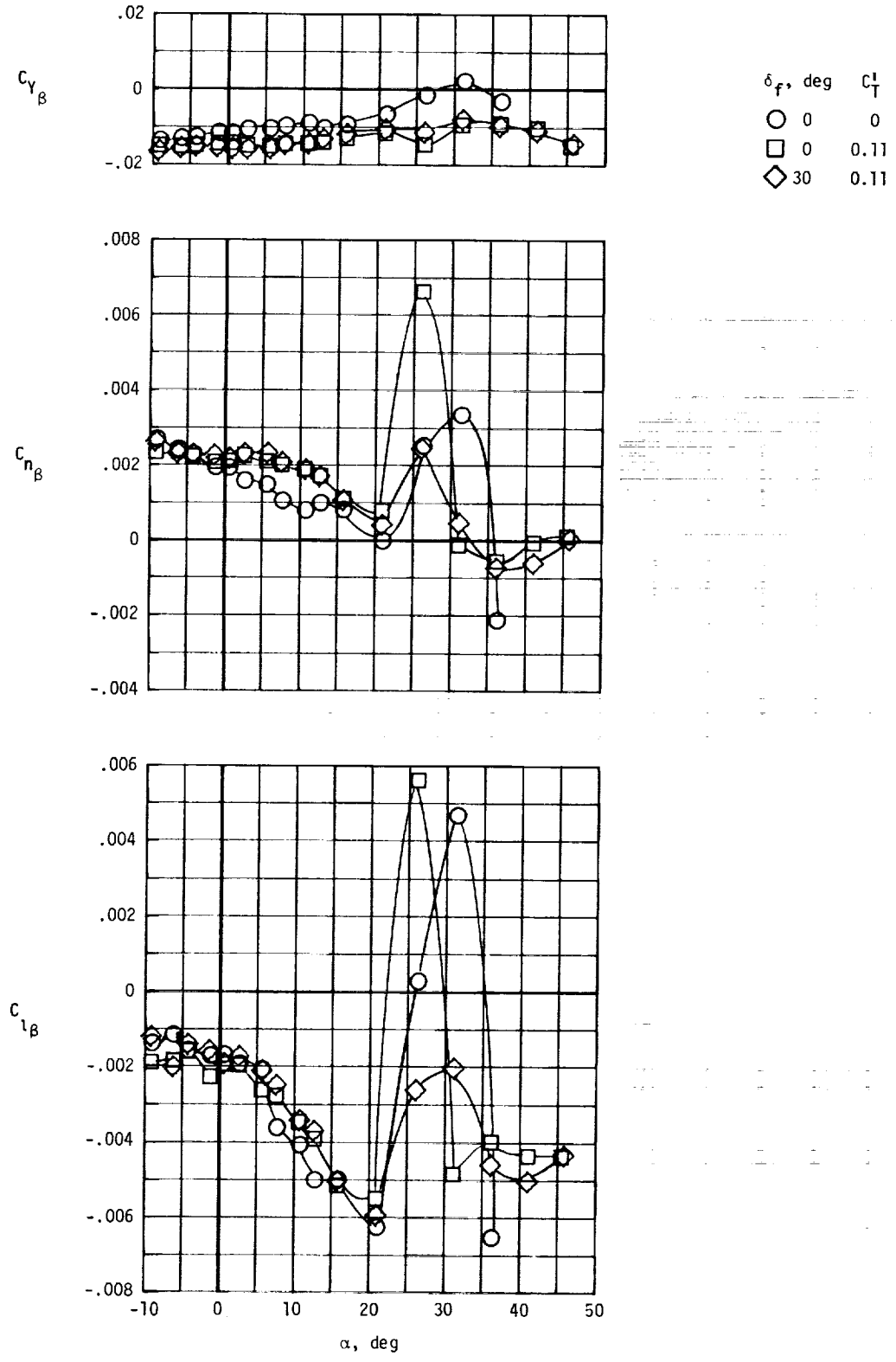

Figure 53.- Lateral-directional characteristics of complete airplane with modification A wing. (See fig. 5(a).)

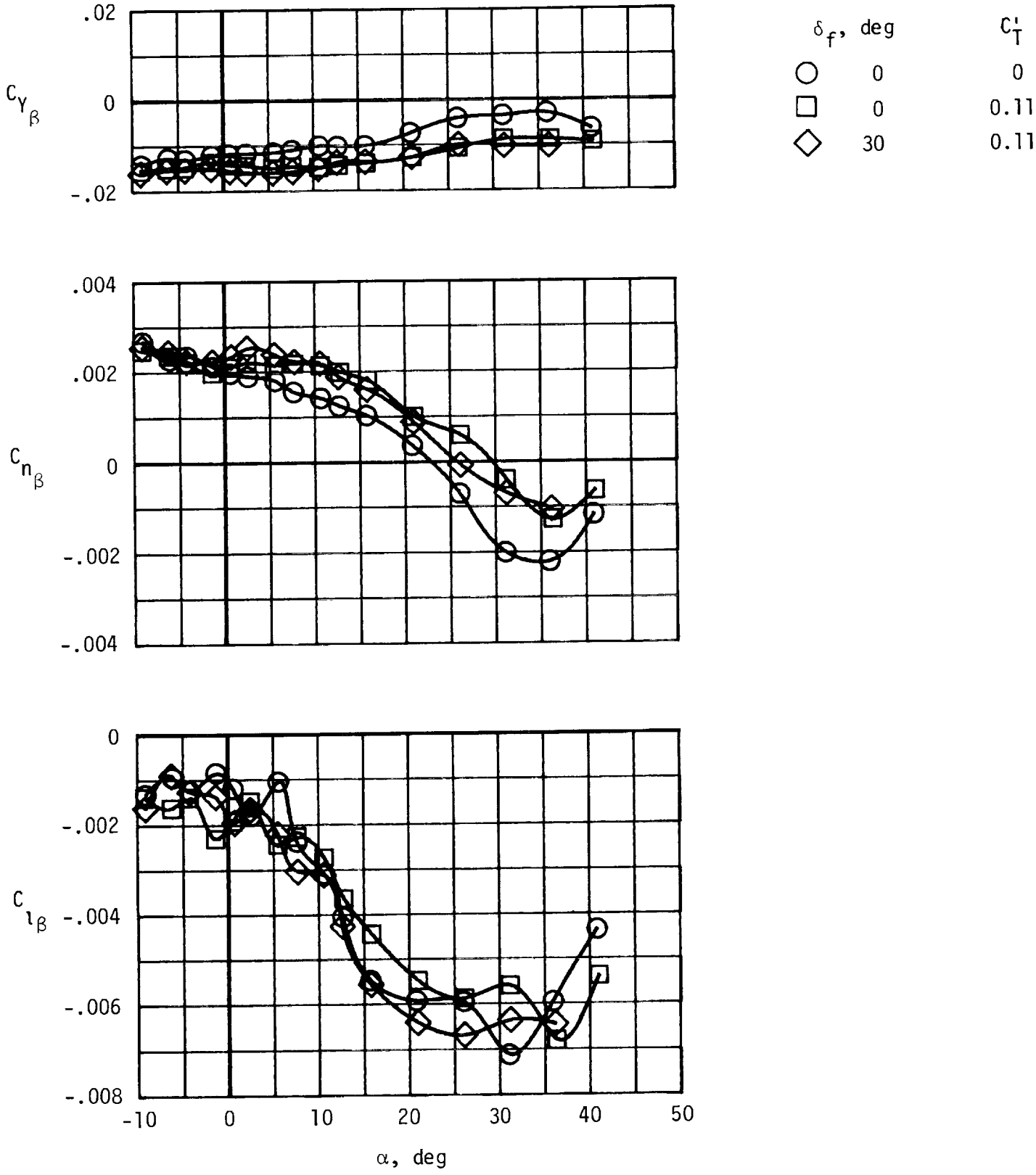

Figure 54.- Lateral-directional characteristics of complete airplane with modification A wing and fillet droop. (See figs. 5(a) and 12(d).)

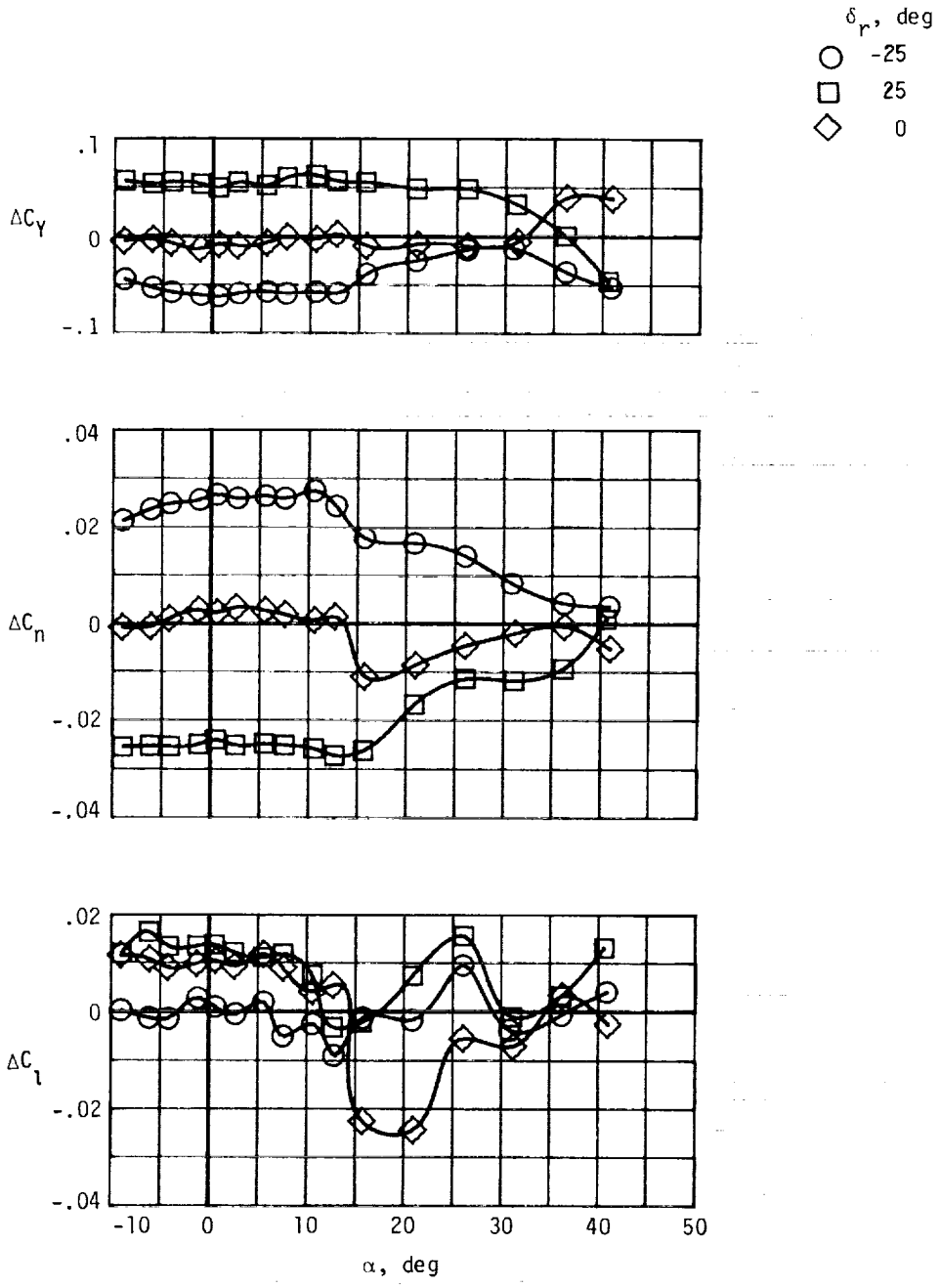

(a) $C_T' = 0.$

Figure 55.- Effect of rudder deflection on lateral-directional aerodynamic characteristics of complete basic airplane.

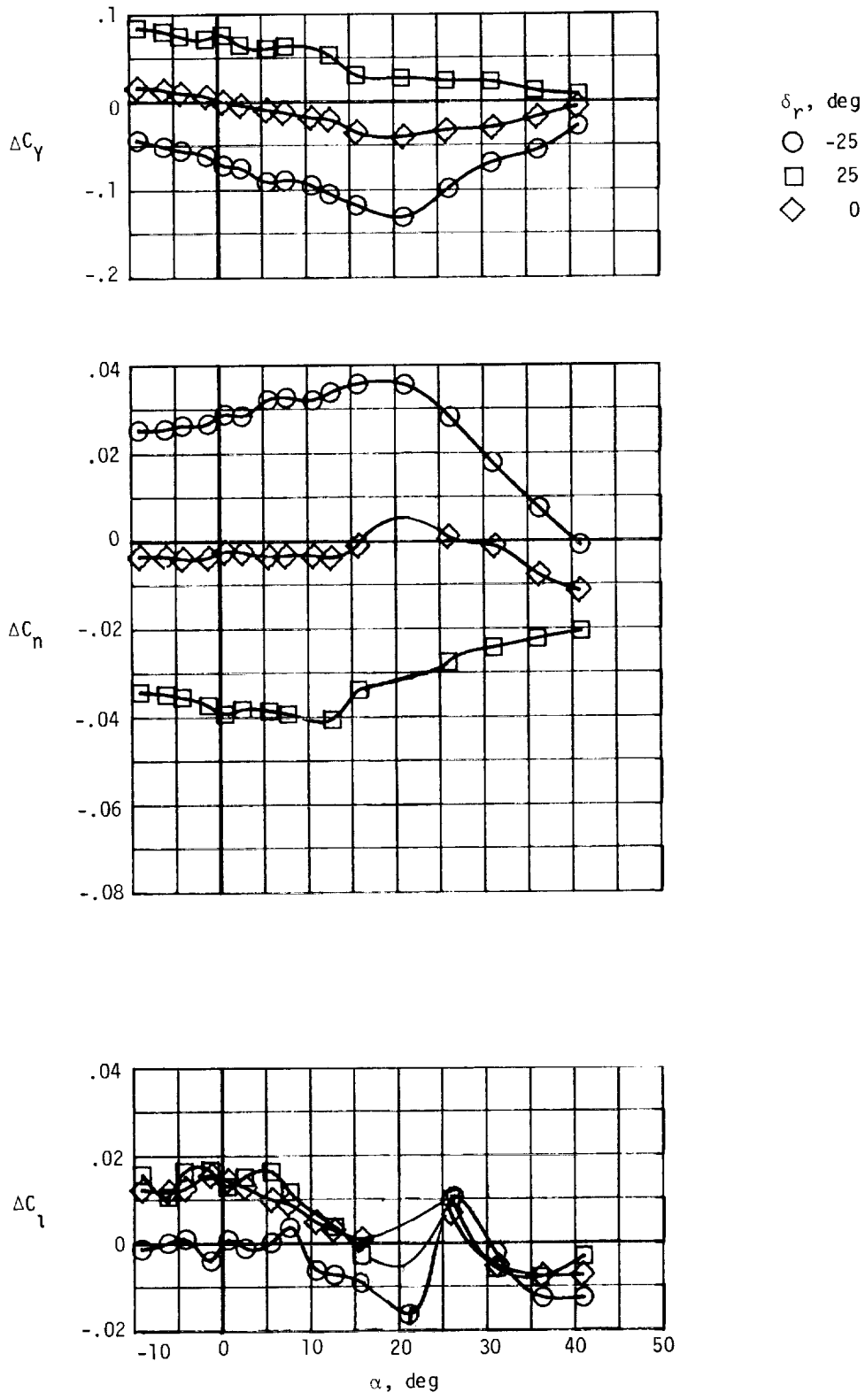

(b) $C_T' = 0.11$.

Figure 55.- Concluded.

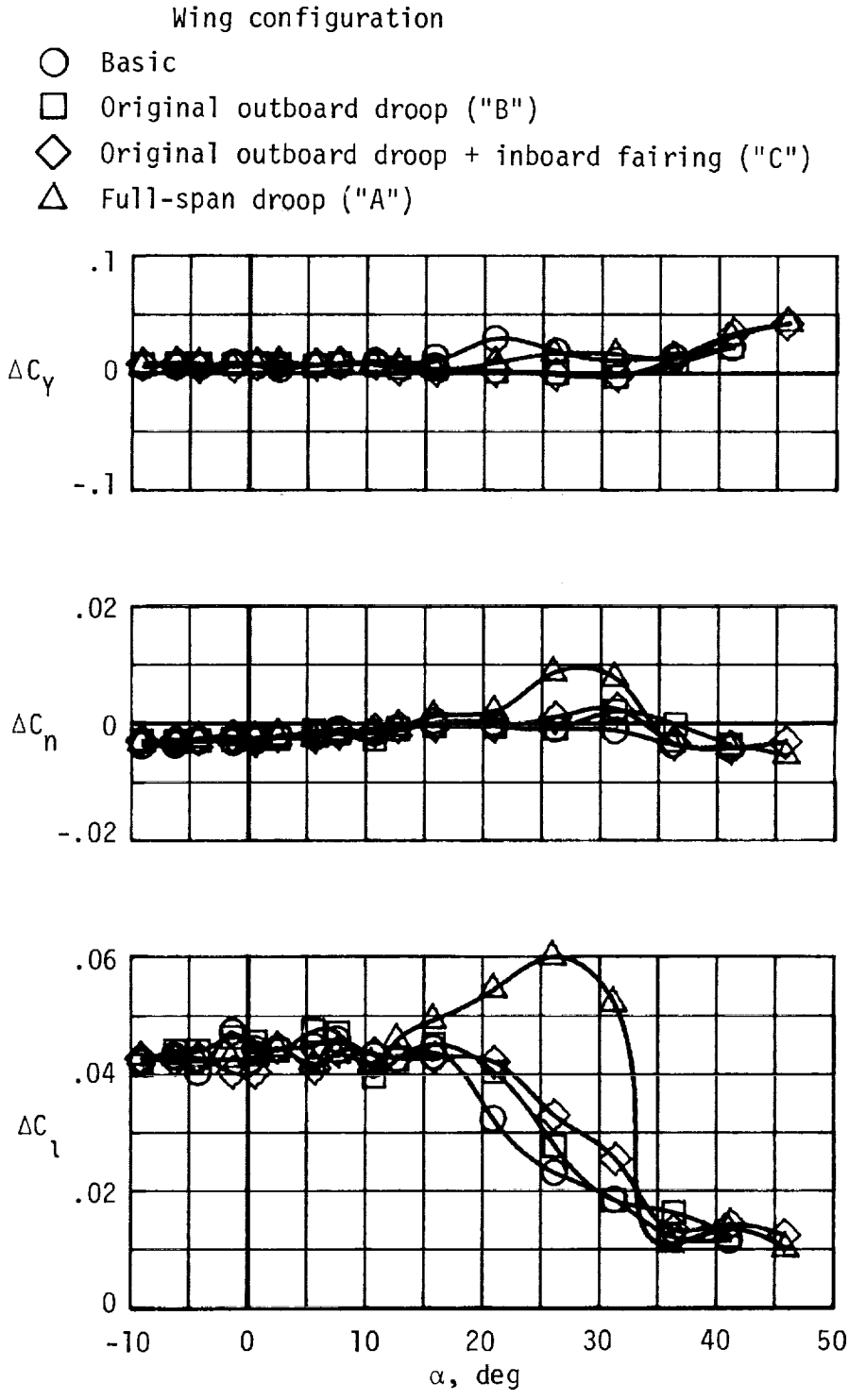

Figure 56.- Effect of aileron deflection on complete airplane with various wing configurations. Aileron deflection = 25° for right roll.

1. Report No.	2. Government Accession No.	3. Recipient's Catalog No.
NASA TP-2011		

4. Title and Subtitle	5. Report Date
EFFECTS OF WING-LEADING-EDGE MODIFICATIONS ON A FULL-SCALE, LOW-WING GENERAL AVIATION AIRPLANE - WIND-TUNNEL INVESTIGATION OF HIGH-ANGLE-OF-ATTACK AERODYNAMIC CHARACTERISTICS	June 1982
	6. Performing Organization Code 505-41-13-02

7. Author(s)	8. Performing Organization Report No.
William A. Newsom, Jr., Dale R. Satran, and Joseph L. Johnson, Jr.	L-15101
	10. Work Unit No.

9. Performing Organization Name and Address	11. Contract or Grant No.
NASA Langley Research Center Hampton, VA 23665	

12. Sponsoring Agency Name and Address	13. Type of Report and Period Covered
National Aeronautics and Space Administration Washington, DC 20546	Technical Paper
	14. Sponsoring Agency Code

15. Supplementary Notes

16. Abstract

The tests were made in the Langley 30- by 60-Foot Tunnel. Wing-leading-edge modifications included leading-edge droop and slat configurations having full-span, partial-span, or segmented arrangements. Other devices included wing-chord extensions, fences, and leading-edge stall strips. Good correlation was apparent between the results of wind-tunnel data and the results of flight tests, on the basis of autorotational stability criterion, for a wide range of wing-leading-edge modifications.

17. Key Words (Suggested by Author(s))	18. Distribution Statement
Spin resistance Stall resistance Wing-leading-edge modifications General aviation	Unclassified - Unlimited Subject Category 01

19. Security Classif. (of this report)	20. Security Classif. (of this page)	21. No. of Pages	22. Price
Unclassified	Unclassified	105	A06

N-305

For sale by the National Technical Information Service, Springfield, Virginia 22161

NASA-Langley, 1982